ANALYSIS OF LOSSY MICROWAVE STRUCTURES AND MICROSTRIP RESONATORS BY THE TLM METHOD

by

SINA AKHTARZAD, B.Sc.

Thesis submitted to the University of Nottingham
for the Degree of Doctor of Philosophy

MAY, 1975

ABSTRACT

Many problems in electrical engineering are associated with the way in which electric and magnetic fields propagate and distribute themselves in various media. Maxwell's equations provide a concise description for the interaction of fields with themselves and with the various boundaries of a problem. Therefore, a numerical procedure for the solution of these equations is an important consideration. This thesis shows how a general three-dimensional medium may be represented by an interconnection of continuous ideal two-wire transmission-lines made up of generalised two-dimensional nodes which are introduced in the earlier chapters. It is then shown how this model may be used for the numerical solution of the electric and magnetic vector fields within the medium. This is the TLM method of numerical analysis.

A universal three-dimensional computer program based on the method is also introduced. This program has been written in only 110 lines of FORTRAN including the subroutines. The ease of application, versatility and accuracy of the TLM method is demonstrated by analysing a wide variety of microwave resonators using this program. The surface mode phenomenon of microstrip is also investigated.

LIST OF AUTHOR'S PUBLICATIONS

A large part of this thesis has appeared in various publications. A list of these, together with related references and abstracts, and other papers which have been submitted to journals and also International and European Microwave conferences is given below:

-

AKHTARZAD, S. and JOHNS, P.B. "Transmission-line matrix solution of waveguides with dielectric losses", Int. J. Num. Meth. Eng., Vol. 9, 1975.

ABSTRACT - The transmission-line matrix method is a time-domain numerical method for solving wave problems. This paper describes how a minor change in the computer program for loss-free dielectrics extends the method to include dielectric losses. Results are given in terms of the wave impedance of a waveguide with losses, and also in terms of power decay due to losses in the dielectric of a resonant cavity.

-

AKHTARZAD, S. and JOHNS, P.B. "Generalized elements for the TLM method of numerical analysis", submitted to Proc. Inst. Elec. Eng., March, 1975.

ABSTRACT - This paper shows how the conduction term in Maxwell's equations can be introduced into the TLM method of numerical analysis. The use of series nodes is also examined thus laying the foundations for the development of the general three-dimensional TLM method.

AKHTARZAD, S. and JOHNS, P.B. "The transmission-line matrix solution of waveguides with wall losses", Electron. Lett., Vol. 9, pp 335-336, July, 1973.

ABSTRACT - The transmission-line matrix method of numerical analysis is developed to account for losses in the walls of a waveguide. Results are given in terms of the wave impedance of a waveguide with losses and also in terms of the power decay due to losses in the walls of a resonant rectangular cavity.

-

AKHTARZAD, S. and JOHNS, P.B. "Numerical solution of lossy waveguides - TLM computer program", Electron. Lett., Vol. 10, pp 309-311, July, 1974.

ABSTRACT - The transmission-line matrix method is a time domain numerical method for solving wave problems. The method uses a mesh of transmission-lines to represent a propagation space and the losses in the space are accounted for by making the transmission-lines lossy. Lossy boundaries are simulated by imperfect boundary reflections on the transmission-lines. A FORTRAN program implementing this technique is presented.

AKHTARZAD, S. and JOHNS, P.B. "The solution of Maxwell's equations in three space dimensions and time by the TLM method of numerical analysis", submitted to Proc. Inst. Elec. Eng., March, 1975.

ABSTRACT - This paper shows how a general three-dimensional medium may be represented by a simple model made up of generalised two-dimensional nodes. It is then shown how this model may be used for the exact numerical solution of electric and magnetic vector fields within the medium without any mathematical formulation of the problem. Results for the resonant frequencies and power decay times of some cavities partially filled with dielectric are given using this method. There has been an excellent agreement in all cases where comparisons could be made.

-

AKHTARZAD, S. and JOHNS, P.B. "The solution of 6-component electromagnetic fields in three space dimensions and time by the TLM method", Electron. Lett., Vol. 10, pp 535-537, December, 1974.

ABSTRACT - The extension of the transmission-line matrix method to three space dimensions is described. The technique provides a solution to the complete set of Maxwell's equations and in particular describes wave propagation in mixed media with or without losses. The method is illustrated by obtaining results for the resonant frequency and field decay time of rectangular cavities partially filled with dielectric.

AKHTARZAD, S. and JOHNS, P.B. "TLM analysis of the dispersion characteristics of microstrip lines on magnetic substrates using three-dimensional resonators", Electron. Lett., Vol. 11, pp 130-131, March, 1975.

ABSTRACT - The dispersion characteristic for a microstrip line on an isotropic magnetic substrate is calculated by the TLM method. The results indicate how errors obtained using approximate TEM analysis vary with frequency. The results also serve to demonstrate the versatility of the three-dimensional TLM program.

-

JOHNS, P.B. and AKHTARZAD, S. "Three-dimensional numerical analysis of microwave cavities using the TLM method", I.E.E.E. MTT-S International Microwave Symposium, Palo Alto, California, U.S.A., May 12-14, 1975.

ABSTRACT - The TLM method of numerical analysis provides a solution for 6-component electromagnetic fields in three space dimensions and time. The universal program is economical and easy to formulate and all the features of a problem are read in as data. The method has been applied to inhomogeneous lossy cavities and cavities containing microstrip discontinuities.

AKHTARZAD, S. and JOHNS, P.B. "The dispersive analysis of microstrip line width change by the TLM method". To be submitted to Electron. Lett., 1975.

ABSTRACT - The TLM method of numerical analysis in three space and time has been successfully applied to microstrip problems. Results indicate good agreement compared with other well known results. In this letter, a general discontinuity problem, namely an abrupt change of width in a microstrip line, is analysed. Comparison is made with an available quasi-TEM data in the literature.

-

AKHTARZAD, S. and JOHNS, P.B. "Three-dimensional TLM computer analysis of microstrip resonators", I.E.E.E. Trans., Microwave Theory Tech., Vol. MTT-23, December, 1975.

ABSTRACT - A wide range of microwave resonators are analysed using the same three-dimensional TLM computer program. The paper demonstrates the ease of application, versatility and accuracy of the TLM method. The results presented include the dispersion characteristics of microstrip on dielectric and magnetic substrate and an example of a microstrip discontinuity. The surface mode phenomenon of microstrip is also investigated.

AKHTARZAD, S. and JOHNS, P.B. "A computer program for the analysis of a wide range of microwave resonators", 5th European Microwave Conference, Hamburg, Germany, September, 1-4, 1975.

ABSTRACT - The solution of large MIC-subassemblies presents a major problem to any numerical method. However, it would seem that the first step should involve a numerical routine of a very general nature for simple discontinuities in three-dimensional structures. Our contribution describes how the TLM method of numerical analysis in form of a very general computer program fulfils this requirement.

-

AKHTARZAD, S. and JOHNS, P.B. "A new model for the numerical solution of Maxwell's equations in three space dimensions and time", 5th Iranian Conference on Electrical Engineering, Pahlavi University, Shiraz, Iran, October 27-30, 1975.

ABSTRACT - This paper shows how a general three-dimensional medium may be represented by an interconnection of continuous ideal two-wire transmission-lines. It is then shown how this model may be used for the numerical solution of the electric and magnetic vector fields within the medium. This is the TLM method of numerical analysis. Results for inhomogeneous lossy cavities and cavities containing microstrip are given.

AKHTARZAD, S., ROWBOTHAM, T.R. and JOHNS, P.B. "The design of coupled microstrip lines", I.E.E.E. Trans., Microwave Theory Tech., Vol. MTT-23, June, 1975.

ABSTRACT - Although graphical results and formulae are available for the design of microstrip couplers, the design procedure is hampered because even- and odd-mode impedances are always expressed in terms of the physical geometry. In practice the designer obtains these impedances and then requires to know the geometry given by them.

A new design procedure for coupled parallel microstrip lines is therefore presented. The technique enables the geometry of the coupled lines to be obtained directly from the required even- and odd-mode impedances and uses single microstrip line geometry as an intermediate step. The results are presented in graphical form using only two universal families of curves. Results are also presented in the form of simple formulae for design programmes and also comparisons with practical results are made.

CONTENTS

CHAPTER 1

THE SOLUTION OF HOMOGENEOUS WAVEGUIDES WITH LOSSY DIELECTRICS

1.1 INTRODUCTION

The transmission-line matrix (TLM) method of numerical analysis provides a time domain, transient solution for the two-dimensional space wave equation,

$$\nabla^2 \underline{E} = \mu\varepsilon \frac{\partial^2 \underline{E}}{\partial t^2}$$

Previous descriptions of the use of this method[1.1-1.3] have considered μ and ε to be real numbers. The modifications to the TLM method required for ε to be complex (lossy dielectrics) is described in the following chapter.

In the TLM method, a homogeneous propagation space is represented by a rectangular mesh of transmission-lines with shunt connections at each crossing point or node, as shown in Fig. 1.1. The matrix is excited at chosen source points, with delta function pulses which then travel along the lines until they meet the next junctions. The computer program is now required to calculate the way in which these pulses are scattered into the four lines at a junction. The appropriate scattering matrix is derived in reference 1.1 and is

$$\frac{1}{2}\begin{pmatrix} -1 & 1 & 1 & 1 \\ 1 & -1 & 1 & 1 \\ 1 & 1 & -1 & 1 \\ 1 & 1 & 1 & -1 \end{pmatrix}$$

The technique is illustrated in Fig. 1.1 by showing the first two iterations for a loss-free dielectric with a point source. This iteration process is repeated a sufficient number of times to give the accuracy of solution required (see reference 1.2). An output impulse function is obtained from a

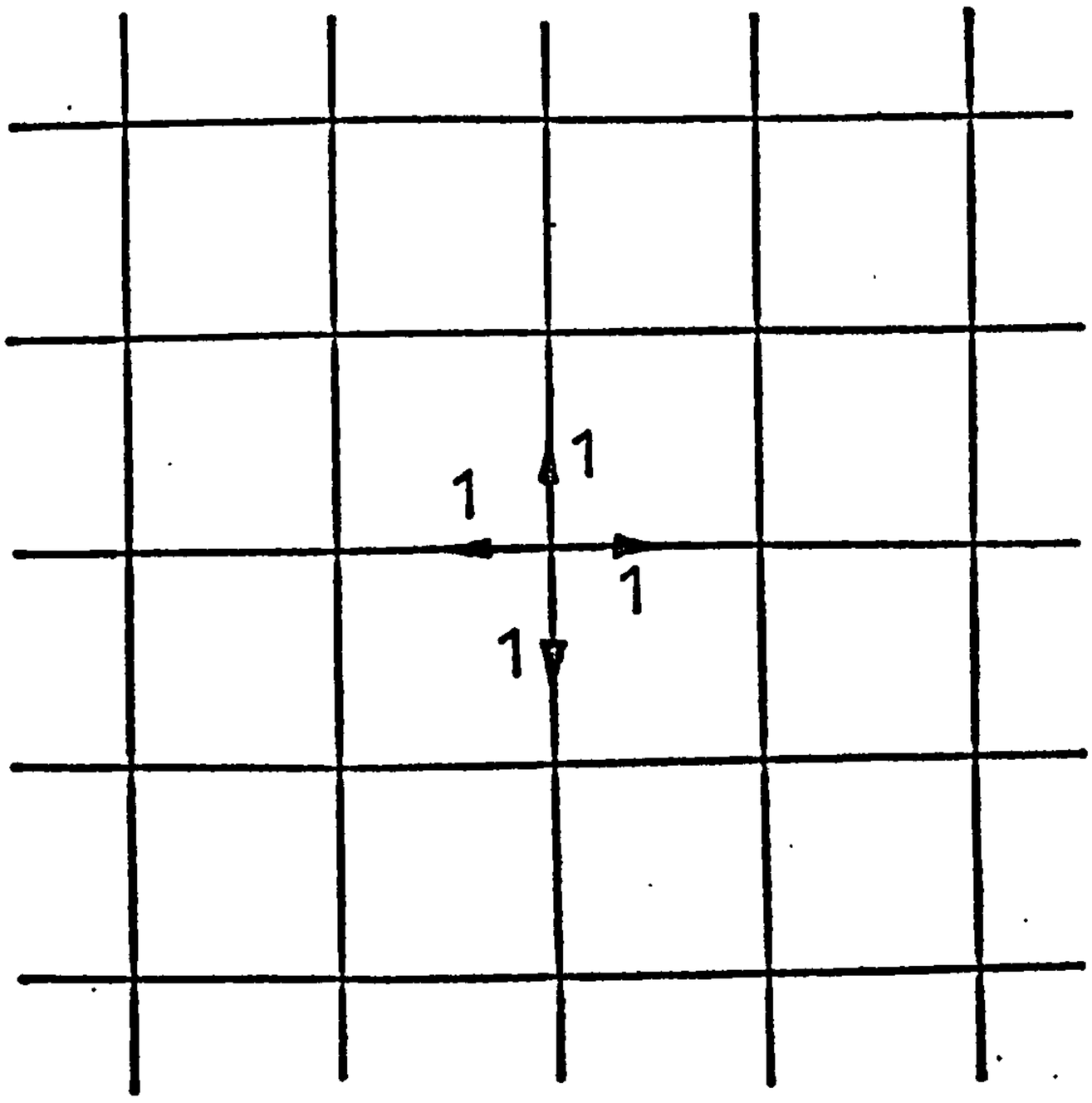

Initial pulse

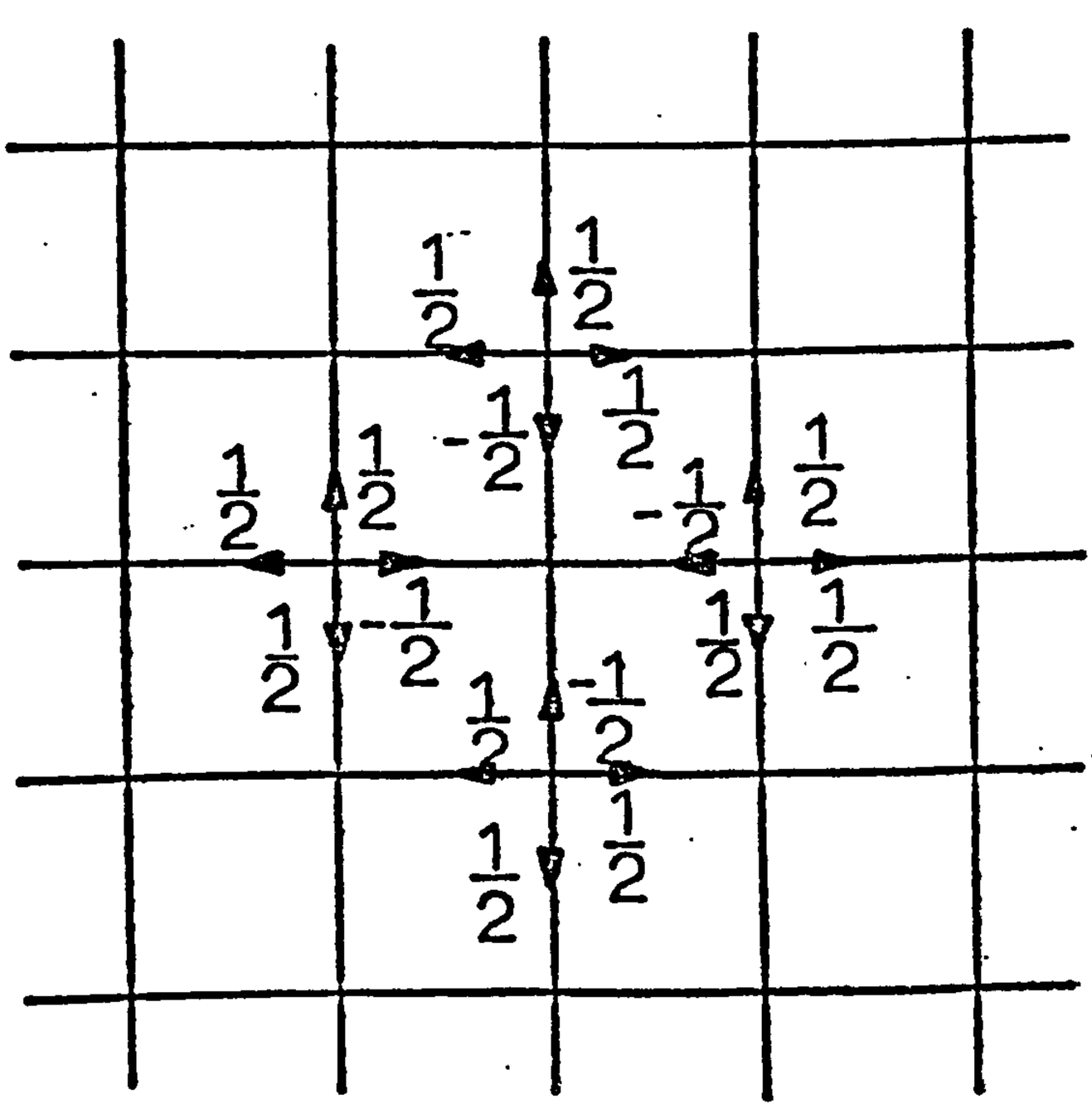

1st iteration

(continued...)

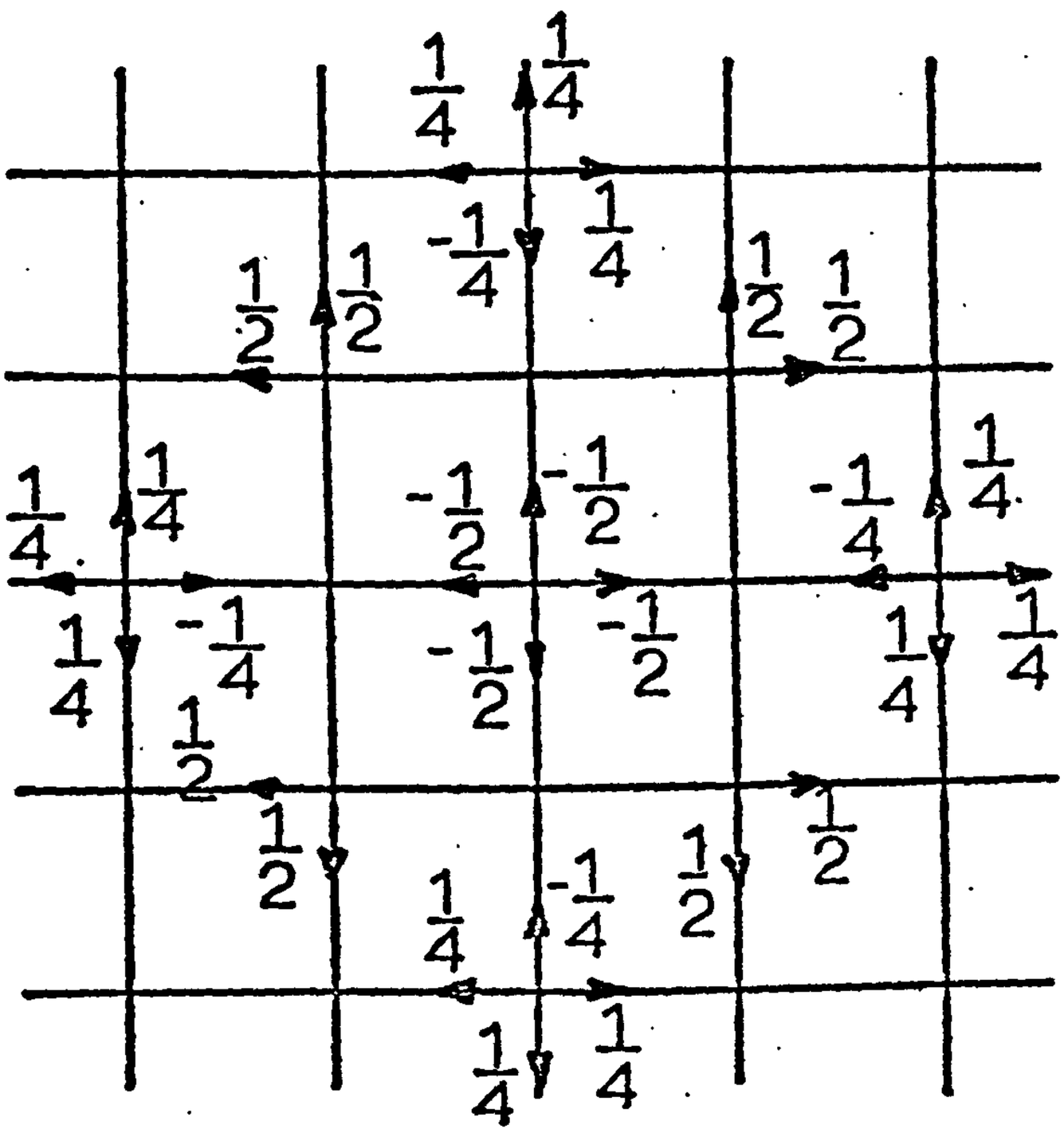

FIG. 1.1 Propagation of a point source on a two-dimensional homogeneous TLM model

a chosen output point by recording the amplitudes of the pulses at that point as time progresses. The Fourier transform of this function is then found, by a simple multiply-and-add procedure, and this gives the spectral response of the system.

The close relationship between the TLM method and the physics of propagation[1,4] allows the method to be extended to account for boundary (see Chapter 3) and dielectric losses. Losses in a medium may be simulated by introducing losses into the component transmission-lines of the TLM model. This means that impulses travelling from one node to the next experience a reduction in amplitude. Restricted to homogeneous wave-guides, the method is particularly useful because this reduction in amplitude of the pulses may be achieved by merely modifying the impulse function obtained under loss-free conditions. The main iteration process of the TLM method is then the same as for the loss-free case. Different loss conditions only require different weighting functions for the amplitude and time of pulses in the impulse function before the Fourier transform is taken.

1.2 THE RELATIONSHIP BETWEEN LINE AND SPACE PARAMETERS

A lossy dielectric may be simulated by introducing losses into the component lines of the transmission-line matrix. In order to show the equivalence between line parameters and space parameters, a junction in the matrix is represented by its lumped parameters. In the numerical calculation, however, the lines will be taken to be distributed parameter transmission-lines.

If the inductance, capacitance and conductance per unit length for an individual line are L, C and G respectively, then the junction between a pair of lines at a mesh node point can be represented by the basic model of Fig. 1.2. The approximate line equations are

$$\left.\begin{aligned} \frac{\partial V_y}{\partial z} &= -L \frac{\partial I_z}{\partial t} \\ \frac{\partial V_y}{\partial x} &= -L \frac{\partial I_x}{\partial t} \\ \frac{\partial I_z}{\partial z} + \frac{\partial I_x}{\partial x} &= -2\left(C + \frac{G}{j\omega}\right) \frac{\partial V_y}{\partial t} \end{aligned}\right\} \quad (1.1)$$

Now the appropriate expansion of Maxwell's equations for $\frac{\partial}{\partial y} = 0$ is

$$\left.\begin{aligned} \frac{\partial E_y}{\partial z} &= \mu \frac{\partial H_x}{\partial t} \\ \frac{\partial E_y}{\partial x} &= -\mu \frac{\partial H_z}{\partial t} \\ \frac{\partial H_x}{\partial z} - \frac{\partial H_z}{\partial x} &= \left(\varepsilon + \frac{\sigma}{j\omega}\right) \frac{\partial E_y}{\partial t} \end{aligned}\right\} \quad (1.2)$$

where σ is the conductivity of the propagation medium. Here the equivalence between line and field parameters can be seen and in particular a conductance of G per unit length of line corresponds to a conductivity of $\sigma = 2G$ in the medium represented. It is often convenient to imagine line geometries such that the impedance $\sqrt{L/C}$ is 1 ohm, and in this case $\sigma = 2G/q$ and $\varepsilon = 2C/q$, where q is numerically equal to the value of $\sqrt{\mu/\varepsilon}$ in ohms.

It is necessary to estimate the frequency range for which the discrete transmission-line model represents continuous space and as usual this is most conveniently done by considering

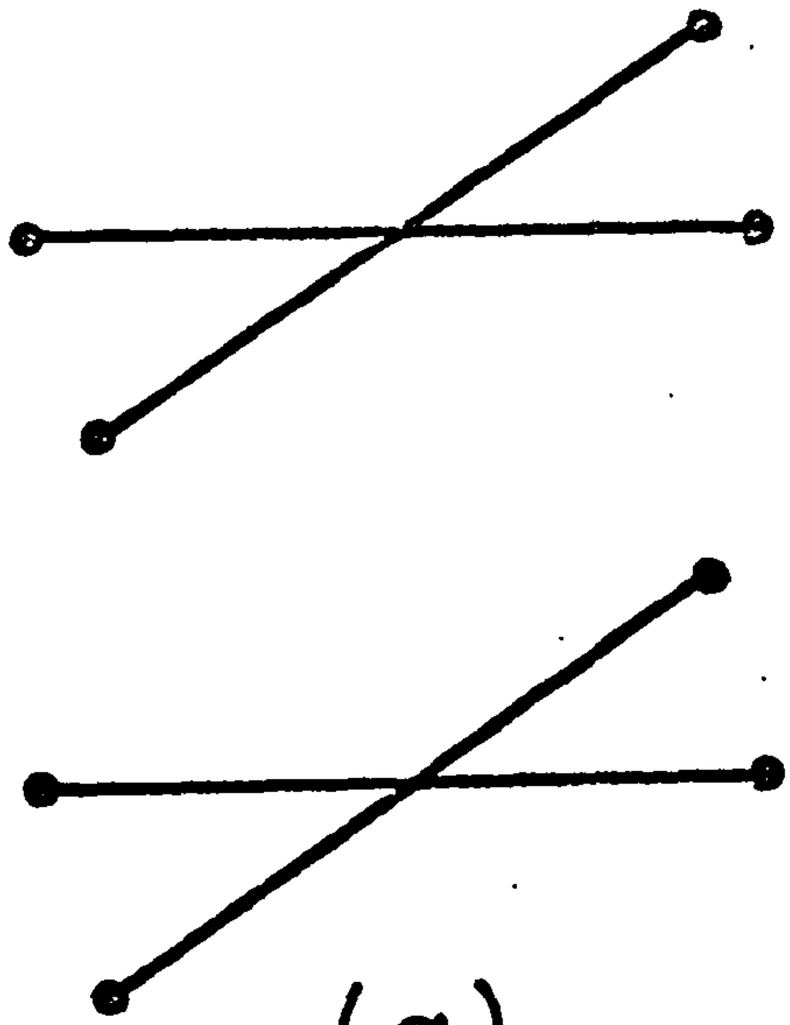

(a)

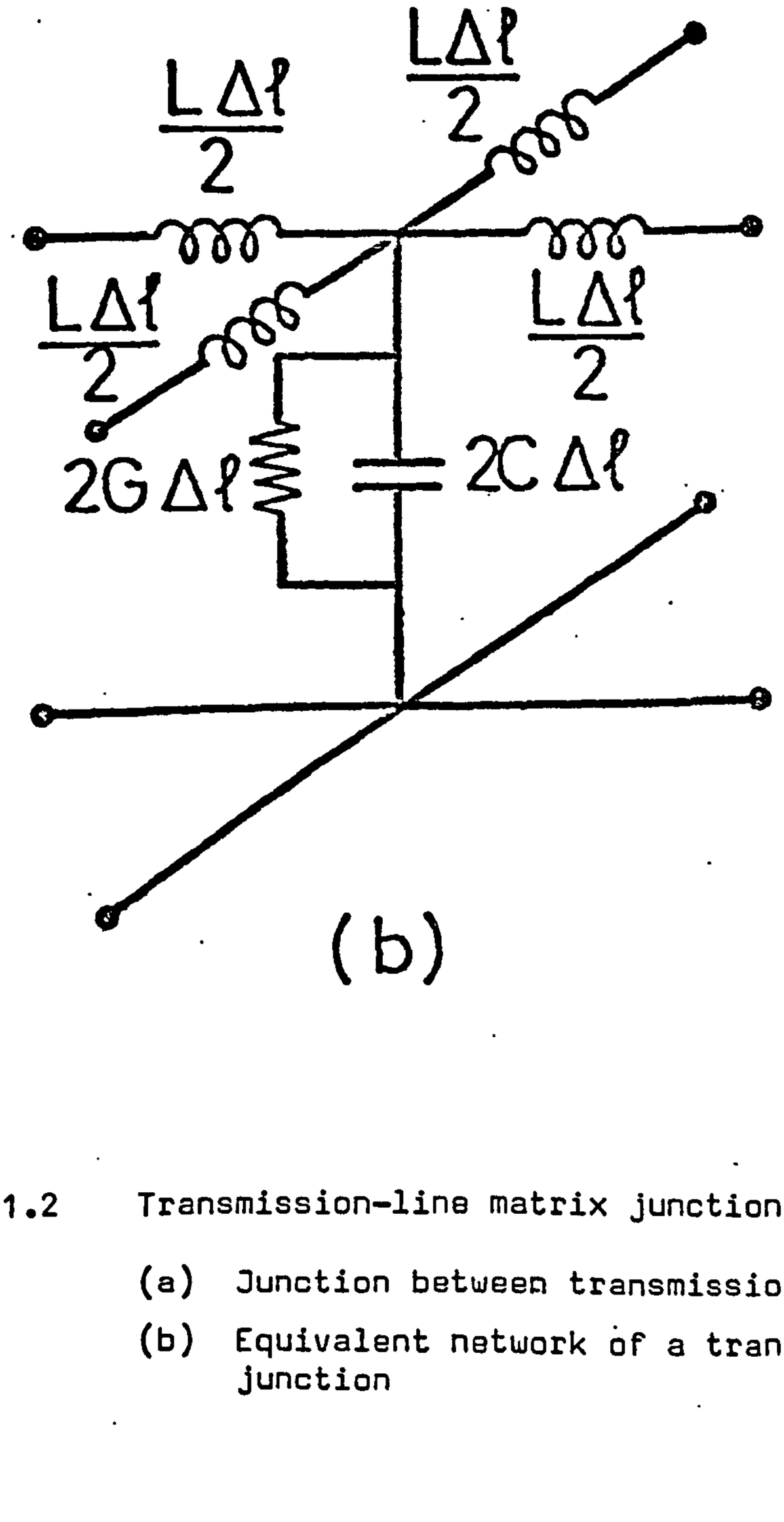

(b)

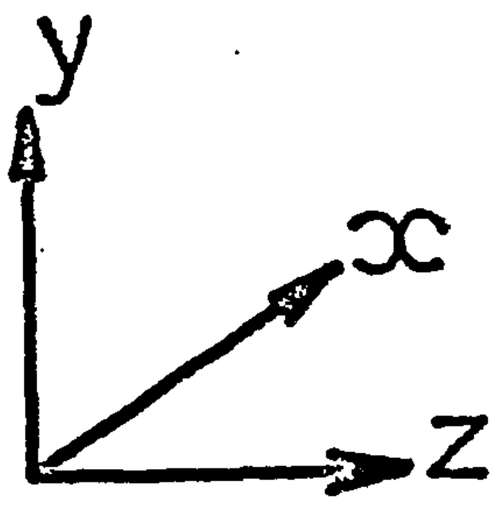

FIG. 1.2 Transmission-line matrix junction

(a) Junction between transmission lines

(b) Equivalent network of a transmission-line junction

the propagation of TEM waves over the matrix. The propagation constant γ for waves on the individual lines is given by

$$\gamma^2 = \omega^2 LC\left(1 + \frac{G}{j\omega C}\right) \qquad (1.3)$$

while for TEM waves of propagation constant γ_n in the medium

$$\gamma^2{}_n = \omega^2 \mu\varepsilon\left(1 + \frac{\sigma}{j\omega\varepsilon}\right) \qquad (1.4)$$

Equations 1.1 to 1.4 show that

$$\gamma_n = \sqrt{2}\,\gamma \qquad (1.5)$$

An exact analysis is needed to find the way in which the accuracy of equation 1.5 deteriorates with rising frequency. The procedure is given in detail in reference 1.1 and a generalisation is required in this version simply to include γ as a complex number. In reference 1.1 it is assumed that TEM waves are travelling in the positive z- direction and are therefore invarient in the x- and y- directions. Hence, it follows that a wave travelling in the medium can be represented by the passage of a wave down a transmission-line with open-circuited stubs of length $\Delta\ell/2$ and spaced at $\Delta\ell$. Now, if the propagation constants of the lines is given by $\gamma = \alpha + \beta$ and the waves on the periodic structure have a propagation constant $\gamma_n = \alpha_n + j\beta_n$, then assuming α and $\alpha_n \ll 1$, the following relationships may be obtained

$$\left.\begin{aligned} \beta/\beta_n &= \frac{\pi\left(\frac{\Delta\ell}{\lambda}\right)}{\sin^{-1}\left[\sqrt{2}\sin\ \pi\left(\frac{\Delta\ell}{\lambda}\right)\right]} \\ \alpha/\alpha_n &\quad \frac{\left[\cos 2\pi\left(\frac{\Delta\ell}{\lambda}\right)\right]^{\frac{1}{2}}}{\sqrt{2}\cos\ \pi\left(\frac{\Delta\ell}{\lambda}\right)} \end{aligned}\right\} \qquad (1.6)$$

where $\beta = \frac{2\pi}{\lambda}$.

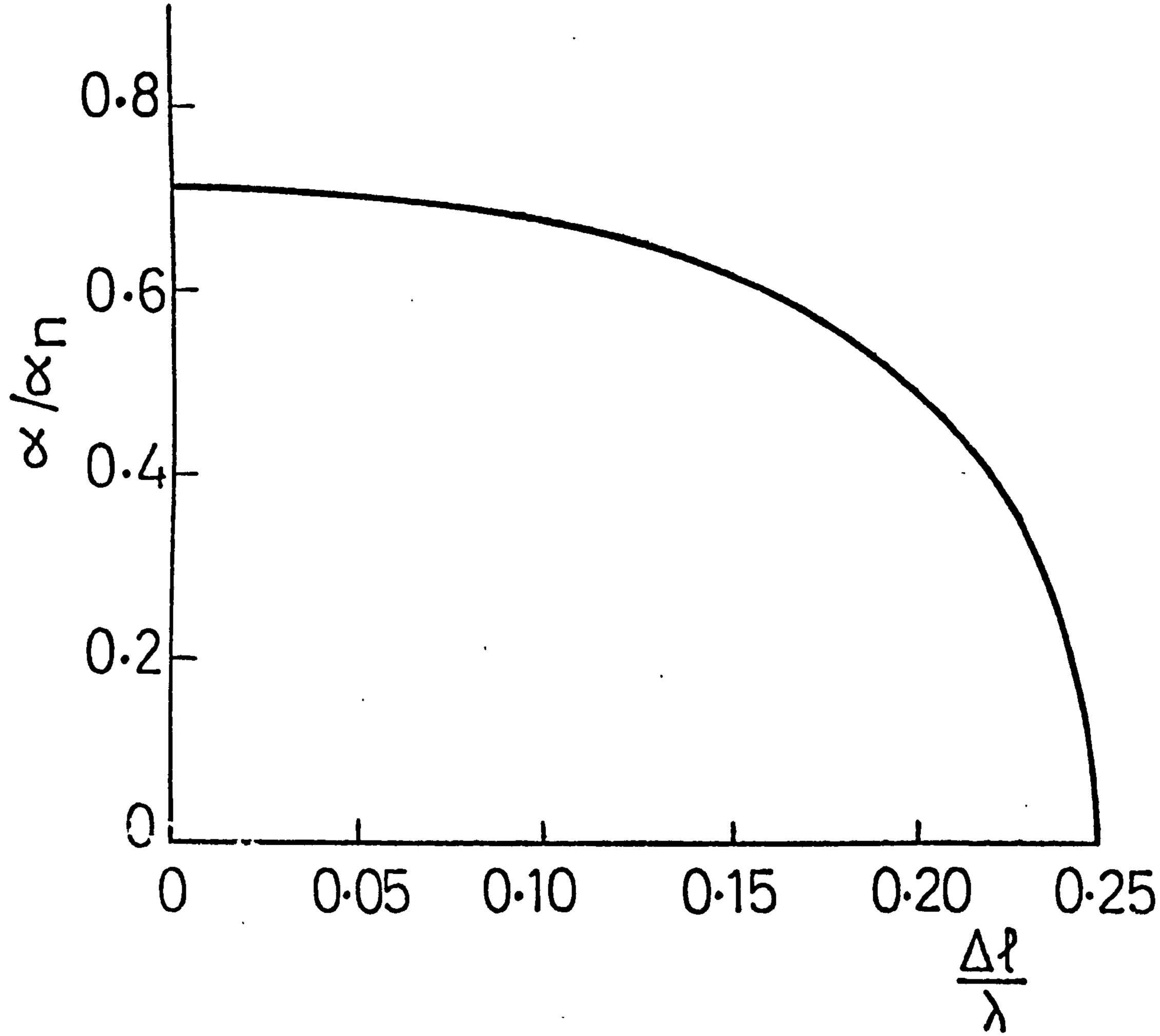

FIG. 1.3 Attenuation characteristic for transverse waves on a transmission-line matrix

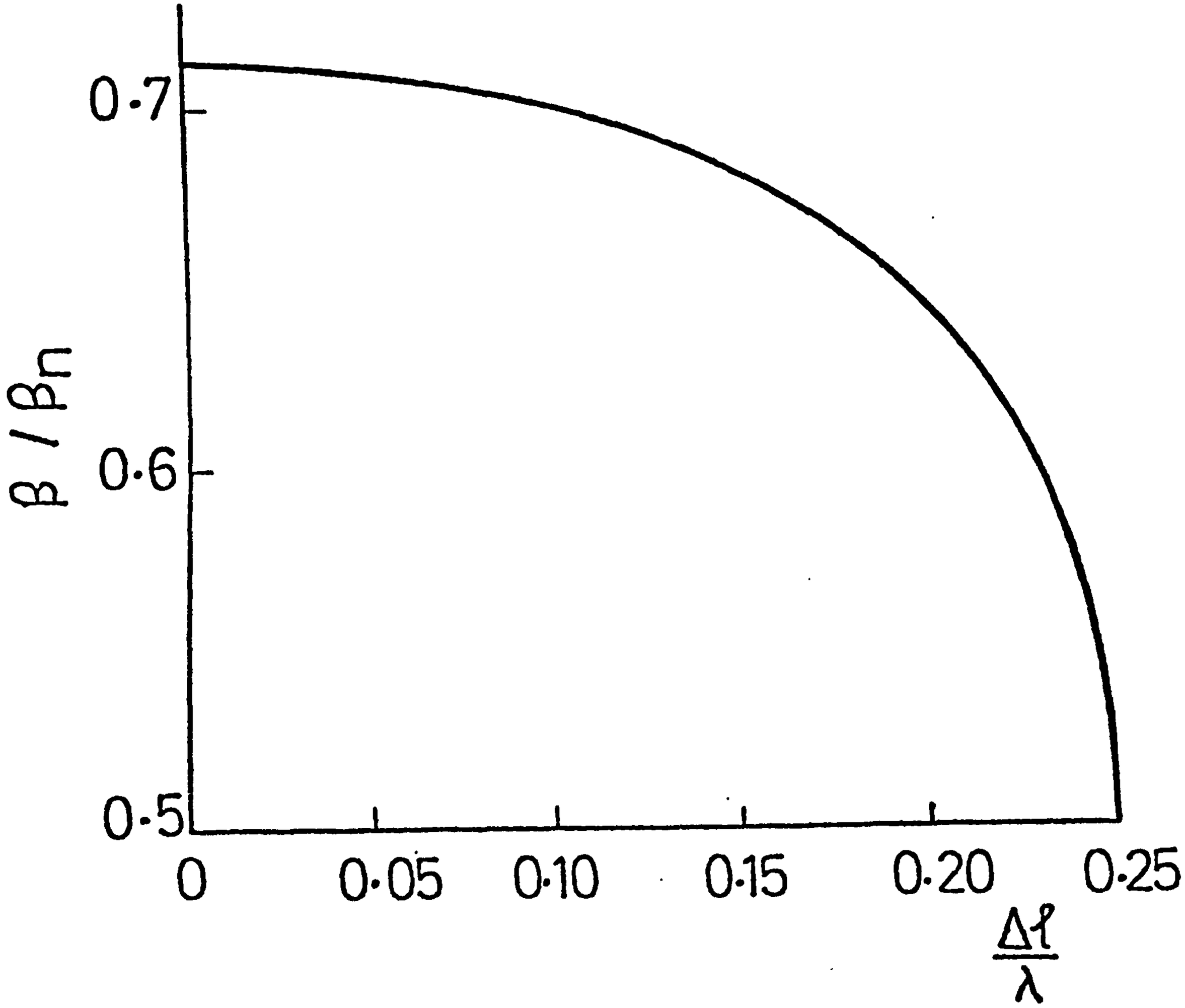

FIG. 1.4 Phase characteristic for transverse waves on a transmission-line matrix

The attenuation constant ratio α/α_n is plotted in Fig. 1.3 and the phase constant ratio β/β_n (which is the same as that derived in reference 1.1) is reproduced for convenience in Fig. 1.4. These curves show that for frequencies well below the network cut off frequency, i.e.

$$\left(\frac{\Delta\ell}{\lambda}\right)_{\text{cut-off}} = \frac{1}{\pi} \sin^{-1}\left(\frac{1}{\sqrt{2}}\right) \qquad (1.7)$$

the propagation constant is given by equation 1.5. It can also be seen that for a given frequency range the errors in α_n will be worse than the errors in β_n. It should be noted that for a given frequency, the error in α_n and β_n vary with the angle of travel of waves over the matrix and that the curves of Fig. 1.3 and Fig. 1.4 give the worst case. Thus, these curves may be used to give a bound on errors in α_n and β_n at a particular frequency (see reference 1.2)

1.3 THE PROCEDURE FOR A LOSSY DIELECTRIC

The procedure for a lossy dielectric is precisely the same as the procedure for loss-free dielectrics except for two modifications. The first of these involves a reduction in the amplitudes of the pulses between iterations to account for the attenuation due to losses, and the second involves altering the time interval between pulses to account for the slower propagation of waves due to losses.

These modifications are derived from the attenuation and phase constants for the individual lines on the matrix. From equation 1.3, these may be written as,

$$\alpha = \omega\sqrt{\frac{LC}{2}} \left[-1 + \sqrt{1 + \left(\frac{G}{\omega C}\right)^2}\right]^{\frac{1}{2}} \qquad (1.8)$$

$$\beta = \omega\sqrt{\frac{LC}{2}}\left[1 + \sqrt{1 + \left(\frac{G}{\omega C}\right)^2}\right]^{\frac{1}{2}} \qquad (1.9)$$

Now, impulses generated at a node in the network have to travel a distance of $\Delta\ell$ before reaching the neighbouring nodes. In travelling this distance they suffer a loss in amplitude corresponding to $(1 - e^{-\alpha\Delta\ell})$ of their value. Therefore, for a lossy dielectric, the TLM model simply requires the impulses on the individual lines to be replaced by $e^{-\alpha\Delta\ell}$ of their value each time the iteration process is repeated. Thus, for homogeneous waveguides, the output impulse response value for fields E or H in a lossy dielectric at the k-th interval of time, ${}_kI'$, are directly related to ${}_kI$ for a non-lossy dielectric by

$${}_kI' = {}_kI\,u^k \qquad (1.10)$$

where

$$u = e^{-\alpha\Delta\ell}$$

and from equation 1.8

$$\alpha\Delta\ell = \sqrt{2}\,\pi\,\frac{\Delta\ell}{\lambda}\left[-1 + \sqrt{1 + (\tan\delta)^2}\right]^{\frac{1}{2}} \qquad (1.11)$$

and $\tan\delta = G/\omega C$ is the loss factor.

Therefore, the losses can be accounted for by adjusting the amplitudes of impulses in the output function according to equation 1.10. Hence, no modification of the main iteration process in the non-lossy dielectric program is necessary and one iteration process can cover any number of different loss factors.

In taking the Fourier transform of the output-impulse function at a node, it must be noted from equation 1.9 that the phase constant, β, has increased by a factor of

$$r = \left[\frac{1 + \sqrt{1+(\tan\delta)^2}}{2}\right]^{\frac{1}{2}} \qquad (1.12)$$

from that of a non-lossy line. Hence, the impulses on the function are separated by a longer time period of $t = r\frac{\Delta\ell}{c}$. Since the function is a series of impulses, the Fourier transform integral may be replaced by a summation, and the real and imaginary parts of the output spectrum are given by

$$\begin{aligned} \text{Re}\left[F(\tfrac{\Delta\ell}{\lambda})\right] &= \sum_{k=1}^{N} {}^{k}Iu^{k} \cos\left(r\frac{2\pi k\Delta\ell}{\lambda}\right) \\ \text{Im}\left[F(\tfrac{\Delta\ell}{\lambda})\right] &= \sum_{k=1}^{N} {}^{k}Iu^{k} \sin\left(r\frac{2\pi k\Delta\ell}{\lambda}\right) \end{aligned} \qquad (1.13)$$

where $F(\frac{\Delta\ell}{\lambda})$ is the frequency response and N is the total number of time intervals for which calculation is made (i.e. the number of iterations).

1.4 NUMERICAL EXAMPLES

1.4.1 Rectangular Waveguide

Numerical calculations for the H_{mo} family of modes were carried out on a 26 x ~~6~~ 12 rectangular matrix with boundaries at x = 0·5 and x = 6·5. By making one of the boundaries (say x = 6·5) an open-circuit, a waveguide of twice the width, as shown in Fig. 1.5, was simulated. The system was excited at all points along the lines z = 1 with impulses corresponding to E_y. The impulse function of the output was taken from the point (x = 6, z = 6) which is 20·5 mesh points away from a discontinuity to an open-circuit at z = 26·5.

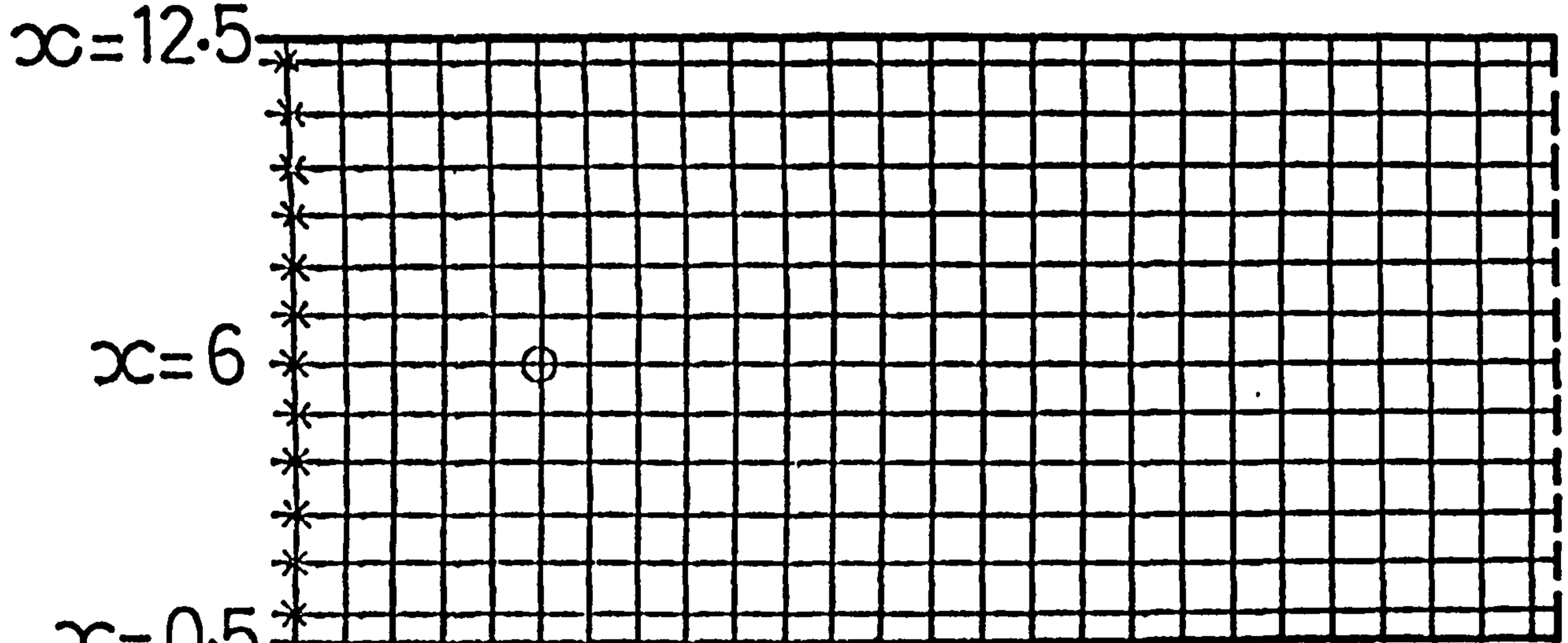

FIG. 1.5 Waveguide model

—— short circuit boundary
– – open circuit boundary
× source point
o output point

A comparison between numerical and theoretical results for normalised values of the wave impedance $Z = E_y/H_x$ for frequencies below and above the first cut-off ($\Delta\ell/\lambda = 0{\cdot}04167/\sqrt{2}$) are shown in Table 1.1, for 750 iterations of the matrix. Results are quoted for a waveguide filled with a dielectric of relative permittivity $\varepsilon_r = 2{\cdot}0$. The effect of the dielectric losses are most easily seen in the results for the argument of the impedance. In loss-free open-circuit waveguides the impedance, in theory, is wholly imaginary and the numerical results in this case are approximately $\pm\pi/2$. In lossy waveguide there is always a real component in the impedance.

In impedance calculations of this type, errors occur in the numerical method for two reasons, both of which arise because the impulse function must be terminated prematurely. The first is associated with the mathematical effect of taking the Fourier transform of a truncated function. The true impulse functions for the E and H fields are multiplied by an aperture in the time domain and this means that the true frequency spectra are convolved by a sinx/x type curve. Thus, if N iterations of the matrix are performed, the magnitude of the convolution function is given in reference 1.2 as,

$$N\,\frac{\Delta\ell}{c}\;\;\frac{\sin(\pi N\Delta\ell/\lambda)}{\pi N\Delta\ell/\lambda}$$

The convolution process causes a smoothing of sharp corners in the spectra and results that are not changing rapidly with frequency are little affected, but where rapid changes occur, errors also occur. Where necessary, this type of error can be taken into account as shown in the resonance problems of reference 1.2

TABLE 1.1

Waveguide with dielectric losses ($\varepsilon_r = 2(1+j0.05)$)

$\Delta\ell/\lambda$	|Z|			ARG(Z)		
	Numerical Method	Theoretical	Error %	Numerical Method	Theoretical	Error %
0.005	0.1221	0.1218	0.24	1.5730	1.5701	0.18
0.009	0.2266	0.2269	0.13	1.5610	1.5682	0.46
0.013	0.3471	0.3477	0.17	1.5514	1.5647	0.85
0.017	0.4988	0.4996	0.16	1.5411	1.5583	1.11
0.021	0.7183	0.7188	0.06	1.5254	1.5448	1.27
0.025	1.1386	1.1364	0.19	1.4837	1.5045	1.40
0.029	3.1460	3.1047	1.33	0.8251	0.8750	6.04
0.033	2.9114	2.8760	1.21	0.8920	0.9231	3.48
0.037	0.8773	0.8815	0.47	-0.9774	-0.9508	2.72
0.041	0.5950	0.5948	0.03	1.0004	1.0260	2.55
0.045	3.3809	3.3749	0.17	0.2931	0.3213	9.62
0.049	0.7838	0.7846	0.10	-1.0197	-0.9963	2.29
0.053	0.2901	0.2833	2.30	0.5384	0.5491	1.98

The second cause of error is more practical and results from the mismatch in the waveguide to the left of the source and solution points in Fig. 1.5. A boundary must be placed behind the source and ideally this would absorb all the reflected energy. However, since the wave impedance in waveguide changes with frequency, there is no simple matrix reflection coefficient which will present a perfect match at all frequencies. Some work has been done in an effort to gradually absorb power, thus simulating a practical wideband waveguide matched load and while this met with some success, it is far simpler to use a matrix reflection coefficient of zero. This means that there is a sudden transition to an impedance of $\sqrt{2}$ times the intrinsic medium within the guide (see reference 1.1). In the numerical method, therefore, the reflected impulsive wave from the termination at z = 26•5 is also partially reflected at z = 0•5 (even though the matrix reflection coefficient is zero at this point). Strictly, the steady-state solution is reached after an infinite amount of time when all the reflections have died away. By taking less than an infinite amount of time, the result only tends to the steady-state solution.

Another form of error occurs in the TLM method. This is the velocity error[1.2], which is well defined and for the values of $\Delta\ell/\lambda$ quoted here is negligible.

1.4.2 Two-Dimensional Rectangular Cavities

The method was also used to calculate the power decay due to losses in the dielectric medium ($\varepsilon_r = 2{\cdot}0$) of a two-dimensional rectangular cavity, with a loss factor of 0•01. A comparison between the numerical and theoretical results for the

TABLE 1.2

Cavity with dielectric losses

($\varepsilon_r = 2(1+j0.01)$, $\Delta\ell = 0.3$ cm)

Number of Mesh points in the x direction	Number of Mesh points in the z direction	Time taken for the power in the cavity to fall to 1/e of its original value		
		Numerical Method ns	Theoretical ns	Error %
5	5	1.594	1.591	0.18
5	10	2.016	2.013	0.14
5	20	2.187	2.183	0.18
5	30	2.223	2.220	0.13
10	30	4.277	4.270	0.16
20	30	7.497	7.491	0.08

time taken for the power in the cavity to fall to 1/e of its original value is shown in Table 1.2. These results provide a direct measure for the Q of the cavity. They also serve to illustrate a calculation technique which is particularly suitable for the TLM method because the method takes place in the time domain and is transient in nature. Decay time calculations are very simple and quick on the computer because the somewhat tedious multiply-and-add routine which converts the time-domain results into the frequency domain are avoided. Also there are no errors due to truncation in the time domain. Thus, by operating in the time domain one of the main sources of error in the TLM method is eliminated and the numerical results are very accurate as can be seen from Table 1.2.

1.5 DISCUSSION

A simple and intuitive modification to the output impulse function of the TLM method has allowed losses in dielectrics to be accounted for. Strictly, however, the method is only formulated for homogeneous problems. The reason for this may be seen from equations 1.8 and 1.9, which give the real and imaginary parts of the complex propagation constant, γ, for waves on the individual lines in the matrix. Difficulty arises, because the intrinsic impedance of the lossy medium then contains an imaginary component. This means that impulses incident on the boundary between two media are not reflected as ideal impulses but have their shape distorted and cannot be handled by the TLM method. However, it is possible to ignore the imaginary component assuming low losses in order to deal with mixed lossy dielectric cases. In fact, tests on inhomogeneous structures with small

dielectric losses have yielded results very close to those obtained by an alternative method explained in the next chapter. In particular, for comparison, the structure in example of section 2.4.3 was tried using the loss method in this chapter, and results showed a maximum error of less than 1% in worst cases. Therefore, it can be concluded that for most inhomogeneous practical engineering problems (for which losses will be generally small), this method provides useful results.

REFERENCES

1.1 JOHNS, P.B. and BEURLE, R.L. "Numerical solution of two-dimensional scattering problems using a transmission-line matrix", Proc. I.E.E., 118, pp 1203-1208, September, 1971.

1.2 JOHNS, P.B. "Application of the transmission-line matrix method to homogeneous waveguides of arbitrary cross-section", Proc. I.E.E., 119, pp 1086-1091, August, 1972.

1.3 JOHNS, P.B. and SLATER, G.F. "Transient analysis of waveguides with curved boundaries", Electron. Lett., 9, pp 486-487, October, 1973.

1.4 JOHNS, P.B. "A new model to describe the physics of propagation", Radio and Electron. Eng., 44, pp 657-666, December, 1974.

1.5 AKHTARZAD, S. and JOHNS, P.B. "Transmission-line matrix solution of waveguides with dielectric losses", Int. J. Num. Meth. Eng., Vol. 9, 1975.

CHAPTER 2

THE SOLUTION OF INHOMOGENEOUS

WAVEGUIDES WITH LOSSY DIELECTRICS

2.1 INTRODUCTION

Waveguides with dielectric boundaries which do not extend across either of the waveguide transverse dimensions find applications in many components. In the general case, there is no analytical solution available and a numerical approach has to be used. The transmission-line matrix (TLM) method of numerical analysis provides a two dimensional time domain, transient solution of such problems. There are a number of other numerical techniques for the solution of inhomogeneous waveguide structures. Most of these techniques are listed in a recent paper by Fook Loy Ng[2.1].

In this chapter a further modification to the TLM method to include solutions for waveguides with inhomogeneous lossy dielectrics is described. The modification used here forms the basis for the dielectric losses considered in the three-dimensinal analysis of the TLM method (see chapter 5). The variation-iteration procedure[2.2] is one of the very few other general numerical methods which have been applied to structures containing inhomogeneous lossy dielectrics. But, unlike the TLM method, it does not include the wall losses.

2.2 BRIEF DESCRIPTION OF THE LOSS-FREE TLM NUMERICAL METHOD FOR INHOMOGENEOUS WAVEGUIDES

Fig. 2.1 shows the transmission-line network model for solving inhomogeneous wave problems (note that in the Figures single lines will be used to represent a pair of wires). The normal rectangular mesh of transmission-lines[2.3,2.4] of unity characteristic admittance has additional open-circuit stubs

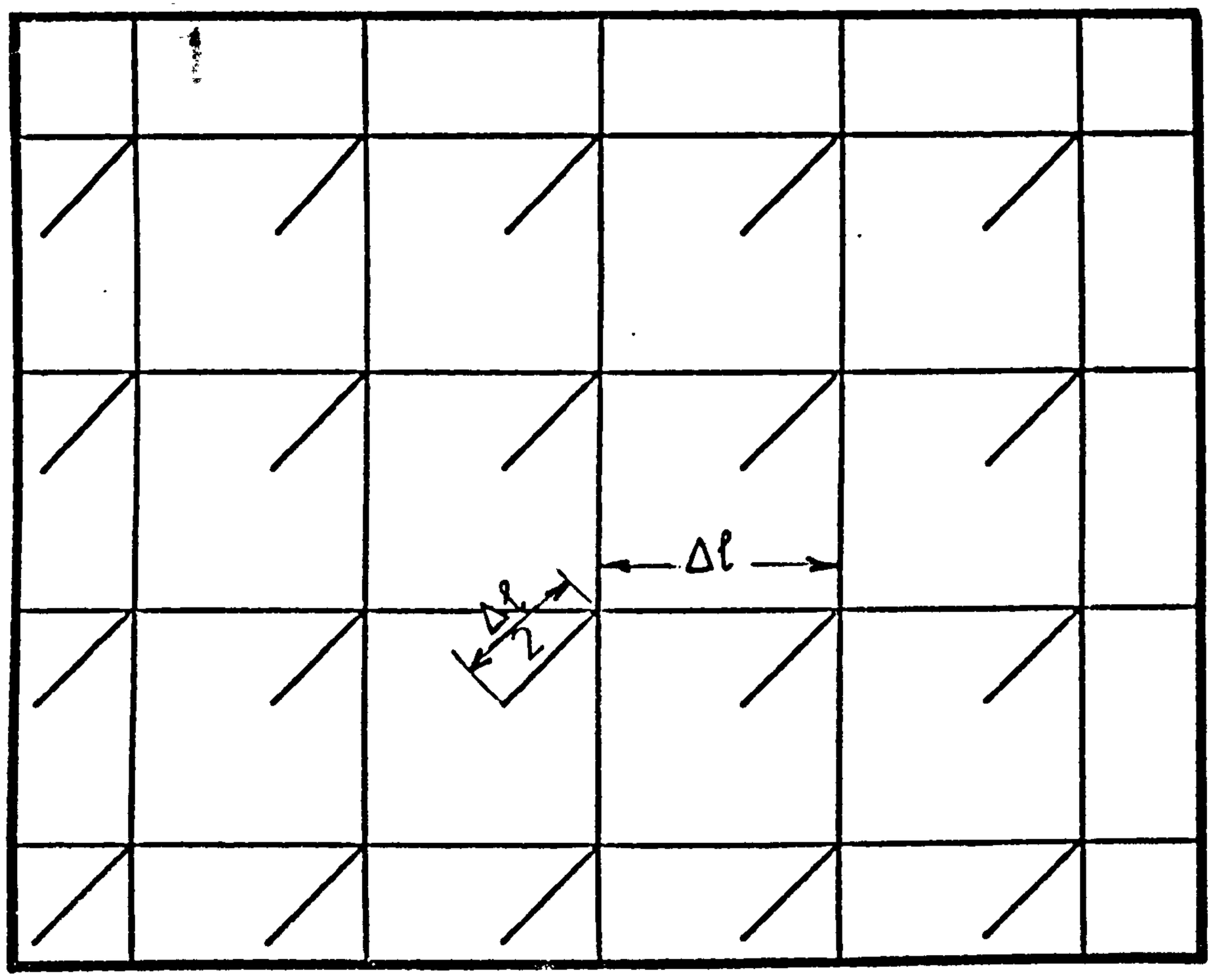

FIG. 2.1 General network configuration

of length $\frac{\Delta\ell}{2}$ and characteristic admittance Y_o, connected in shunt at each node (see Fig. 2.2(a) and (b)). The value required for Y_o for these stubs (referred to as permittivity-stubs from here onwards) determines the permittivity of the space being simulated. Waves may propagate in the two component directions on such a model and thus be propagated at any angle. A direct analogy between the model and the space it represents, will result in relationships between voltages and currents on the component lines of the model and electric and magnetic fields in the space[2.4].

The model may be excited by launching a voltage-impulse delta function on the lines joining a particular node to neighbouring nodes and also on its respective stub. The impulse function will travel along the lines and on arrival at a node it will spread out along the five lines forming the discontinuity.

These new impulses, in turn, will be transmitted and reflected on their arrival at neighbouring nodes and hence will form yet other impulses. The process will go on with time progressing and impulses will fill the model after enough repetition of the process. Arrival of each impulse at a node at a certain instant of time is ensured by the equi-length of line, $\Delta\ell$, that each impulse will have to travel between two neighbouring nodes. By the careful choice of length $\frac{\Delta\ell}{2}$ for the stubs and also placing the reflecting bounds half-way between the nodes, the synchronization mechanism of iteration process is followed by both former and latter.

The network described is of slow wave nature, i.e. at low frequencies waves propagating in the component directions and stubs are slowed down to $1/\sqrt{2(1 + Y_o/4)}$ of the free space velocity (see

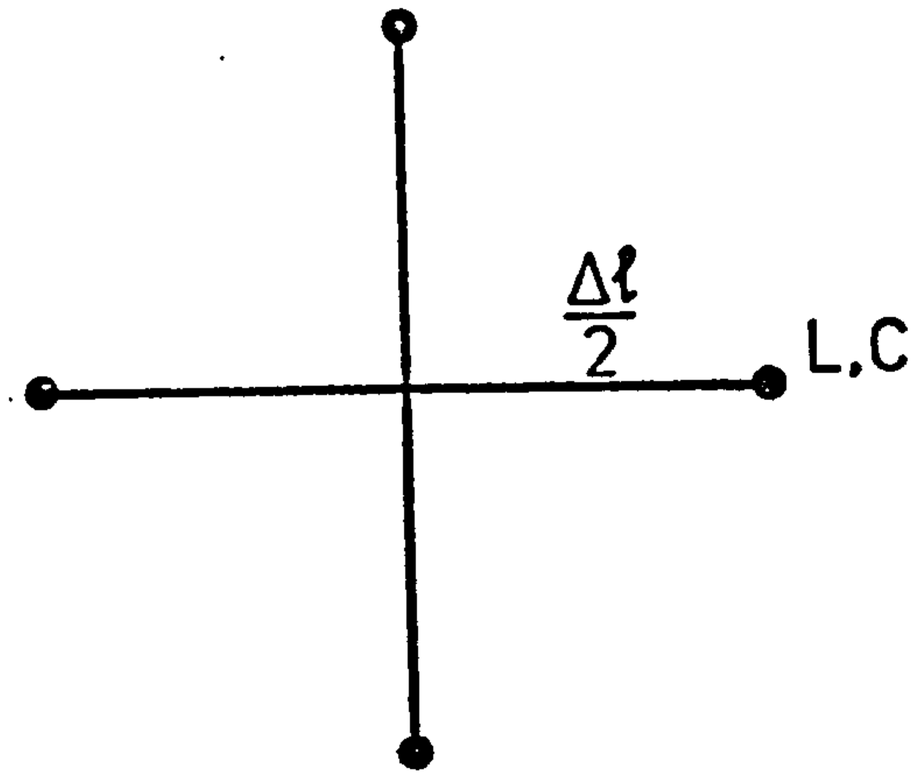

(a)

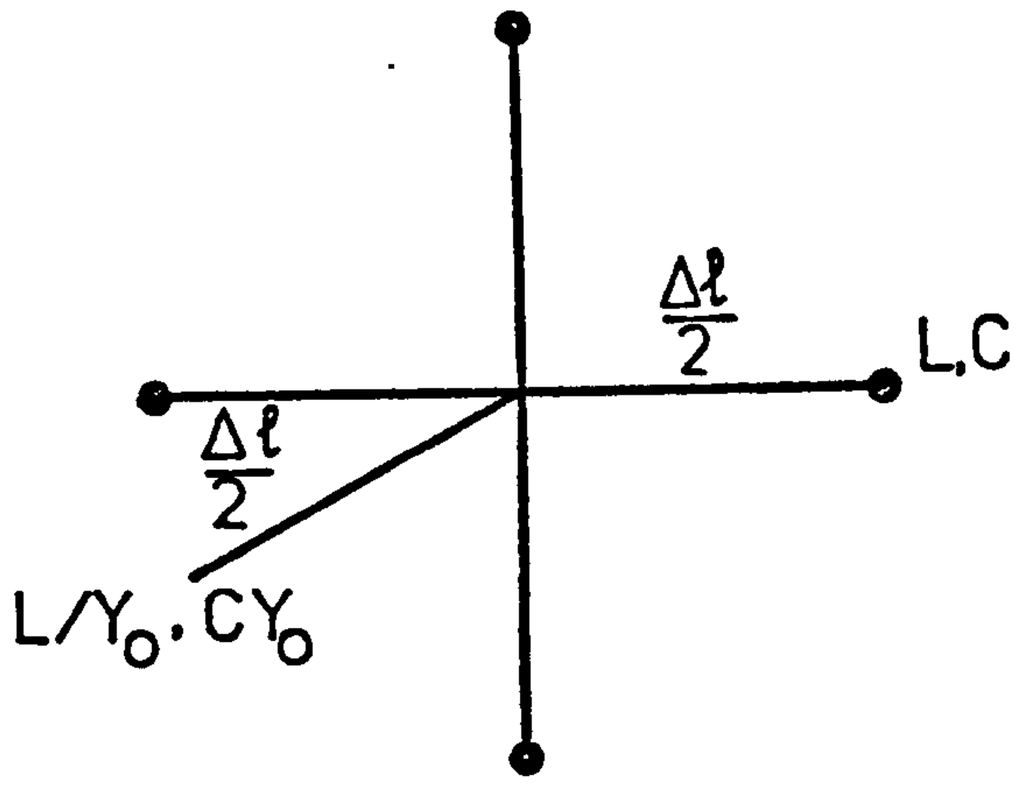

(b)

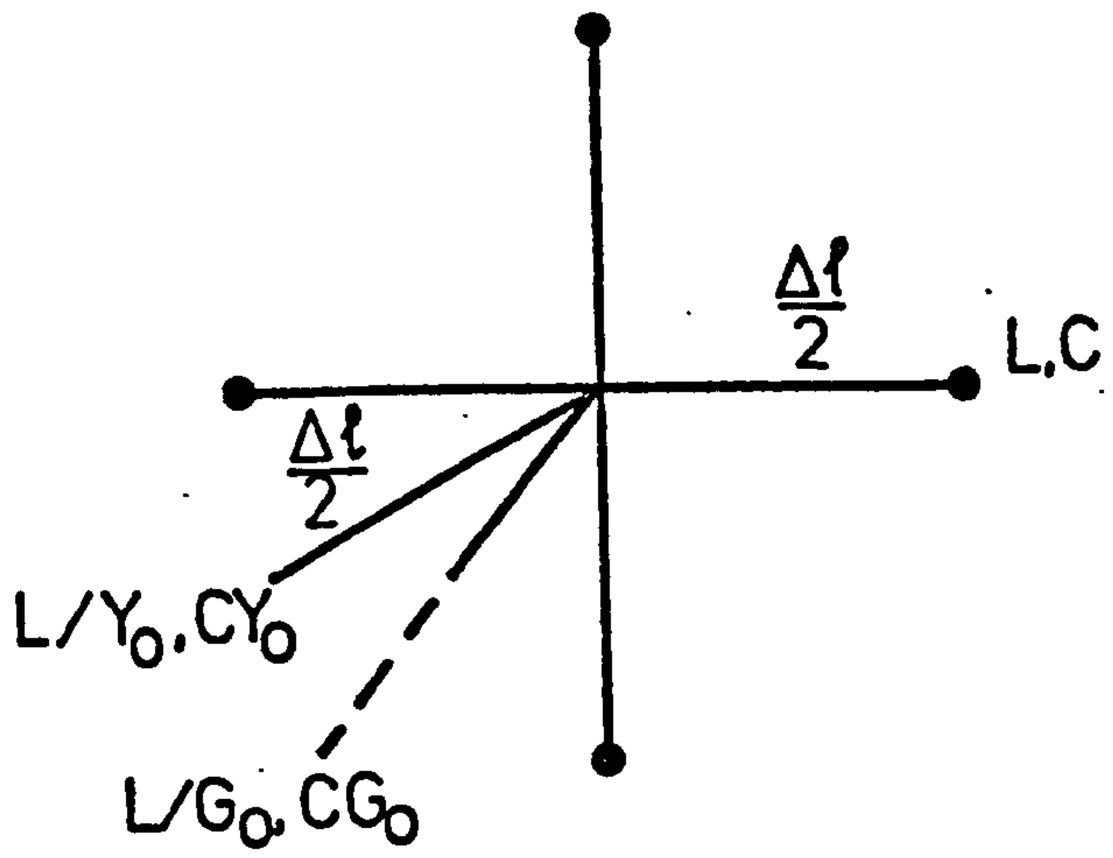

(c)

FIG. 2.2 A node of TLM model, (a) without stubs, (b) with permittivity-stub, (c) with permittivity- and loss-stubs

reference 2.5), where Y_o is the variable characteristic admittance of the stubs relative to the unity characteristic admittance assumed for the main matrix of transmission lines.

If ${}_kV_n(z,x)$ is unit voltage-impulse reflected from the node at (z,x) into the n^{th} co-ordinate direction at time $k\frac{\Delta\ell}{c}$, the iteration process at the node (z,x) is summarised by,

$$\begin{pmatrix} V_1(z,x) \\ V_2(z,x) \\ V_3(z,x) \\ V_4(z,x) \\ V_5(z,x) \end{pmatrix}_{k+1} = \mathbf{S} \cdot \begin{pmatrix} V_3(z,x-1) \\ V_4(z-1,x) \\ V_1(z,x+1) \\ V_2(z+1,x) \\ V_5(z,x) \end{pmatrix}_{k} \qquad (2.1)$$

where scattering matrix

$$\mathbf{S} = \frac{2}{Y} \begin{pmatrix} 1 & 1 & 1 & 1 & Y_o \\ 1 & 1 & 1 & 1 & Y_o \\ 1 & 1 & 1 & 1 & Y_o \\ 1 & 1 & 1 & 1 & Y_o \\ 1 & 1 & 1 & 1 & Y_o \end{pmatrix} - \mathbf{I} \qquad (2.2)$$

and $Y = 4 + Y_o$ (2.3)

and $\mathbf{I}$ is the unit matrix, c is the velocity of light. The co-ordinate directions 1, 2, 3 and 4 correspond to -x, -z, +x and +z respectively and 5 refers to the stub.

2.3 DEVELOPMENT OF THE NUMERICAL METHOD FOR THE LOSSY DIELECTRICS

In the new matrix intended for lossy dielectrics, an additional length of line of variable characteristic admittance, G_o, relative to the unity characteristic admittance assumed for the main lines of transmission-line matrix, is connected in parallel at each node. The new stub (loss-stub) is of infinite length or otherwise terminated in its own characteristic impedance so that the incident voltage pulses on this stub are not reflected back on to the node. Hence, at each node, incorporating both permittivity and loss-stubs, there are five incident voltage pulses. Therefore, in the computer program analysis of the TLM method we still have to store the current values of voltage pulses on the four main lines (V_1, V_2, V_3 and V_4) and that of the dielectric-stub (V_5). Pulse analysis for each node including the loss-stub gives the new version of equation 2.1 as before with

$$Y = 4 + Y_o + G_o \qquad (2.4)$$

At low frequencies the effect of the loss-stub is to add to each matrix node a lumped shunt conductance of $\frac{G_o}{Z_o \Delta \ell}$ per unit length, where Z_o is the characteristic impedance of free space. The matrix as a whole represents a lossy space of conductivity σ . Hence, G_o in terms of σ of space is given by

$$G_o = \sigma . Z_o . \Delta \ell \qquad (2.5)$$

Thus the losses on the matrix are now made variable simply by altering the value of the constant G_o.

As the frequency increases, the fact that the loss-stub is a distributed conductance and not lumped becomes important. As before (section 1.2) an exact analysis is needed to establish

the range of frequencies over which the equation 5 is reasonably accurate. Again, the procedure is straight forward and is explained in reference 2.5. The following transmission equations connect the input voltages and currents (V_i and I_i) with the output voltages and currents (V_{i+1} and I_{i+1}) of one cell of the periodic structure involved (Fig. 2.2(c)). For propagation in the direction of one of the matrix co-ordinates the equation is

$$\begin{pmatrix} V_i \\ I_i \end{pmatrix} = \begin{pmatrix} \cos\theta & j\sin\theta \\ j\sin\theta & \cos\theta \end{pmatrix} \cdot \begin{pmatrix} 1 & 0 \\ G_o + j(2+Y_o)\tan\theta & 1 \end{pmatrix} \cdot \begin{pmatrix} \cos\theta & j\sin\theta \\ j\sin\theta & \cos\theta \end{pmatrix} \cdot \begin{pmatrix} V_{i+1} \\ I_{i+1} \end{pmatrix} \qquad (2.6)$$

$$\text{where} \quad \theta = \beta \frac{\Delta\ell}{2} = \pi \frac{\Delta\ell}{\lambda} . \qquad (2.7)$$

If the waves on the periodic structure have a propagation constant of $\gamma_n = \alpha_n + \beta_n$,then we also have

$$\begin{pmatrix} V_i \\ I_i \end{pmatrix} = \begin{pmatrix} e^{\gamma_n \Delta\ell} & 0 \\ 0 & e^{\gamma_n \Delta\ell} \end{pmatrix} \cdot \begin{pmatrix} V_{i+1} \\ I_{i+1} \end{pmatrix} \qquad (2.8)$$

Solutions of equations 2.6 and 2.8, assuming $\alpha_n \Delta\ell \ll 1$, gives

$$\left.\begin{aligned} \frac{\beta}{\beta_n} &= \frac{\theta}{\sin^{-1}\left[\sqrt{2(1+Y_o/4)}\,\sin\theta\right]} \\ \frac{\alpha}{\alpha_n} &= \frac{\left[1-2(1+Y_o/4)\sin^2\theta\right]^{\frac{1}{2}}}{\sqrt{2(1+Y_o/4)}\cos\theta} \end{aligned}\right\} \qquad (2.9)$$

where

$$\alpha = \frac{G_o}{8\Delta\ell(1+Y_o/4)} \qquad (2.10)$$

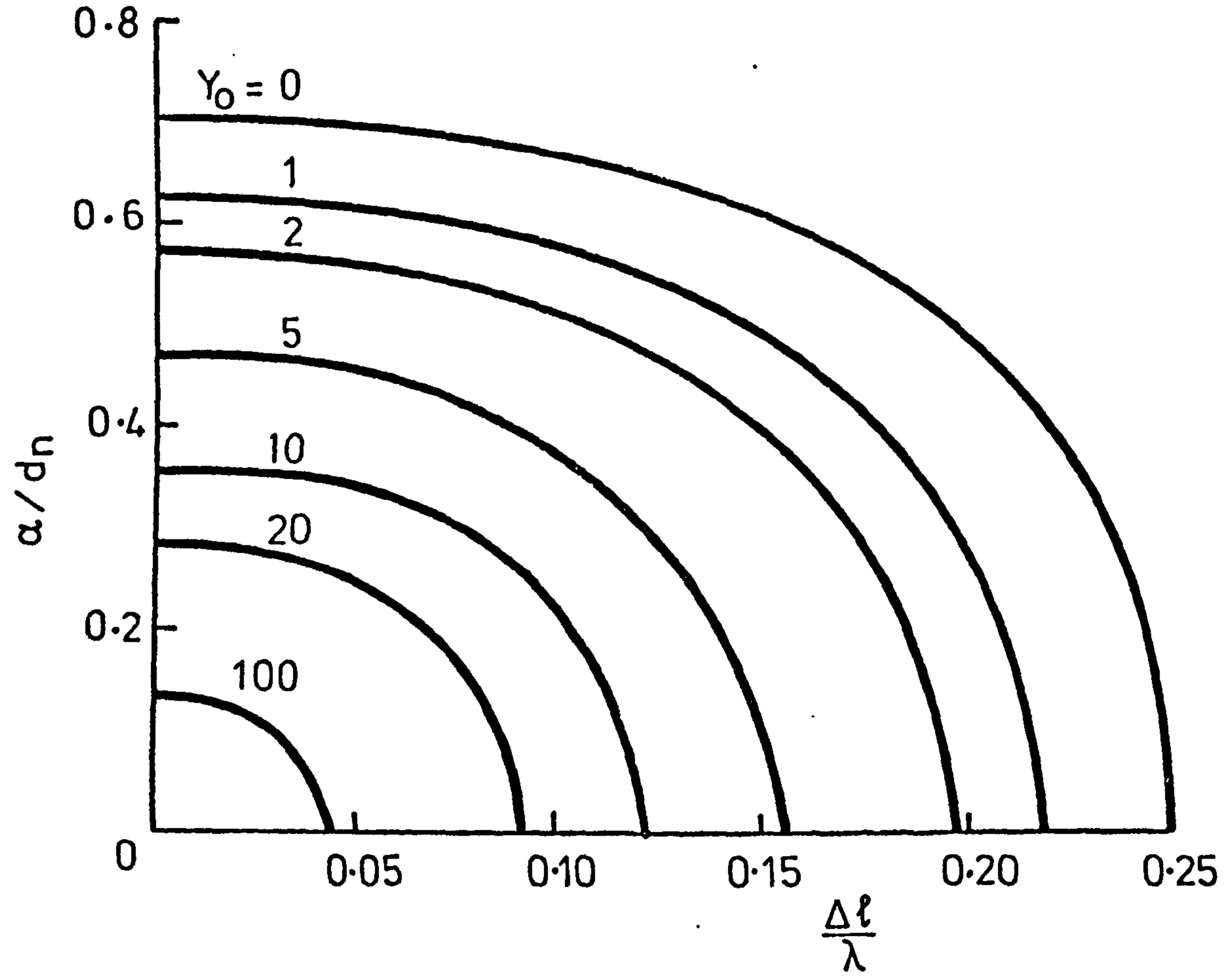

FIG. 2.3 Attenuation characteristic for transverse waves on a stub loaded transmission-line matrix

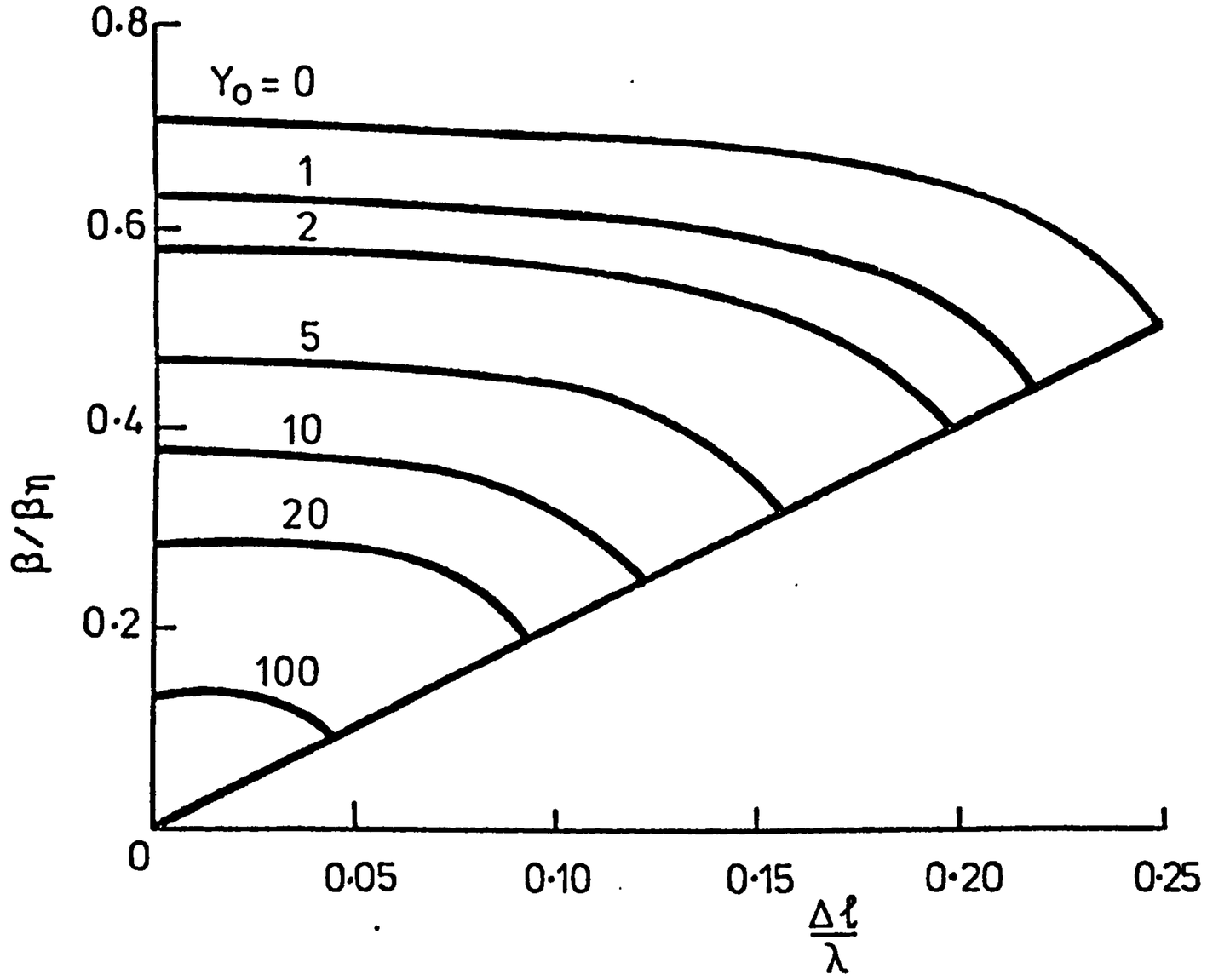

FIG. 2.4 Phase characteristic for transverse waves on a stub loaded transmission-line

Results of equation 2.9 are presented graphically in Fig. 2.3 and Fig. 2.4. It can be seen that for frequencies well below the network cut-off frequency,

$$\left(\frac{\Delta \ell}{\lambda}\right)_{\text{cut off}} = \frac{1}{\pi} \sin^{-1}\left[\frac{1}{\sqrt{2(1+Y_o/4)}}\right] \qquad (2.11)$$

the propagation constants α_n and β_n of the network are fairly constant, so that equation 2.9 reduces to

$$\gamma_n = \sqrt{2(1+Y_o/4)}\,\gamma \qquad (2.12)$$

where $\gamma = \alpha + \beta$. β and α are given by equations 2.7 and 2.10 respectively.

2.4 NUMERICAL EXAMPLES

2.4.1 Lossy Homogeneously Filled Waveguide

The first problem checked on a matrix of transmission-lines simulated on a digital computer corresponded to a two-dimensional magnetic type field, H_{mo} family of modes. Fig. 2.5 shows the geometry of a guide 6 cm wide and 13 cm long filled with a dielectric of relative permittivity $\epsilon_r = 4.9$ and conductivity $\sigma = 0.05$ S/m terminated in an open-circuit discontinuity. This geometry was simulated on a matrix of 12 nodes across and 26 nodes along. The matrix was excited at all points along the line $z = 1$ with impulses corresponding to E_y. The impulse function of the output was taken from the point $(x = 6, z = 6)$ as shown in Fig. 2.5.

A comparison between numerical and theoretical results for normalised values of the wave impedance $Z = \frac{E_y}{H_x}$ for frequencies below and above the first cut-off are shown in Table 2.1 for 750 iterations of matrix network. As it can be seen from the table,

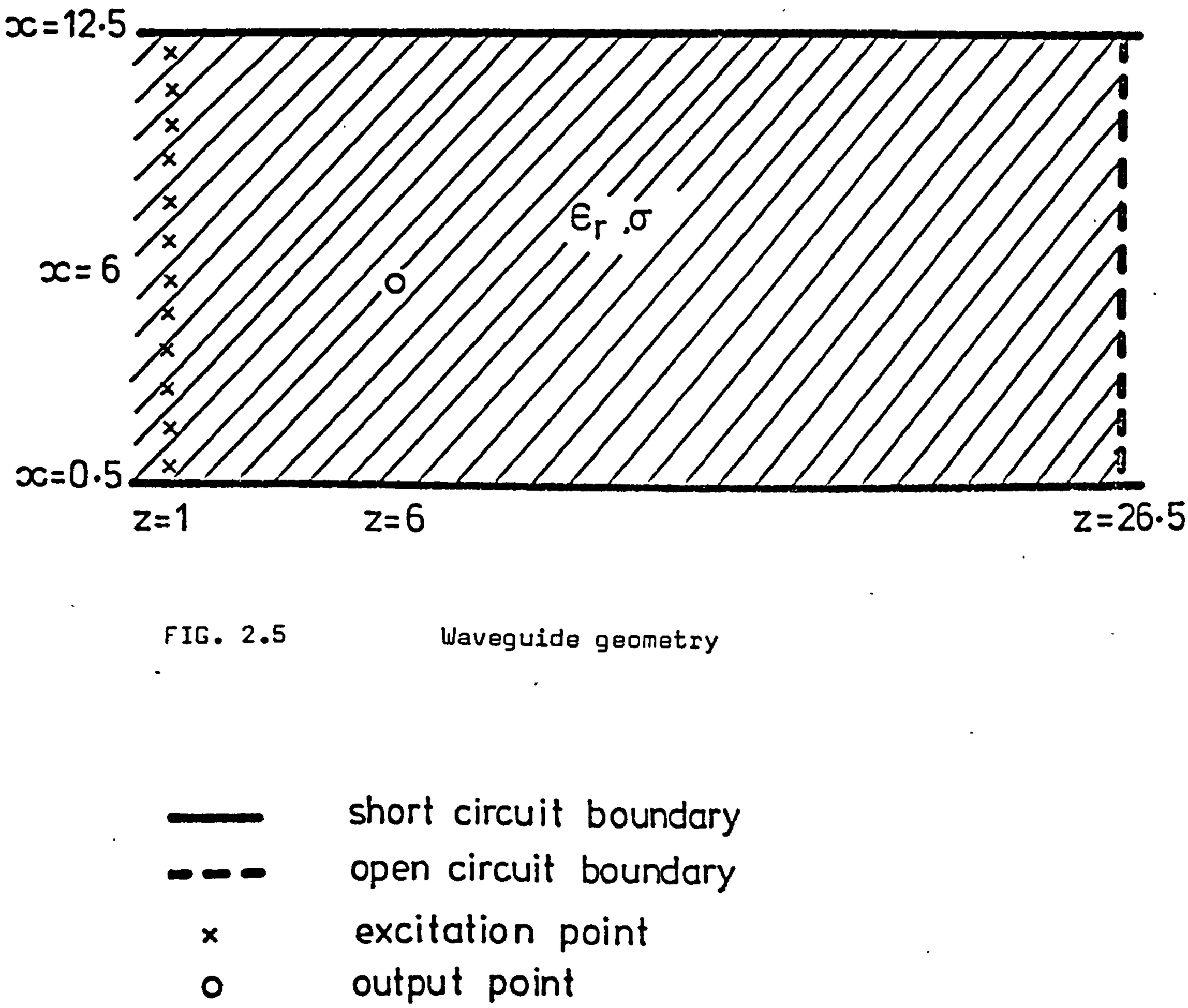

FIG. 2.5 Waveguide geometry

——— short circuit boundary

– – – open circuit boundary

× excitation point

o output point

TABLE 2.1

Waveguide with dielectric losses

($\varepsilon_r = 4.9, \sigma = 0.05$ S/m)

$\Delta\ell/\lambda$	$\lvert Z \rvert$			ARG(Z)		
	TLM	Theoretical	Error %	TLM	Theoretical	Error %
0.003	0.0725	0.0729	0.55	1.5573	1.5575	0.01
0.006	0.1511	0.1518	0.46	1.5414	1.5420	0.04
0.009	0.2446	0.2453	0.28	1.5195	1.5205	0.07
0.012	0.3706	0.3712	0.16	1.4824	1.4840	0.11
0.015	0.5803	0.5792	0.19	1.3945	1.3977	0.23
0.018	1.0000	0.9979	0.21	0.9930	1.0065	1.34
0.021	1.1735	1.1676	0.51	0.4991	0.5121	2.53
0.024	0.5032	0.5093	1.19	-0.2046	-0.2141	3.21
0.027	0.6766	0.6609	2.37	0.6780	0.6853	1.06
0.030	0.8733	0.8921	2.11	-0.4185	-0.4185	4.31

the agreement between numerical and theoretical results is good both below and above the first cut-off which occurs at $\frac{\Delta \ell}{\lambda} = 0.0188$.

2.4.2 Two-Dimensional Rectangular Cavity

Next the method was used to check the power decay due to losses in the dielectric medium ($\varepsilon_r = 6.0$) of a two-dimensional rectangular cavity with a loss factor of 0.2. This problem was set up on a number of variable sizes of matrix networks. H_{101} mode was isolated by choosing the position and relative magnitude of the excitation points to correspond approximately to the field values of the mode.

The analysis was carried out at the resonant frequency of H_{101} mode. Table 2.2 shows the results of decay time for various sizes of cross section of cavity (a x b). It is noticed that the accuracy of the numerical results is independent of the size of the cavity and in all cases considered the error is less than 1%.

2.4.3 A General Inhomogeneous Bifurcated Waveguide

Finally, to demonstrate the flexibility and easiness with which the losses in general can be introduced and be taken care of by the described procedures, configuration of Fig. 2.6(a) is considered. The guide with its walls 4 cm apart is assumed to possess losses in the walls ($\sigma_\omega = 0.278 \times 10^3$ S/m), bifurcation ($\sigma_b = 1.111 \times 10^3$ S/m) and also in the dielectric slab ($\tan\delta = 0.05$). ε_n is equivalent to the relative permittivity of the basic matrix network and is equal to 2. Fig. 2.6(a) and Fig. 2.6(b) show frequency runs for the wave impedance in magnitude and phase looking into the dielectric slab.

TABLE 2.2

Cavity with dielectric losses

(ε_r = 6.0, $\tan\delta$ = 0.02, $\Delta\ell$ = 0.2 cm)

$\frac{a}{\Delta\ell}$	$\frac{b}{\Delta\ell}$	Time taken for the power in the cavity to fall to 1/e of its original value		
		TLM ns	Theoretical ns	Error %
1	3	0.246	0.246	0.0
6	9	0.305	1.297	0.62
6	15	1.457	1.447	0.69
9	15	2.014	2.005	0.45
15	20	3.128	3.118	0.32
20	30	4.337	4.325	0.28

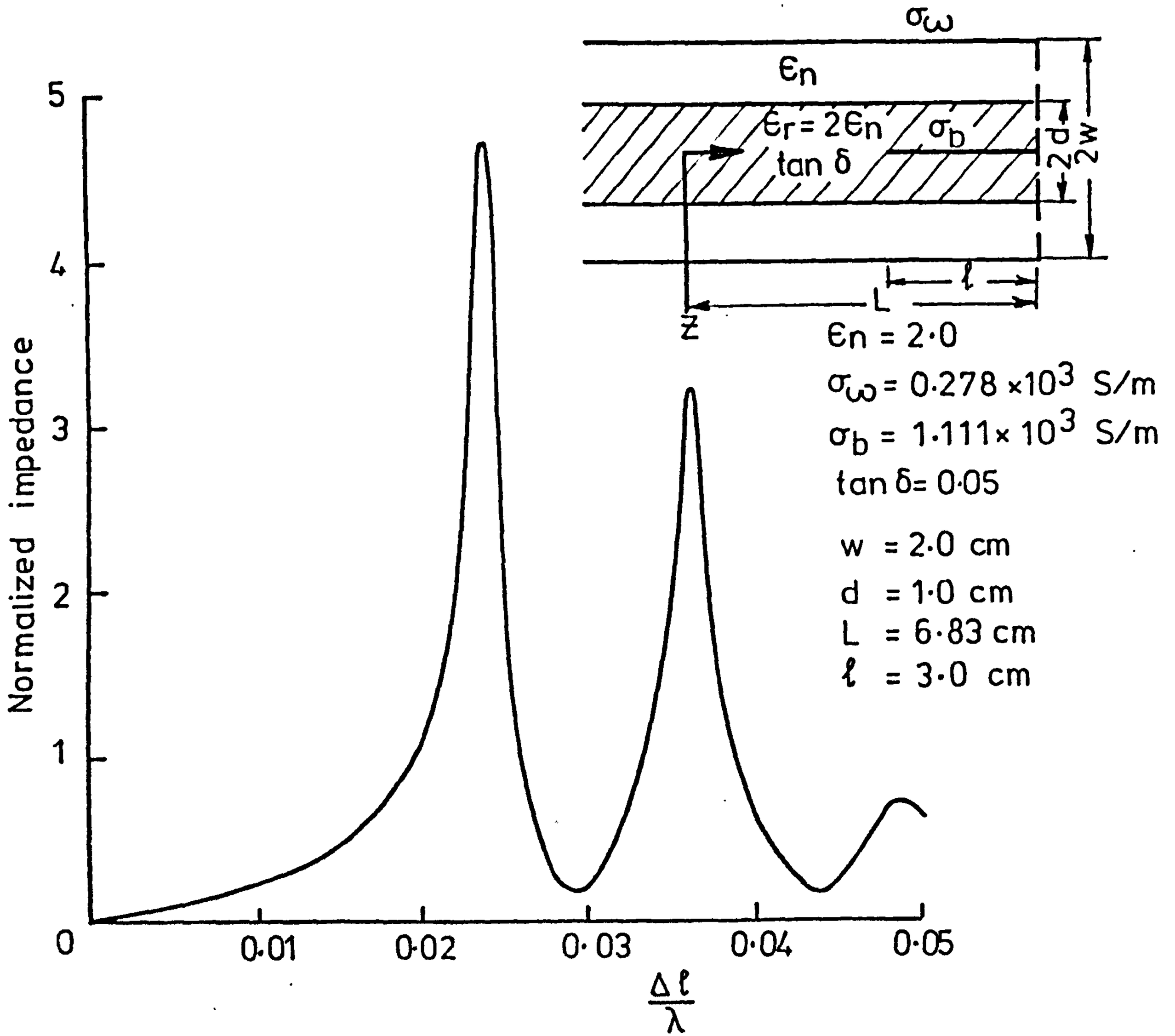

FIG. 2.6(a) Magnitude of impedance in an inhomogeneous lossy waveguide

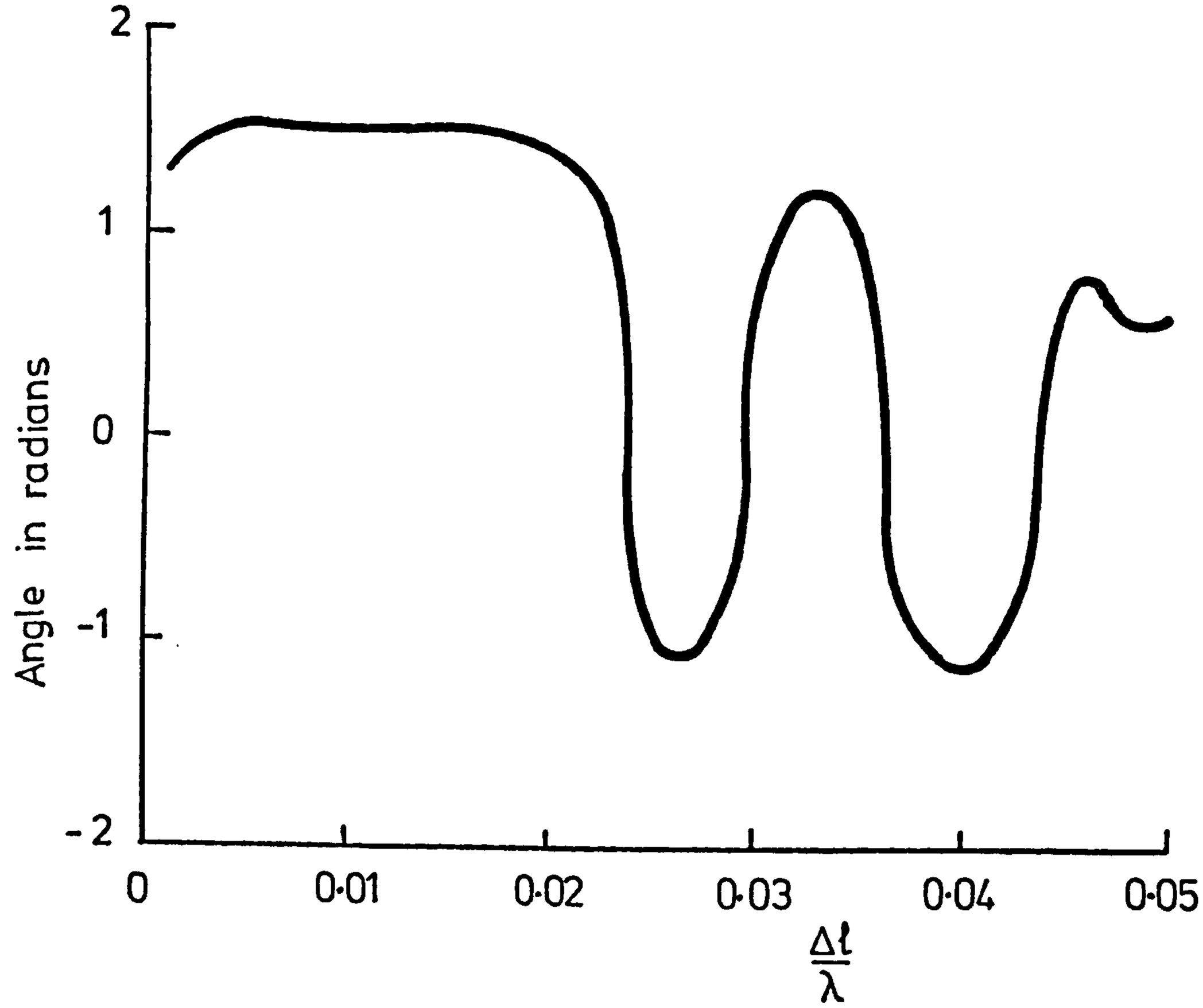

FIG. 2.6(b) Angle of impedance in the waveguide

2.5 Discussion

The variation-iteration procedure is one of the very few other general numerical methods which have been applied to structures containing lossy dielectrics[2.2]. The technique does not include wall losses and is a steady-state procedure requiring the solution of a complex eigenvalue matrix equation. Results are given in terms of dispersion curves assuming a continuous waveguide in the third space dimension. This type of formulation is impossible in the TLM method as described here, because it operates only in two space dimensions. A different model is needed for problems involving three space dimensions as described in Chapter 5. TLM results for the cut-off frequency for such guides with losses give a damped resonant curve corresponding to the indefinite cut-off conditions shown by La Loux et al[2.2].

Because the TLM method operates in the time domain, it does not require the laborious solution of simultaneous equations and this tends to make programming easier (see Chapter 4) than in steady-state procedures. Also, for a given mesh coarseness, the accuracy of the TLM method is often better than steady-state results as discussed in references 2.4, 2.5 and 2.6.

REFERENCES

2.1 FOOK, L.N. "Tabulation of methods for the numerical solution of the hollow waveguide problem", I.E.E.E. Trans., MTT-22, pp 322-329, March, 1974.

2.2 LALOUX, A.A., GOVAERTS, R.J.M. and VANDER VOST, A.S., "Application of a variation-iteration method to waveguides with inhomogeneous lossy loads", I.E.E.E. Trans., MTT-22, pp 229, 236, March, 1974.

2.3 JOHNS, P.B. and BEURLE, R.L. "Numerical solution of two-dimensional scattering problems using a transmission-line matrix", Proc. I.E.E., 118, pp1203-1208, September, 1971.

2.4 JOHNS, P.B. "Application of the transmission-line matrix method to homogeneous waveguides of arbitrary cross-section", Proc. I.E.E., 119, pp 1086-1091, August, 1972.

2.5 JOHNS, P.B. "The solution of inhomogeneous waveguide problems using a transmission-line matrix", I.E.E.E. Trans., MTT-22, pp 210-215, March, 1974.

2.6 JOHNS, P.B. and SLATER, G.F. "Transient analysis of waveguides with curved boundaries", Electron. Lett., 9, pp 486-487, October, 1973.

2.7 AKHTARZAD, S. and JOHNS, P.B. "Generalized elements for the TLM method of numerical analysis", Submitted to Proc. I.E.E., (March, 1975).

CHAPTER 3

THE SOLUTION OF WAVEGUIDES WITH LOSSY WALLS

3.1 INTRODUCTION

In a perfect conductor, the conductivity is assumed to be infinite and any electromagnetic radiation is perfectly reflected from the surface of a perfect conductor. In this case, for the mode representations in the TLM method, loss-free boundary walls are represented by short- and open-circuits on the matrix[3.1]. However, in many practical microwave engineering problems, the finite conductivity of a conductor cannot be neglected and must be taken into account. Hence, the TLM method is further modified to take account of boundary losses as well as dielectric losses described in previous chapters.

In the TLM method, as described in the following section, boundary losses may be simulated by introducing suitable reflection coefficients where component lines meet the boundaries.

3.2 CONDUCTING BOUNDARIES OF FINITE CONDUCTIVITY

Short-circuit walls of finite conductivity, such as lossy waveguide walls, bifurcation or diaphragm, can be accounted for by replacing the perfect short-circuit boundary with an impedance wall whose surface impedance[3.2] is given by

$$Z_c = \sqrt{\frac{\mu\omega}{2\sigma}}(1 + j) \qquad (3.1)$$

where μ and σ are the permeability and conductivity values for the specific conducting boundary.

The conducting boundaries on the matrix are perpendicular to the transmission-lines which intersect them, and the voltage reflection coefficient for impulses on these lines is given by

$$\rho = \frac{Z_c - Z_o}{Z_c + Z_o} \qquad (3.2)$$

Z_o is the characteristic impedance of waves on the transmission-lines in the matrix, i.e.

$$Z_o = \sqrt{\frac{\mu_o}{\varepsilon_o}} \qquad (3.3)$$

where μ_o and ε_o are permeability and permittivity of free space.

For small losses, Z_c is small compared to Z_o and the imaginary part of ρ can be neglected. Thus, if $\mu = \mu_o$, ρ is given approximately by,

$$\rho = -1 + 2\sqrt{\frac{\varepsilon_o \omega}{2\sigma}} \qquad (3.4)$$

Since ρ depends on the frequency ω, the iterations of the numerical method must be repeated for each value of $\Delta\ell/\lambda$ used.

For other lossy boundaries such as a resistive strip of zero thickness inside a waveguide parallel to the electric field, procedure is as before with Z_c replaced by the resistance R of the resistive strip. Hence, the reflection coefficient of impulses reaching the strip is given as

$$\rho = 1 - \frac{2}{(R/Z_o) + 1} \qquad (3.5)$$

In this case, ρ as can be seen from equation 3.5, is not dependent on the frequency ω, and hence the iterations of the numerical method will not have to be repeated for each value of $\Delta\ell/\lambda$ used.

3.3 NUMERICAL EXAMPLES

3.3.1 Rectangular Waveguides

(a) Waveguide with lossy walls - Numerical calculations for the H_{mo} family of modes were carried out on a 61 x 8 rectangular matrix with boundaries at x = 0·5 and x = 8·5 as shown in Fig. 3.1. By making one of the boundaries (say x = 8·5) an open circuit, a waveguide of twice the width is simulated. The system was excited

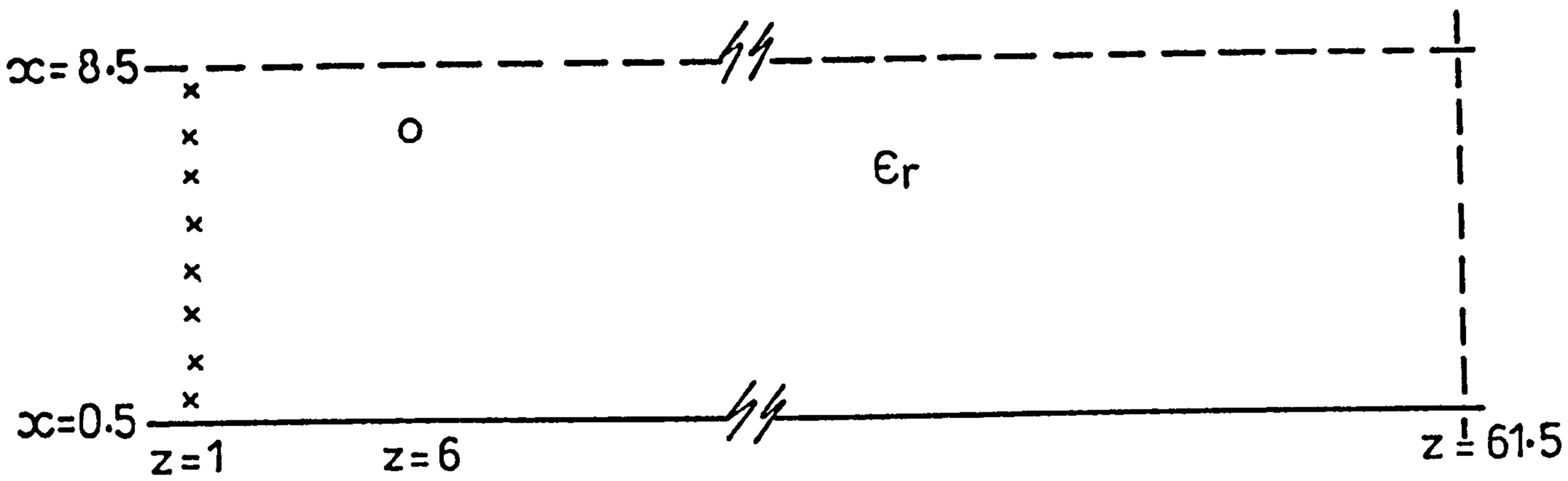

FIG. 3.1 The waveguide geometry

——— short circuit boundary

– – – open circuit boundary

× excitation point

o output point

TABLE 3.1

Waveguide with loss-free walls ($\varepsilon_r = 2.0$)

$\Delta\ell/\lambda$	|Z|		ARG(Z)	
	Numerical Method	Theoretical	Numerical Method	Theoretical
0.023	6.2296	482.0395	-0.9263	-1.5708
0.025	2.2531	2.6599	1.8694	1.5708
0.027	0.2550	0.2527	-1.5309	-1.5708
0.029	6.8085	6.6448	1.5923	1.5708
0.031	0.2706	0.2826	-1.5582	-1.5708
0.033	1.8526	1.8320	1.5787	1.5708
0.035	0.8573	0.8521	-1.5569	-1.5708
0.037	0.4875	0.4796	1.5548	1.5708
0.039	5.9766	6.0828	-1.5633	-1.5708
0.041	0.2076	0.2118	-1.5488	-1.5708

TABLE 3.2

Waveguide with wall losses

($\varepsilon_r = 2.0$, $\sigma = 0.278 \times 10^3$ mho/m)

$\Delta\ell/\lambda$	|Z|		ARG(Z)	
	Numerical Method	Theoretical	Numerical Method	Theoretical
0.023	4.1981	6.1272	-0.2806	-0.0106
0.025	2.3822	2.4898	1.2546	1.0610
0.027	0.3281	0.3252	-0.7952	-0.8554
0.029	5.2724	5.1637	0.8459	0.8678
0.031	0.2963	0.3039	-1.1340	-1.1610
0.033	1.8117	1.8038	1.3408	1.3384
0.035	0.8505	0.8529	-1.3820	-1.4025
0.037	0.4912	0.4838	1.3914	1.3932
0.039	5.3772	5.4883	-1.1022	-1.1155
0.041	0.2115	0.2179	-1.2795	-1.3174

at all the points along the line z = 1 with impulses corresponding to E_y. The impulse function of the output was taken from the point (x = 7, z = 6) which is 55•5 mesh points away from a discontinuity to an open-circuit at z = 61•5.

A comparison between numerical and theoretical results for normalised values of the wave impedance $Z = E_y/H_x$ for frequencies above cut-off are shown in Table 3.1 for a loss-free waveguide. Table 3.2 shows the results when the walls of the waveguide are taken to be 6 cm apart and are given a conductivity of $\sigma = 0{\cdot}278 \times 10^3$ mho/m. The discrepancy between theoretical and numerical results near cut-off is due to the truncation error[3.2], caused by the 550 iterations of the matrix used for these calculations. The effect of truncating the iteration process is to cause the field values, expressed as a function of frequency, to be convolved with a sin f/f type curve. This causes smoothing out of high, narrow peaks of the output function.

(b) Waveguide with lossy bifurcation - The method is also demonstrated by applying it to a waveguide of width 4 cm, with a lossy centre bifurcation of finite conductivity $\sigma_b = 0{\cdot}278 \times 10^3$ S/m as shown in Fig. 3.2. Results for the impedance at the output point are presented graphically in Fig. 3.2.

(c) Waveguide with centre resistive card - Fig. 3.3 shows an example of lossy waveguide where equation 2.5 is used. The structure shown is a waveguide with a resistive card at the centre position ($R = 100\ Z_0$). Results are shown in Table 3.3 for the impedance at the output point, in the frequency range containing the dominant mode and are compared with the results obtained from reference 3.3.

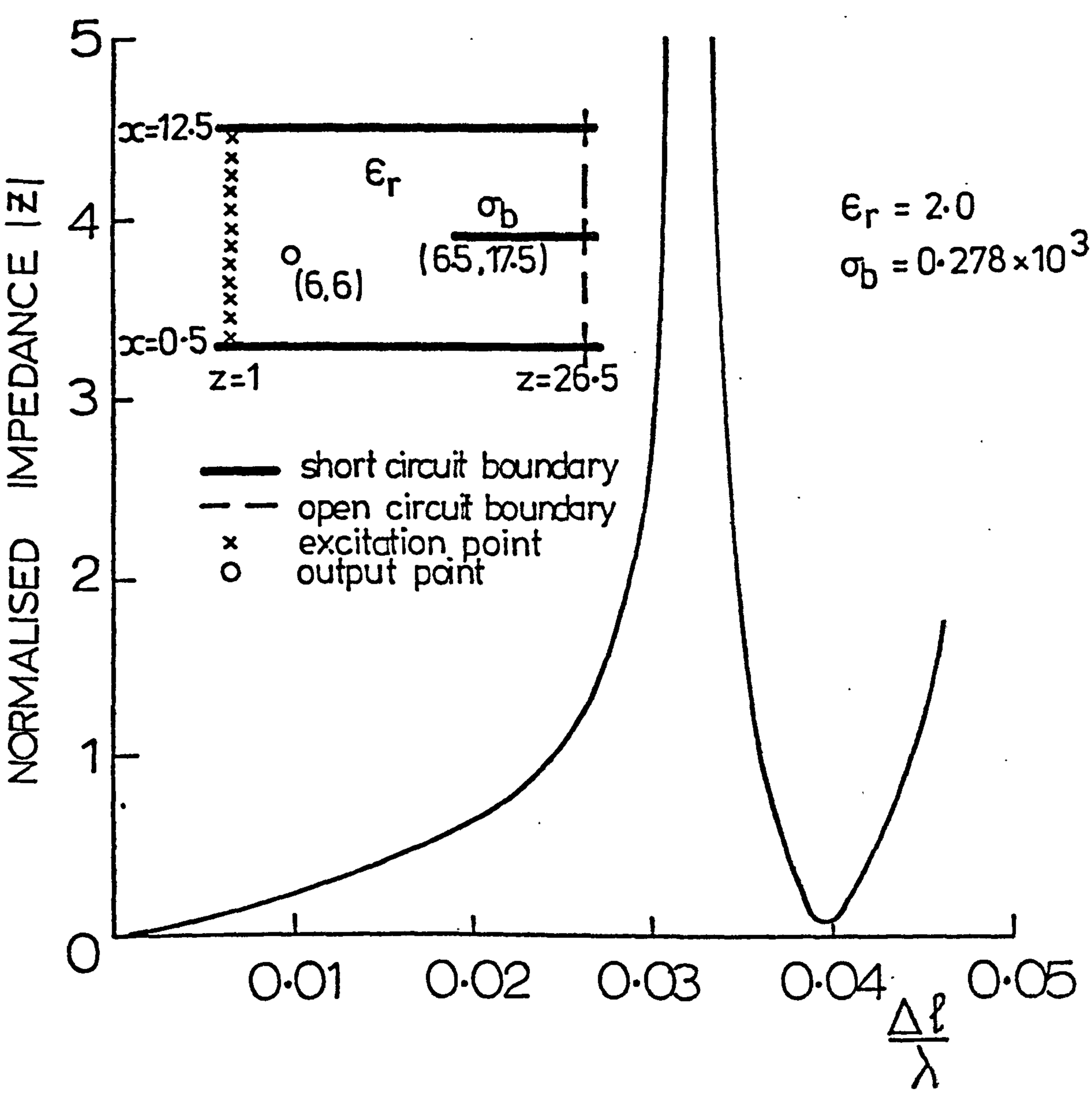

FIG. 3.2 Magnitude of impedance in a waveguide with a symmetrical lossy bifurcation

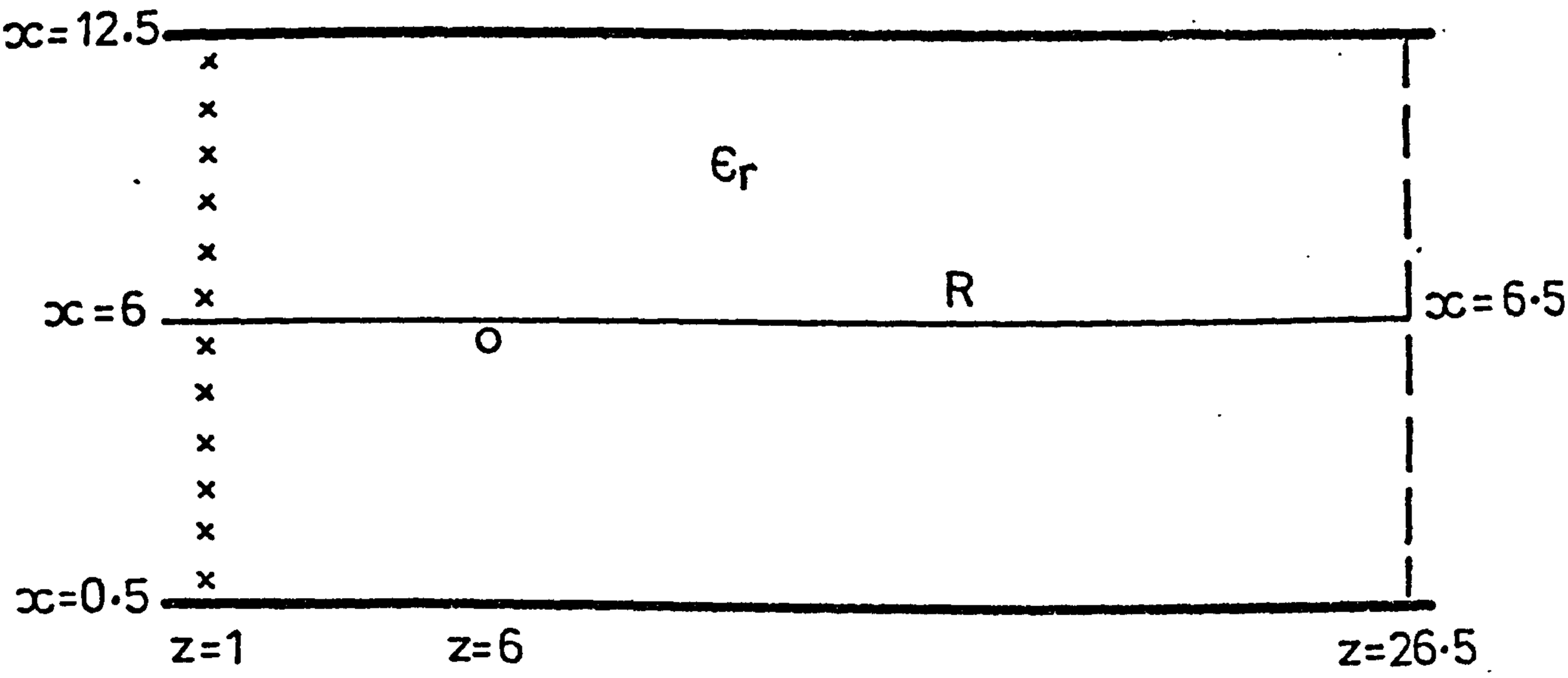

FIG. 3.3 Waveguide geometry including a centre resistive strip

——— short circuit boundary

— — open circuit boundary

× excitation point

o output point

TABLE 3.3

Waveguide with resistive strip ($\varepsilon_r = 2.0$, $R = 100\ Z_o$)

$\Delta\ell/\lambda$	|Z|		ARG(Z)	
	Numerical Method	Marcuvitz	Numerical Method	Marcuvitz
0.020	0.6769	0.6539	1.5579	1.5680
0.024	1.0447	0.9963	1.5599	1.5653
0.028	2.6096	2.3107	1.5539	1.5439
0.032	1.4742	1.5332	1.4059	1.5220
0.036	1.6712	1.7049	-1.4810	-1.5212
0.040	0.2246	0.2287	1.3923	1.4891
0.044	2.7814	2.7651	1.4585	1.5209
0.048	1.2555	1.2581	-1.5058	-1.5363
0.052	0.0482	0.0444	-0.9579	-1.2818
0.056	0.9235	0.8916	1.5091	1.5440

3.3.2 TWO-DIMENSIONAL RECTANGULAR CAVITIES

The method was also used to calculate the power decay due to losses in the walls of a two-dimensional ractangular cavity. A comparison between the numerical and theoretical results for the time taken for the power in the cavity to fall to 1/e of its original value is shown in Table 3.4. In the numerical method, the H_{101} mode was isolated by choosing the position and relative magnitude of the excitation points to correspond approximately to the field values of the mode. Also, the analysis was carried out at the resonant frequency of the H_{101} mode.

TABLE 3.4

Cavity with wall losses

($\epsilon_r = 2.0$, $\sigma = 0.278 \times 10^3$ S/m, $\Delta\ell = 0.3$ cm)

No. of mesh points in the x-direction	No. of mesh points in the z-direction	Time taken for the power in the cavity to fall to 1/e of its original value	
		Numerical Method ns	Theoretical ns
5	5	0.40	0.40
5	10	0.50	0.49
10	30	1.39	1.39
20	20	3.11	3.16
20	30	3.79	3.82

REFERENCES

3.1 JOHNS, P.B. "Application of the transmission-line matrix method to homogeneous waveguides of arbitrary cross-section", Proc. I.E.E., 119, pp 1086-1091, August, 1972.

3.2 COLLIN, R.E. "Foundations for microwave engineering", New York, McGraw-Hill, pp 78, 1966.

3.3 MARCUVITZ, N. "Waveguide hand book", New York, McGraw-Hill, pp 402-404, 1951.

3.4 AKHTARZAD, S. and JOHNS, P.B. "Transmission-line matrix solution of waveguides with wall losses", Electron. Lett., 9, pp 335-336, July, 1973.

CHAPTER 4

TLM COMPUTER PROGRAMMING TECHNIQUE

4.1 INTRODUCTION

Programming forms a significant part of any numerical method. With a proper technique, the programmer will save both computer time and storage. This saving could prove to be of great importance when limited time or storage, especially the latter, is available on the computer. It is perhaps equally important that a new user of the program should be able to adapt to it in a short while and also be able to feed into the computer the general data on a problem. With regard to these points, a general two-dimensional program was developed in which any number of boundaries (conducting or dielectric, with or without losses) are read in as data. The program will then exit with required information, tabulated against the frequency.

In this chapter, the basis of a simple version of a TLM computer program incorporating dielectric losses as discussed in Chapter 1 and also wall losses (Chapter 3) is fully analysed. It is hoped that it will give an insight into the programming side of the TLM method, which forms an important part of it. A feature of particular interest in this program is the technique used for nodal calculations in order to halve the storage requirements (see program listing - Appendix A). It was subsequently used in the final general two-dimensional program which includes dielectric- and loss-stubs.

The FORTRAN program implementing the TLM method requires the user to insert,

(a) the limits of the matrix in the x- and y- co-ordinate directions,

(b) position of boundaries together with their appropriate boundary code and reflection coefficient,

(c) excitation points or lines together with their appropriate excitation code and initial value,

(d) the output point,

(e) the output code,

(f) number of iterations required (NI),

(g) loss factor (tanδ),

(h) frequency range ($\frac{\Delta\ell}{\lambda}$).

The program then exits with values of EHMOD, the output magnitude tabulated against frequency $\frac{\Delta\ell}{\lambda}$.

If the following equivalences apply between fields E and H in the medium and voltages and currents V and I on the matrix (see reference 4.1),

(i) E ≡ V and H ≡ I

then for output code L = 1,2,3, EHMOD = $|H_y|$, $|H_x|$, $|E_z|$ respectively

(ii) H ≡ V and E ≡ I

then for output code L = 1,2,3, EHMOD = $|E_y|$, $|E_x|$, $|H_z|$ respectively.

4.2 PROGRAM DESCRIPTION

The program consists of main program TLM, which calls subroutine OUTPUT

(a) Language: FORTRAN IV

(b) Number of variables:

scalars (integer or real):	25	in TLM
	16	in OUTPUT
arrays:	6	in TLM
	1	in OUTPUT

(c) The program is written for single precision arithmetic

(d) Number of statements: 55 in TLM

26 in OUTPUT

4.3 INPUT DATA

The program consists of two subroutines. The main subroutine is TLM, which calls the auxiliary subroutine OUTPUT.

The calling sequence is:

```
CALL  OUTPUT  (NI)
```

where NI is input parameter to the OUTPUT subroutine.

4.3.1 The Input-Parameter Definitions:

(i) TLM

NX: x-direction range limit

NY: y-direction range limit

IB(KB,M): boundary parameter

M=1,8

KB internal counter (for number of boundaries)

†* M=1 x-low

* M=2 x-high

* M=3 y-low

* M=4 y-high

M=5,8 boundary code (see later)

R(KB): boundary reflection coefficient

IE(KE,M): excitation parameter

M=1,7

KE internal counter (for number of excitation points or lines)

§ M=1 x-low

M=2 x-high

M=3 y-low

M=4 y-high

M=5,7 excitation code (see later)

VA(KE): excitation amplitude

IO: x-value of output node

JO: y-value of output node

L: output choice code (see output sheet)

NI: number of iterations required

(* Boundaries should fall within the range limits (1,NX) in the x-direction and (1,NY) in the y-direction.

† A value of zero for x-low declares the end for input boundary data.

§ A value of zero for x-low declares the end for input excitation data.)

(ii) OUTPUT

D1: frequency-low ($\frac{\Delta \ell}{\lambda}$, matrix mesh size to free space wavelength)

D2: frequency-high

DS: frequency-increment

T: loss factor of the dielectric (tanδ)

4.3.2 The Input Codes

(a) Boundary codes

a.1 Horizontal boundary

code: 1310

a.2 Vertical boundary

code: 2401

(b) Excitation codes

b.1 Impulses on top and bottom lines

code: 123

b.2 Impulses on left and right lines

code: 224

b.3 Impulses on top, bottom, left and right lines

code: 114

4.3.3 The Input-Parameter Format

(i) TLM

Col. 1-5	6-10	11-15	16-20	21-25	26-35
NX	NY				
IB(1,1)	IB(1,2)	IB(1,3)	IB(1,4)	IB(1,M) M = 5,8	R(1)
.	.	.	.	.	.
.	.	.	.	.	.
IB(KB,1)	IB(KB,2)	IB(KB,3)	IB(KB,4)	IB(KB,M) M = 5,8	R(KB)
0					
IE(1,1)	IE(1,2)	IE(1,3)	IE(1,4)	IE(1,M) M = 5,7	VA(1)
.	.	.	.	.	.
.	.	.	.	.	.
IE(KE,1)	IE(KE,2)	IE(KE,3)	IE(KE,4)	IE(KE,M) M = 5,7	VA(KE)
0					
10	JO	L	NI		

(ii) OUTPUT

Col. 1-10	11-20	21-30
T		
D1	D2	DS

4.4 OUTPUT DATA

The output-impulse function EH(IC) (in time domain) processed in the main subroutine TLM is turned over to the auxiliary subroutine OUTPUT. This routine performs the Fourier transformation on the impulse function taking note of loss factor T. The program then exits with values of EHMOD, the output magnitude, tabulated against frequency $\frac{\Delta \ell}{\lambda}$.

If the following equivalences apply between fields E and H in the medium and voltages and currents V and I on the matrix (see reference 4.2).

(i) $E \equiv V$ and $H \equiv I$

then for output code L = 1,2,3, EHMOD = $|H_y|, |H_x|, |E_z|$ respectively.

(ii) $H \equiv V$ and $E \equiv I$

then for output code L = 1,2,3, EHMOD = $|E_y|, |E_x|, |H_z|$ respectively.

4.5 FLOW DIAGRAM CHARTS

4.5.1 TLM

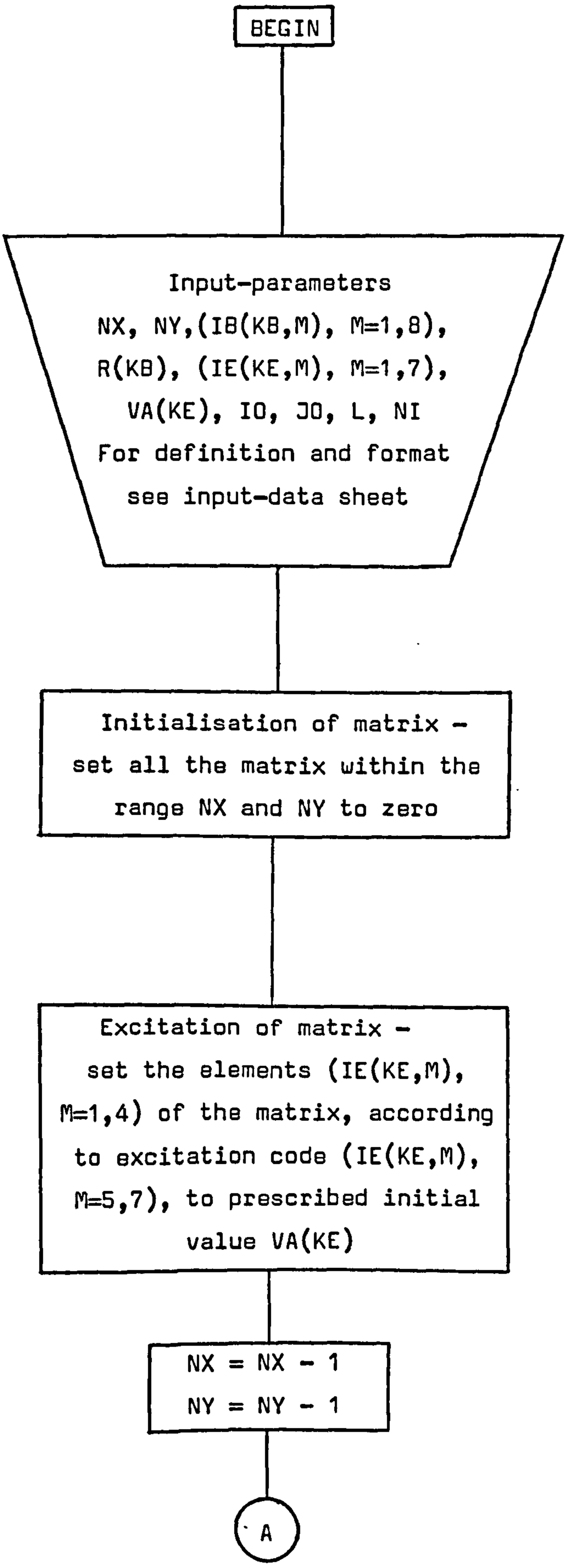

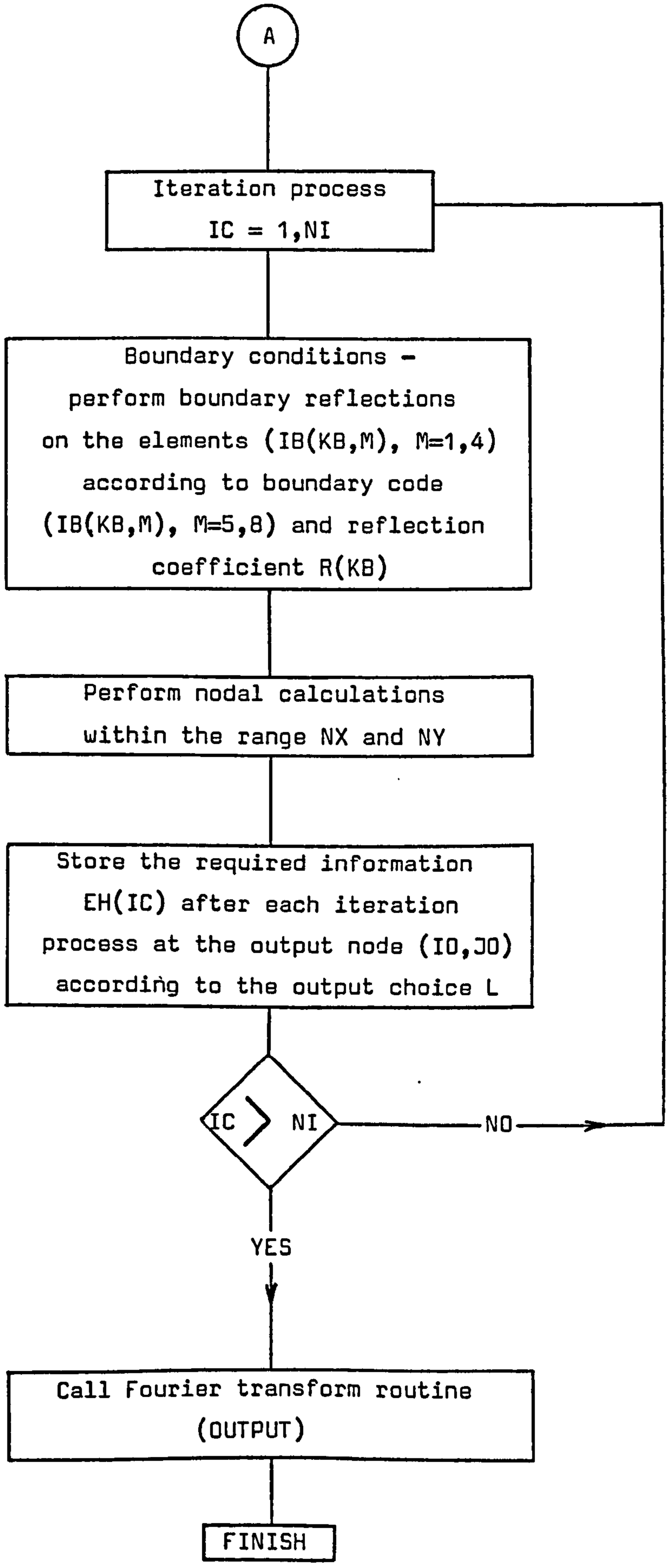
A
Iteration process
IC = 1,NI
Boundary conditions -
perform boundary reflections
on the elements (IB(KB,M), M=1,4)
according to boundary code
(IB(KB,M), M=5,8) and reflection
coefficient R(KB)
Perform nodal calculations
within the range NX and NY
Store the required information
EH(IC) after each iteration
process at the output node (IO,JO)
according to the output choice L
IC > NI
NO
YES
Call Fourier transform routine
(OUTPUT)
FINISH

4.5.2 OUTPUT

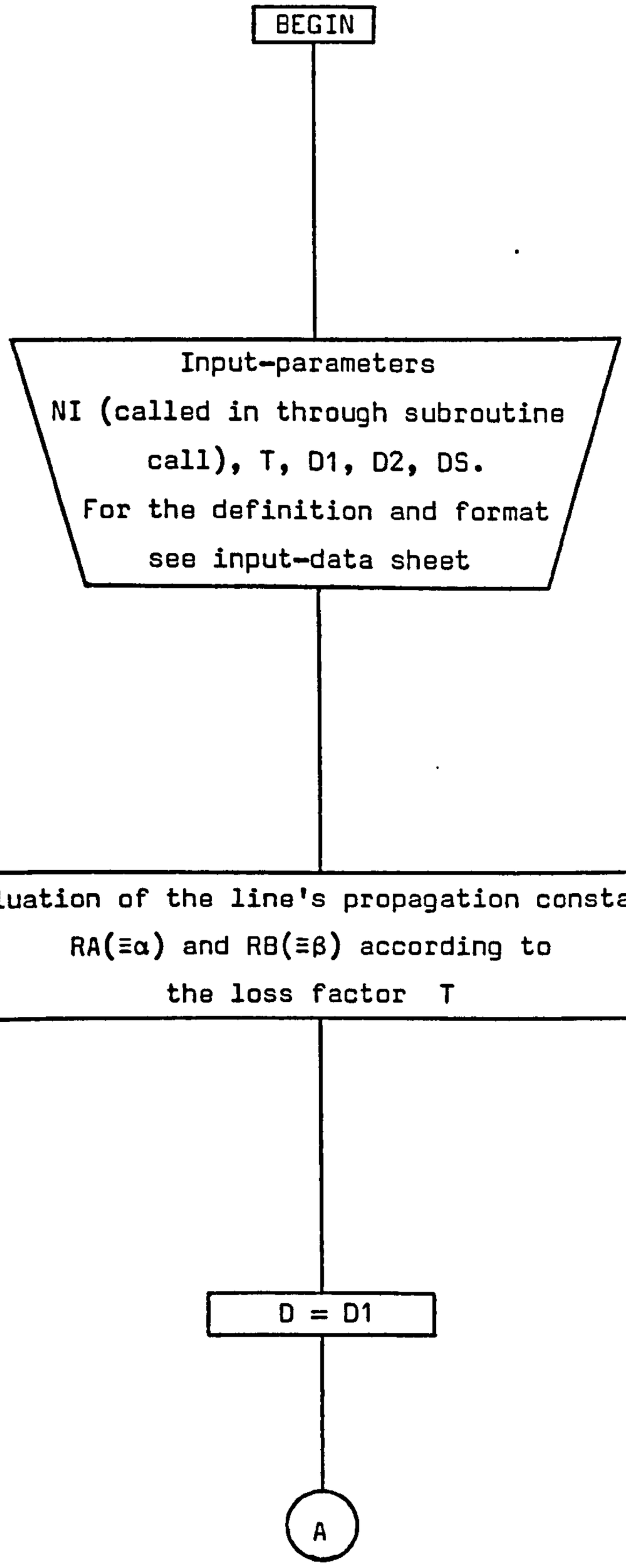
BEGIN
Input-parameters
NI (called in through subroutine call), T, D1, D2, DS.
For the definition and format see input-data sheet
Evaluation of the line's propagation constants RA(≡α) and RB(≡β) according to the loss factor T
D = D1
A

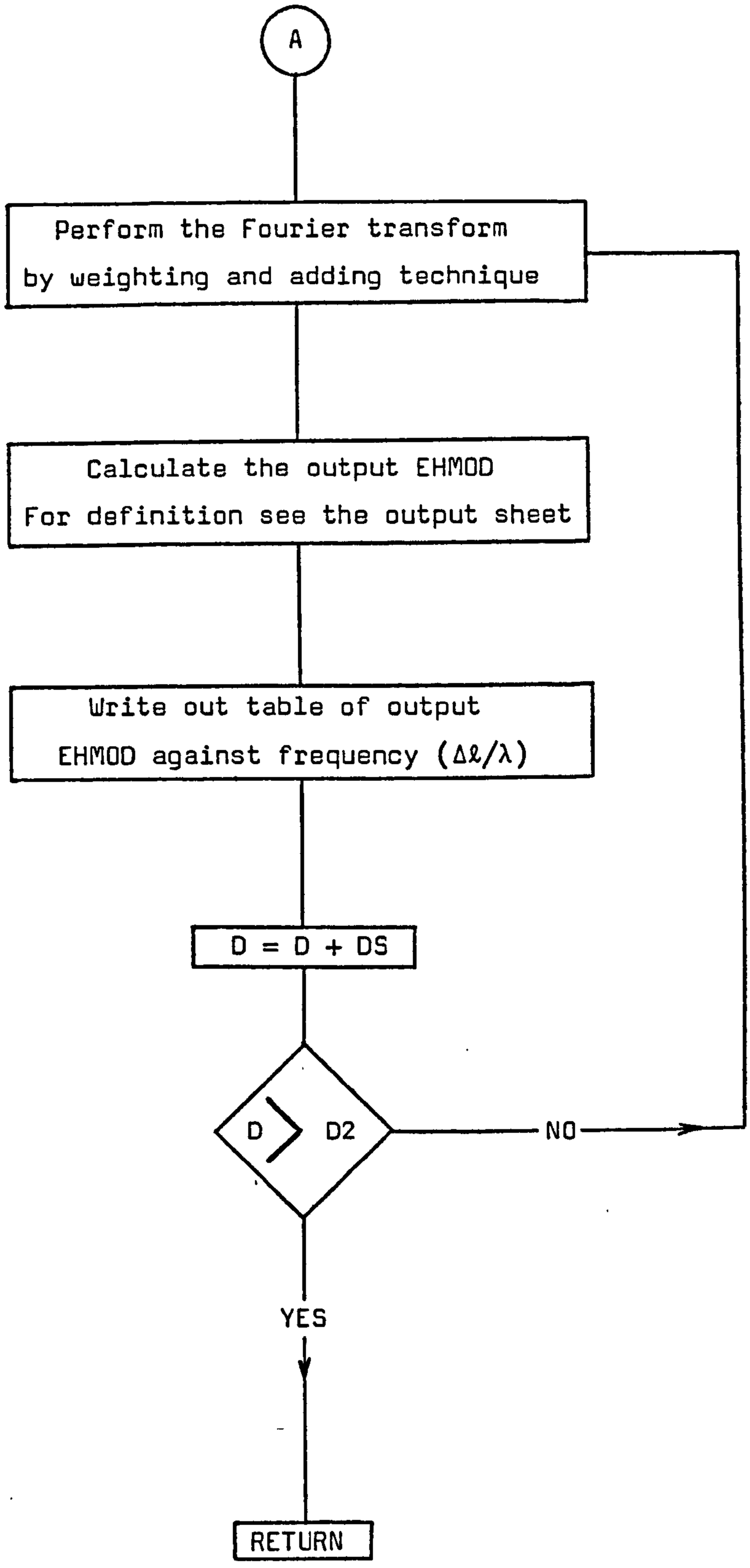
A
Perform the Fourier transform
by weighting and adding technique
Calculate the output EHMOD
For definition see the output sheet
Write out table of output
EHMOD against frequency (Δℓ/λ)
D = D + DS
D > D2
NO
YES
RETURN

4.6 USAGE DEMONSTRATION

4.6.1 Numerical Example

As a demonstration, a numerical example of the TLM method has been carried out on a multi-ridged waveguide with a short-circuit plane of symmetry half-way across the cross section. Fig. 4.1 shows the geometry for the calculation. The problem was simulated on a matrix of size 12 x 11 for NI = 200 iterations. H_z was excited along a line through the node x = 10. The output impulse function E_y was calculated at the output node (2,8) and then the frequency spectrum of the impulse function was obtained at intervals of $\Delta\ell/\lambda$ = 0·0005 up to 0·025. Fig. 4.2 shows the frequency spectrum containing the dominant mode $[(\Delta\ell/\lambda)_{cut\ off} = 0{\cdot}0125 = S/2]$.

The errors involved[4.1] are:

(i) Truncation error

$$\Delta S = \frac{3}{SN^2\pi^2}$$

$$\text{Error} < 1{\cdot}2\%$$

(ii) Velocity error - negligible.

(iii) Field description error - estimated to be less than 1%.

4.6.2 Performance Guide

(a) Computer used: ICL 1906A of the Cripps Computing Centre of the University of Nottingham.

(b) Maximum core size used: 6000 bytes.

(c) Time to calculate main program (200 iterations) and output routine (50 frequency values for Fig. 4.1 - see Appendix A): 20 S

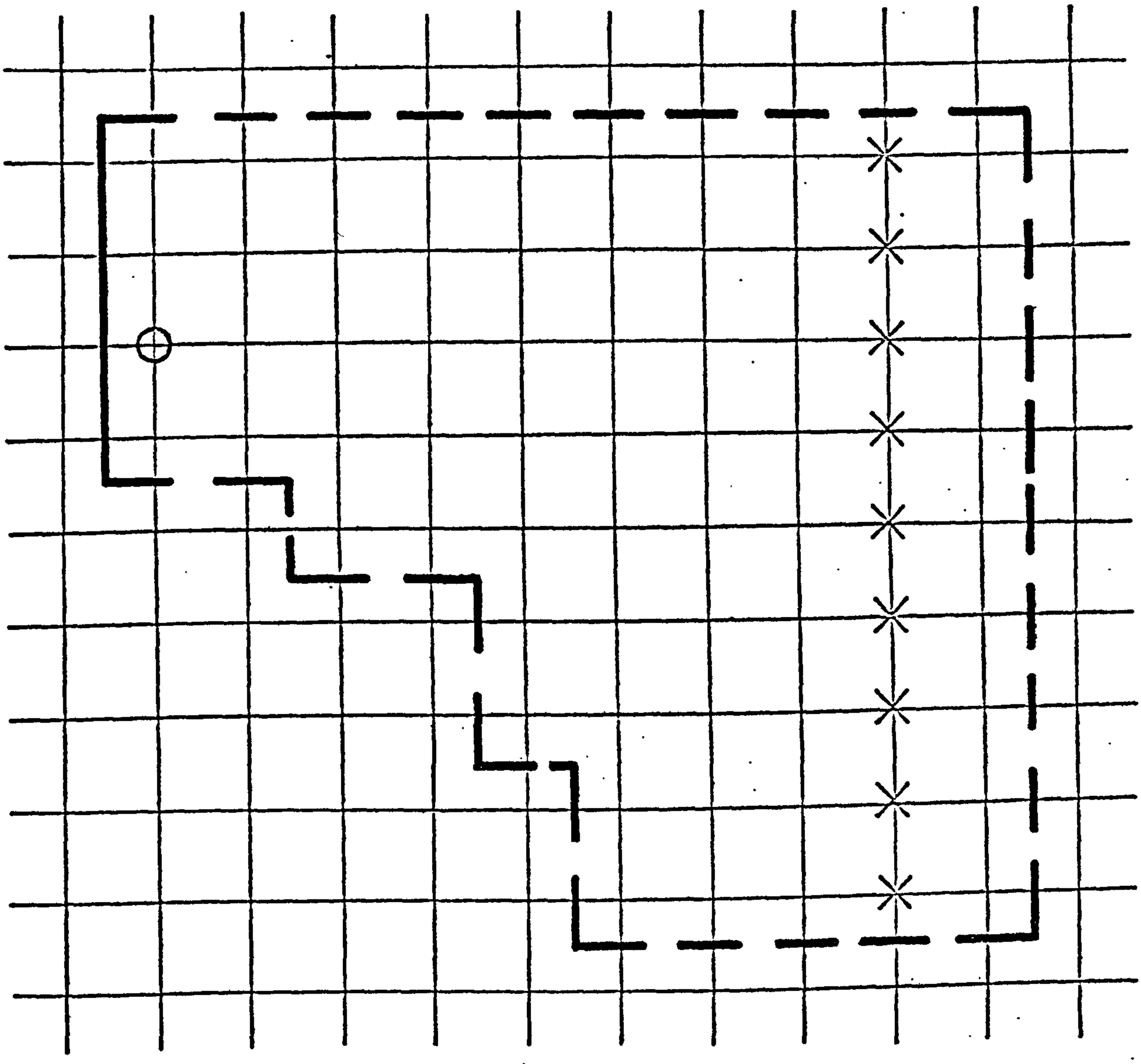

FIG. 4.1 Half-cross-section geometry of the multi-ridge waveguide

——— short circuit boundary

— — open circuit boundary

× source point

○ output point

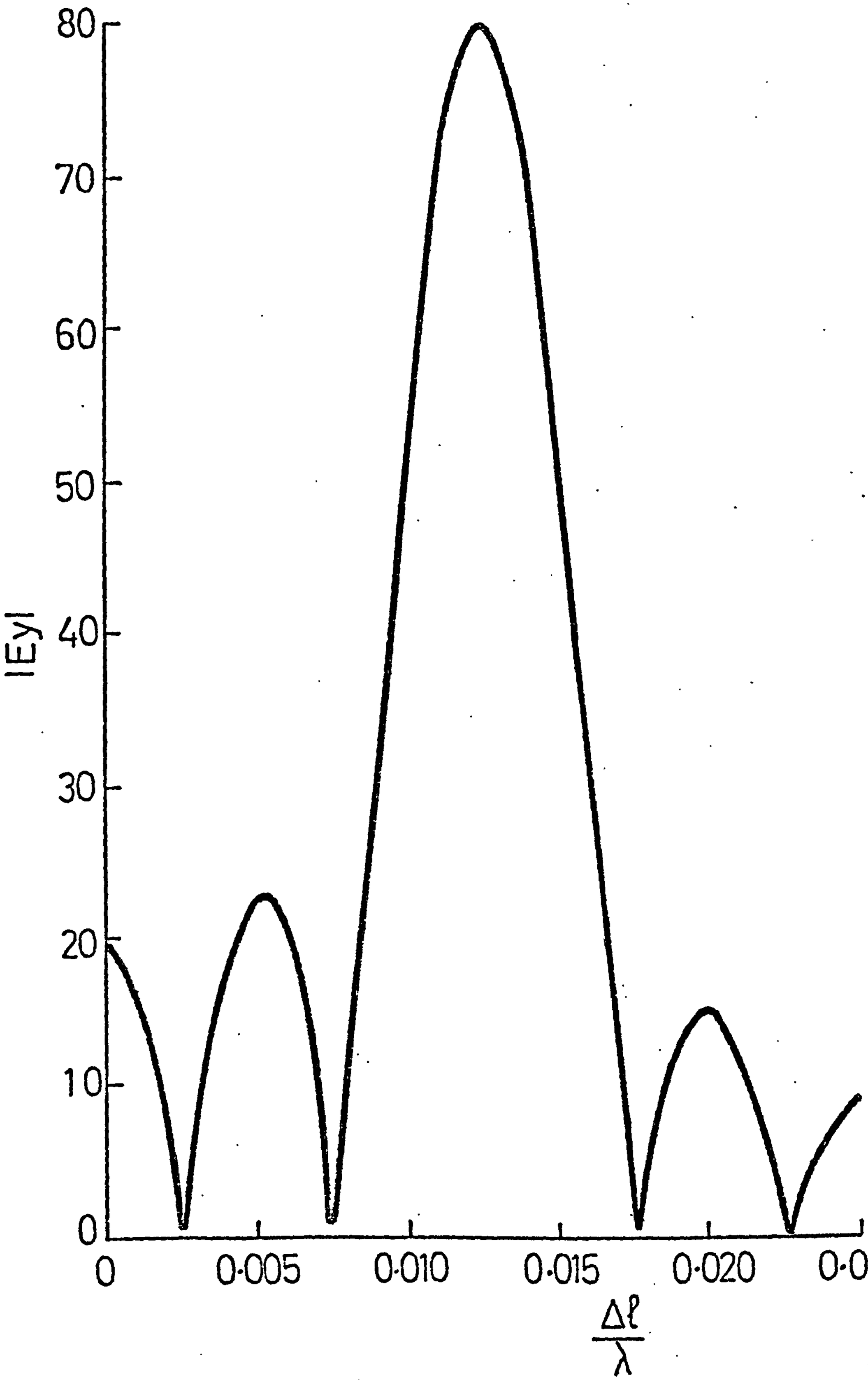

FIG. 4.2 Solution for dominant mode of the multi-ridged waveguide

REFERENCES

4.1 JOHNS, P.B. "Application of the transmission-line matrix method to homogeneous waveguides of arbitrary cross-section", Proc. I.E.E., 119, pp 1086-1091, August, 1972.

4.2 AKHTARZAD, S. and JOHNS, P.B. "Numerical solution of lossy waveguides - TLM computer program", Electron. Lett., 10, pp 309-311, July, 1974.

CHAPTER 5

THE COMPLETE SOLUTION OF MAXWELL'S EQUATIONS IN THREE SPACE DIMENSIONS AND TIME

5.1 INTRODUCTION

Many problems in electrical engineering are associated with the way in which electric and magnetic fields propagate and distribute themselves in various media. Maxwell's equations provide a concise description for the interaction of these fields with themselves and with the various boundaries of a problem, and therefore a numerical procedure for the complete solution of these equations is an important consideration. In this chapter, the extension of the TLM method to three space dimensions for the complete solution of Maxwell's equations is described[5.1]. It will be shown how a general three dimensional medium may be represented by an interconnection of continuous ideal two-wire transmission-lines and how this model may be used for the numerical solution of the electric and magnetic vector fields within the medium.

The three-dimensional model is basically made up of shunt nodes already used in the construction of the two-dimensional model and also series nodes which will be discussed in the next section. Media represented by the model may be inhomogeneous with any value of permeability, μ, or permittivity, ϵ, and lossy with conductivity, σ, taking any value from zero (loss-free medium) to infinity (ideal conductor).

5.2 GENERAL TWO-DIMENSIONAL TRANSMISSION-LINE ELEMENTS

As was described in the previous chapters, the two-dimensional TLM method is based on a network of transmission-lines consisting of the interconnection of elements of shunt connected parallel open wires. A general shunt connected node of the network, for convenience, is shown in Fig. 5.1. Now, if the voltage on the transmission-lines represents the E-field

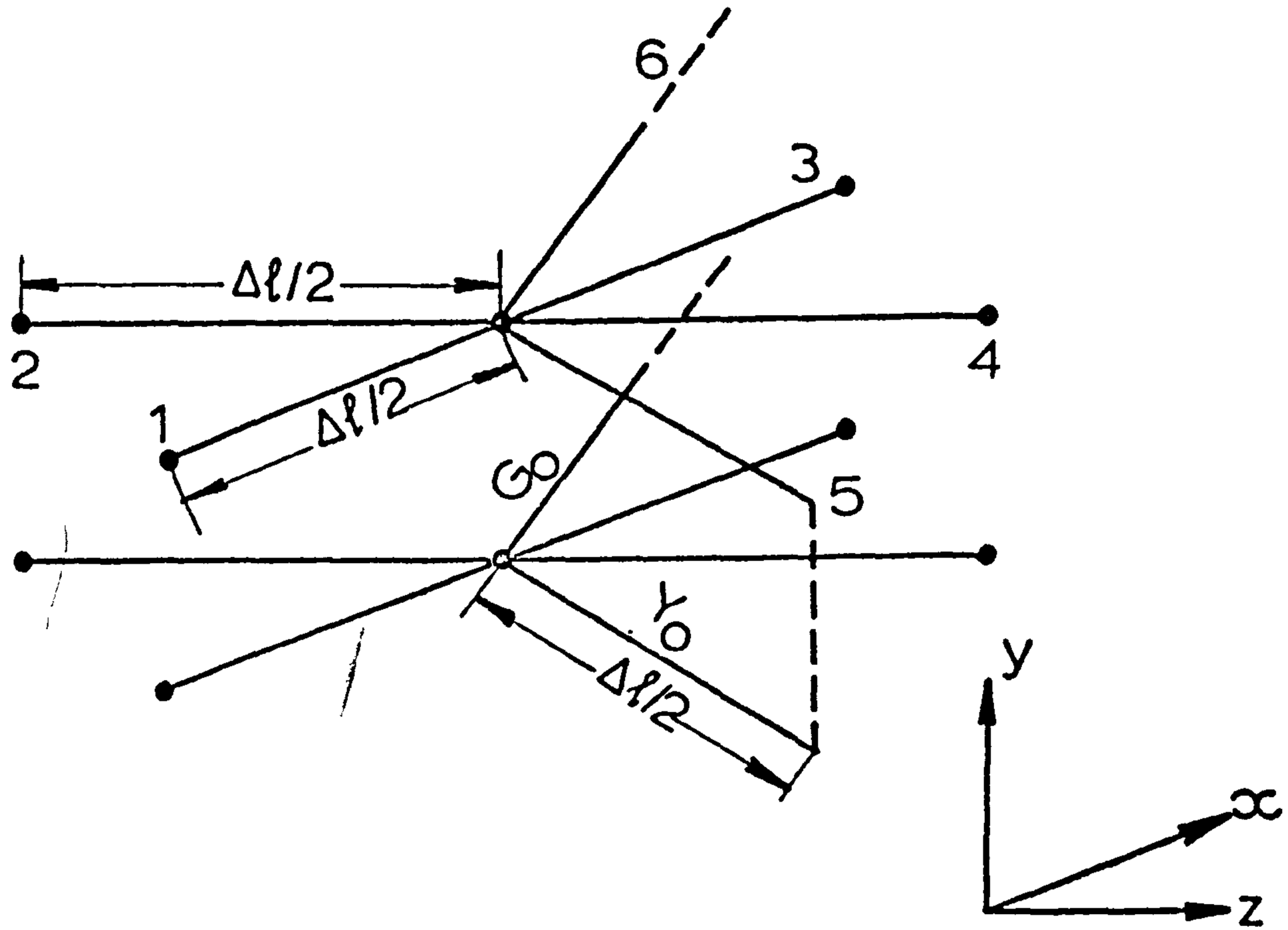

FIG. 5.1 The general shunt connected node with permittivity- and loss-stubs

— — — — open circuit

——— — — infinite length

in the propagation medium, the set of Maxwell's equations described in the x-z plane (for example) are,

$$\left.\begin{aligned} \frac{\partial H_x}{\partial z} - \frac{\partial H_z}{\partial x} &= \varepsilon' \frac{\partial E_y}{\partial t} \\ \frac{\partial E_y}{\partial z} &= \mu \frac{\partial H_x}{\partial t} \\ \frac{\partial E_y}{\partial x} &= -\mu \frac{\partial H_z}{\partial t} \end{aligned}\right\} \qquad (5.1)$$

where ε' is the complex permittivity.

The time-domain impulse function of the two-dimensional array of scattering elements describing a problem is obtained by iteration of the voltage impulse scattering matrix for a single element. This is given by equation 2.2.

Now consider the basic scattering element of Fig. 5.2. It consists of a four terminal series connected junction of ideal transmission-lines with a fifth line in the form of a short-circuited stub of variable characteristic impedance, Z_o. If the voltage on the lines of the series element represents the E-field in the propagation medium, the set of Maxwell's equations described in the x-z plane are,

$$\left.\begin{aligned} \frac{\partial E_x}{\partial z} - \frac{\partial E_z}{\partial x} &= -\mu \frac{\partial H_y}{\partial t} \\ -\frac{\partial H_y}{\partial z} &= \varepsilon \frac{\partial E_x}{\partial t} \\ \frac{\partial H_y}{\partial x} &= \varepsilon \frac{\partial E_z}{\partial t} \end{aligned}\right\} \qquad (5.2)$$

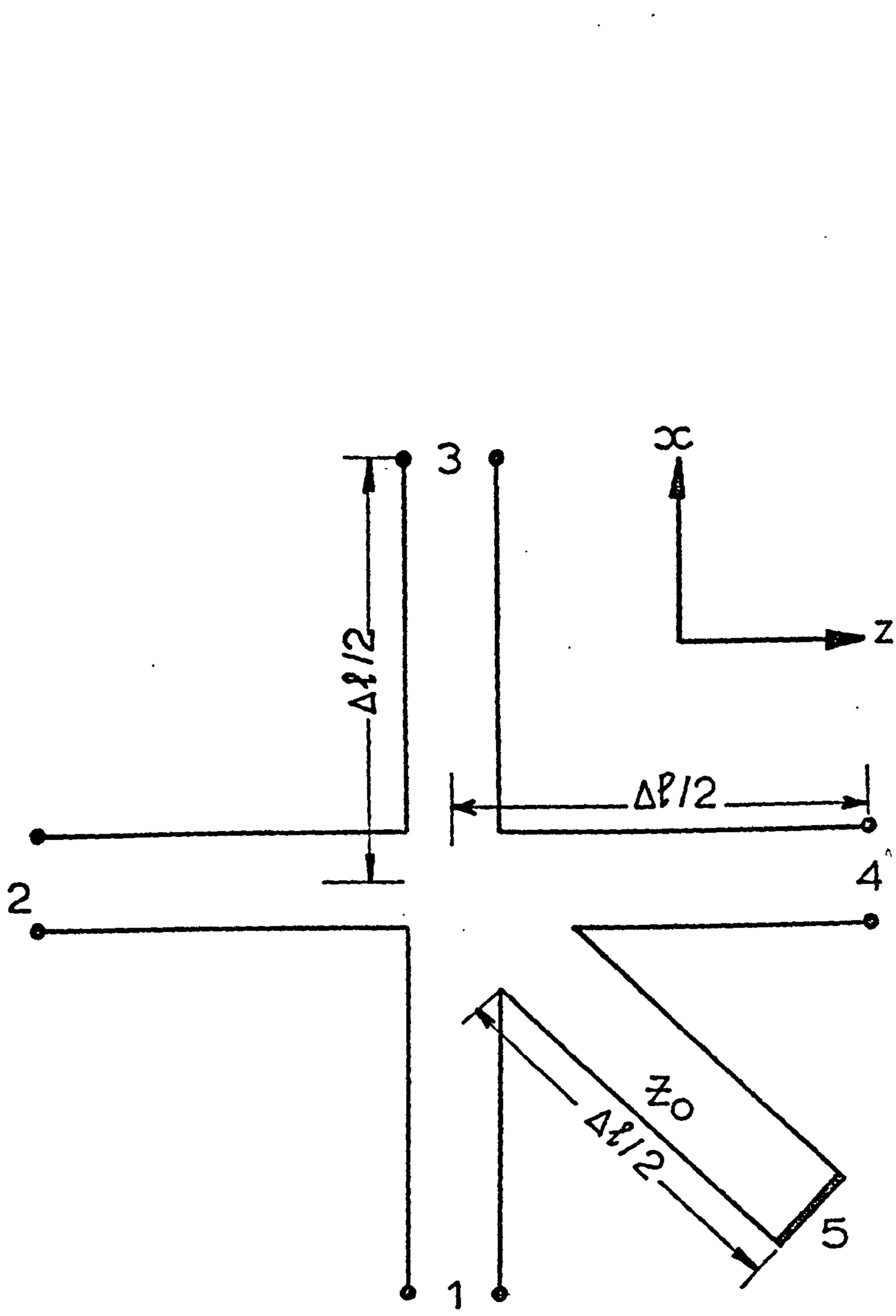

FIG. 5.2 The general series connected node with permeability-stub

—— short circuit

A direct comparison between equation 5.2 and the transmission-line equations of the series element will show that,

$$\mu \equiv 2(1 + Z_o/4) \tag{5.3}$$

Hence, it can be seen that, the variable impedance stub, Z_o, describes the permeability of the medium. Therefore it will be referred to as permeability-stub.

The voltage impulse scattering matrix for the series element is

$$\frac{1}{Z_o+4}\begin{pmatrix} (Z_o+2) & 2 & 2 & -2 & -2 \\ 2 & (Z_o+2) & -2 & 2 & 2 \\ 2 & -2 & (Z_o+2) & 2 & 2 \\ -2 & 2 & 2 & (Z_o+2) & -2 \\ -2Z_o & 2Z_o & 2Z_o & -2Z_o & -(Z_o-4) \end{pmatrix} \tag{5.4}$$

Thus, if voltages on the two-dimensional matrix elements always represent E-fields in the medium, the shunt connected matrix provides a solution for two-dimensional $\underline{H}_{mo}$ modes in the x-z plane (H_z, H_x and $\underline{E}_y$ fields) and the series connected matrix provides a solution for E_{mo} modes in the x-z plane (E_z, E_x and H_y fields). Therefore, these two separate matrices will solve the two separate sets of three equations (5.1 and 5.2) given by the expansion of Maxwell's equations in two dimensions. Note also that losses are not included in the series matrix because there is no corresponding loss term in Maxwell's equations.

The slow wave properties of the series matrix are similar to the shunt matrix. In particular, if a one dimensional (TEM) wave propagates in the z-direction on the matrix shown in

Fig. 5.3, then any current pulse travelling from B to A (say) is met by a similar current pulse travelling from A to B. (Note that for simplicity the permeability-stub at the nodes are omitted in Fig. 5.3). Hence, a one-dimensional wave travelling over the matrix in the z-direction may be represented by the passage of a wave down a transmission-line having short-circuited stubs of length $\Delta\ell/2$, as shown in Fig. 5.3(b). This is the exact dual of the parallel case[5.2] and the transmission equation, taking the permeability-stub into account, becomes

$$\begin{pmatrix} V_i \\ I_i \end{pmatrix} = \begin{pmatrix} \cos\theta/2 & j\sin\theta/2 \\ j\sin\theta/2 & \cos\theta/2 \end{pmatrix} \cdot \begin{pmatrix} 1 & j(2+Z_o)\tan\theta/2 \\ 0 & 1 \end{pmatrix} \cdot$$

$$\begin{pmatrix} \cos\theta/2 & j\sin\theta/2 \\ j\sin\theta/2 & \cos\theta/2 \end{pmatrix} \cdot \begin{pmatrix} V_{i+1} \\ I_{i+1} \end{pmatrix} \qquad (5.5)$$

where

$$\theta = \frac{\omega\Delta\ell}{c} = 2\pi\frac{\Delta\ell}{\lambda} \qquad (5.6)$$

The velocity characteristic for the two-dimensional series matrix then becomes

$$\sin\left(\frac{\beta_n\Delta\ell}{2}\right) = \sqrt{2(1+Z_o/4)}\ \sin\left(\frac{\omega\Delta\ell}{2c}\right) \qquad (5.7)$$

where β_n represents the propagation constant of the network (medium).

Equation 5.7 shows that, say for $Z_o = 0$, for low frequencies ($\Delta\ell/\lambda$ < about 0·1) the velocity of waves on the matrix is $1/\sqrt{2}$ of the free-space velocity. This corresponds to the fact that the stubs have doubled the inductance per unit length, the capacitance

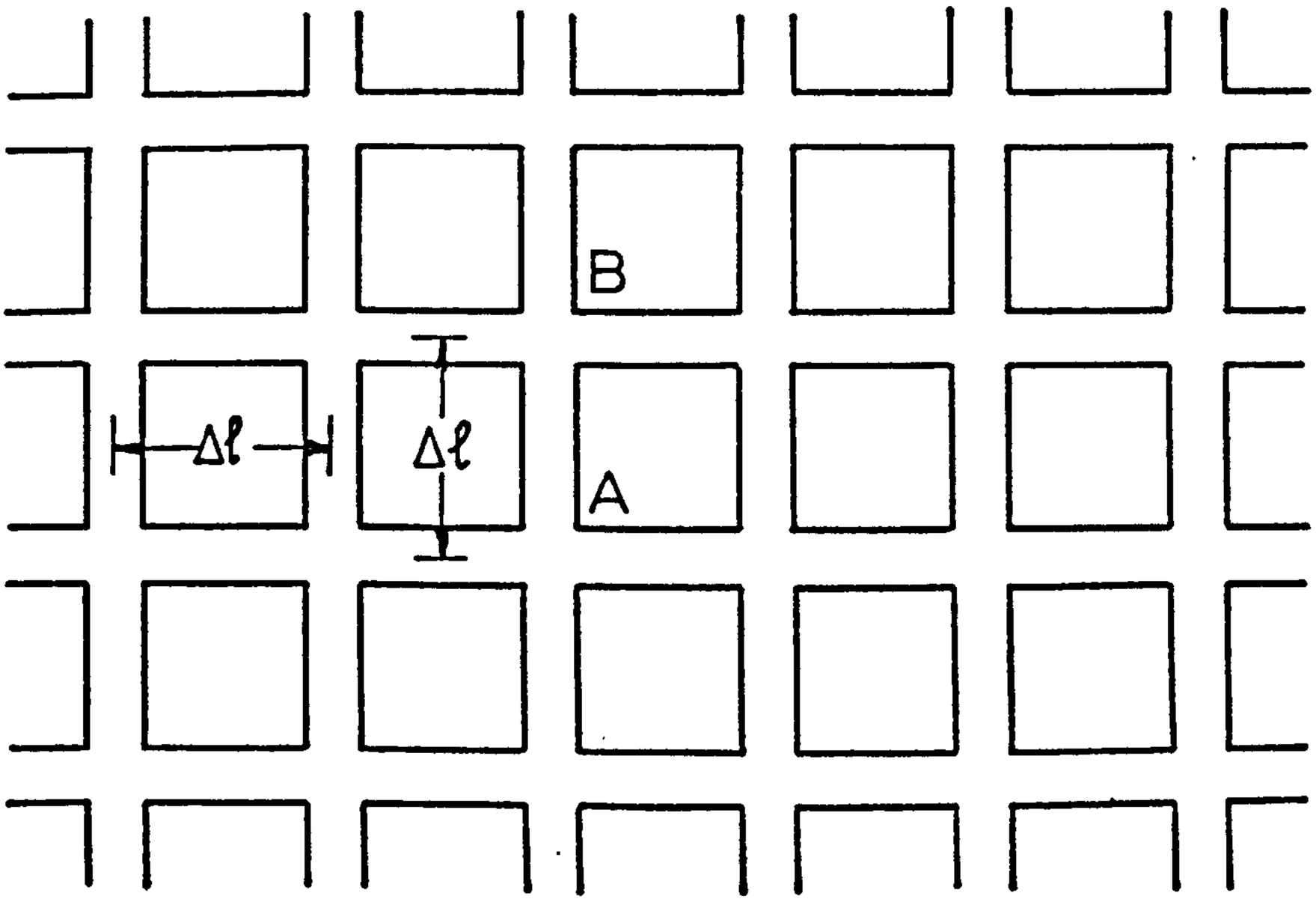

(a)

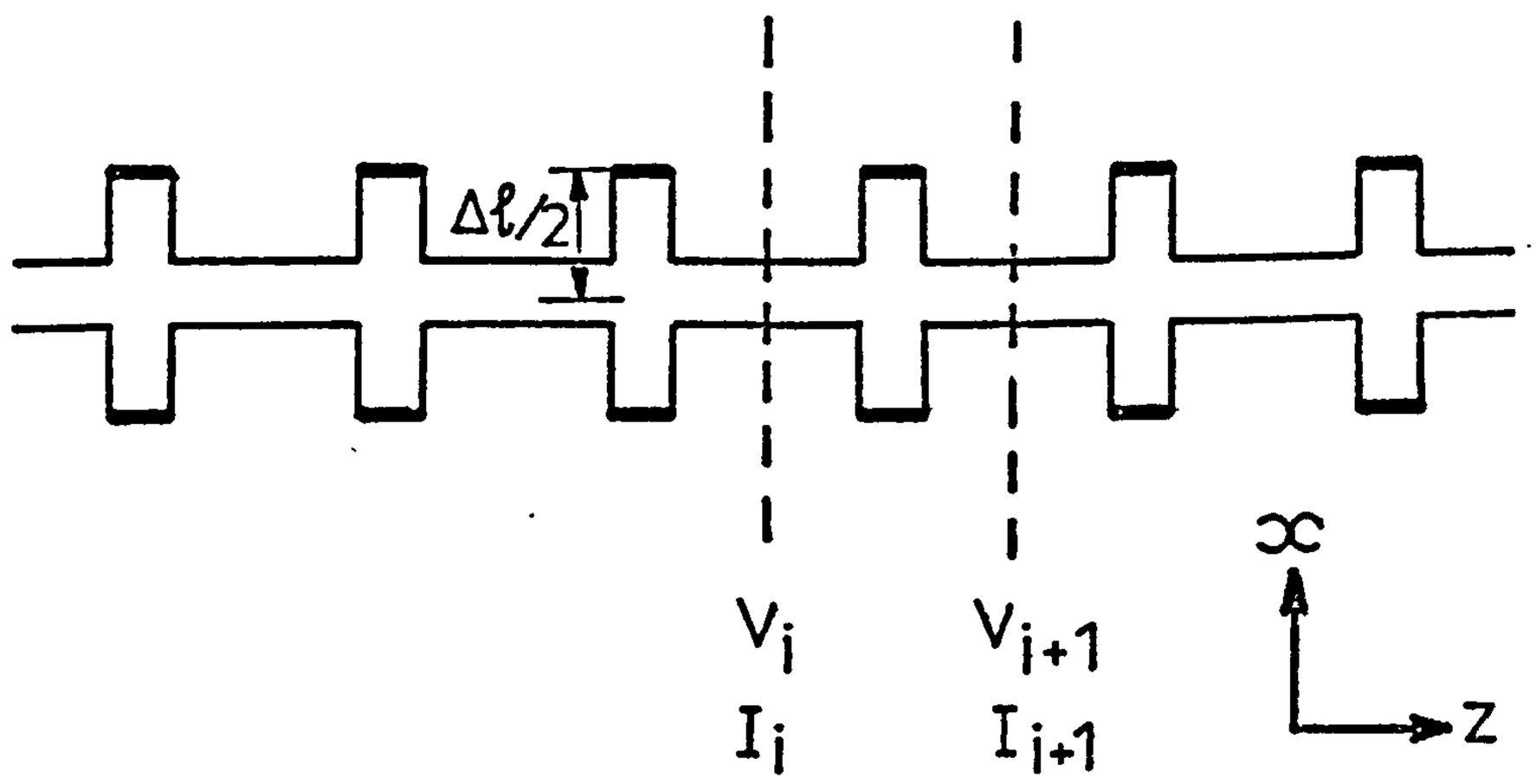

(b)

FIG. 5.3 Series connected network model

(a) two-dimensional equivalent network

(b) one-dimensional equivalent network

—— short circuit

per unit length remaining unchanged. In the parallel case, the capacitance was doubled and the inductance was unchanged. A one-dimensional wave travelling diagonally across the series matrix sees matched conditions as in the parallel case, but because the distance around the transmission-lines is $\sqrt{2}$ times the diagonal distance, the effective velocity along the diagonal can be shown[5.2] is $\sqrt{2}$ times the value for waves propagating in the direction of the co-ordinates. Thus, the effective velocities of the waves travelling in the two directions are the same.

5.3 THE THREE-DIMENSIONAL MATRIX USING TWO-DIMENSIONAL NODES

Among other properties, the three-dimensional matrix must be able to support both E-modes and H-modes in any plane. Equations 5.1 and 5.2 indicate therefore that there must be a parallel matrix and a series matrix in each plane. A three-dimensional model may be built by stacking two-dimensional matrices on top of each other and an obvious way to do this is by having alternate parallel and series matrices spaced from each other by $\Delta\ell/2$. Since the model must appear the same when viewed along any of the three co-ordinate axes, the method of interconnecting the matrices can be visualised.

For the purpose of analysis, the three-dimensional model is first made up for the non-lossy homogeneous field problems. Then in the next section, properties of the model for inhomogeneous media are studied and are further extended to also include the lossy cases.

Consider now a parallel connection in the x-z plane connected to a series connection in the y-z plane and a series connection in the x-y plane as shown in Fig. 5.4. At the parallel connected point, the voltage is common to both lines and therefore the following equation applies,

$$\frac{\partial H_x}{\partial z} - \frac{\partial H_z}{\partial x} = \varepsilon \frac{\partial E_y}{\partial t} \qquad (5.8)$$

Also, the current is common in the series matrix and so for the y-z plane,

$$\frac{\partial E_z}{\partial y} - \frac{\partial E_y}{\partial z} = -\mu \frac{\partial H_x}{\partial t} \qquad (5.9)$$

Similarly for the series connection in the x-y plane,

$$\frac{\partial E_y}{\partial x} - \frac{\partial E_x}{\partial y} = -\mu \frac{\partial H_z}{\partial t} \qquad (5.10)$$

Equations 5.8, 5.9 and 5.10 make up half of Maxwell's equations. The remaining half of the equation may be obtained from the series connection in the x-z plane connected to the parallel connection in the y-z and x-y planes shown in Fig. 5.5. Thus, the equations describing the circuit of Fig. 5.5 are,

$$\frac{\partial E_x}{\partial z} - \frac{\partial E_z}{\partial x} = -\mu \frac{\partial H_y}{\partial t} \qquad (5.11)$$

$$\frac{\partial H_z}{\partial y} - \frac{\partial H_y}{\partial z} = \varepsilon \frac{\partial E_x}{\partial t} \qquad (5.12)$$

$$\frac{\partial H_y}{\partial x} - \frac{\partial H_x}{\partial y} = \varepsilon \frac{\partial E_z}{\partial t} \qquad (5.13)$$

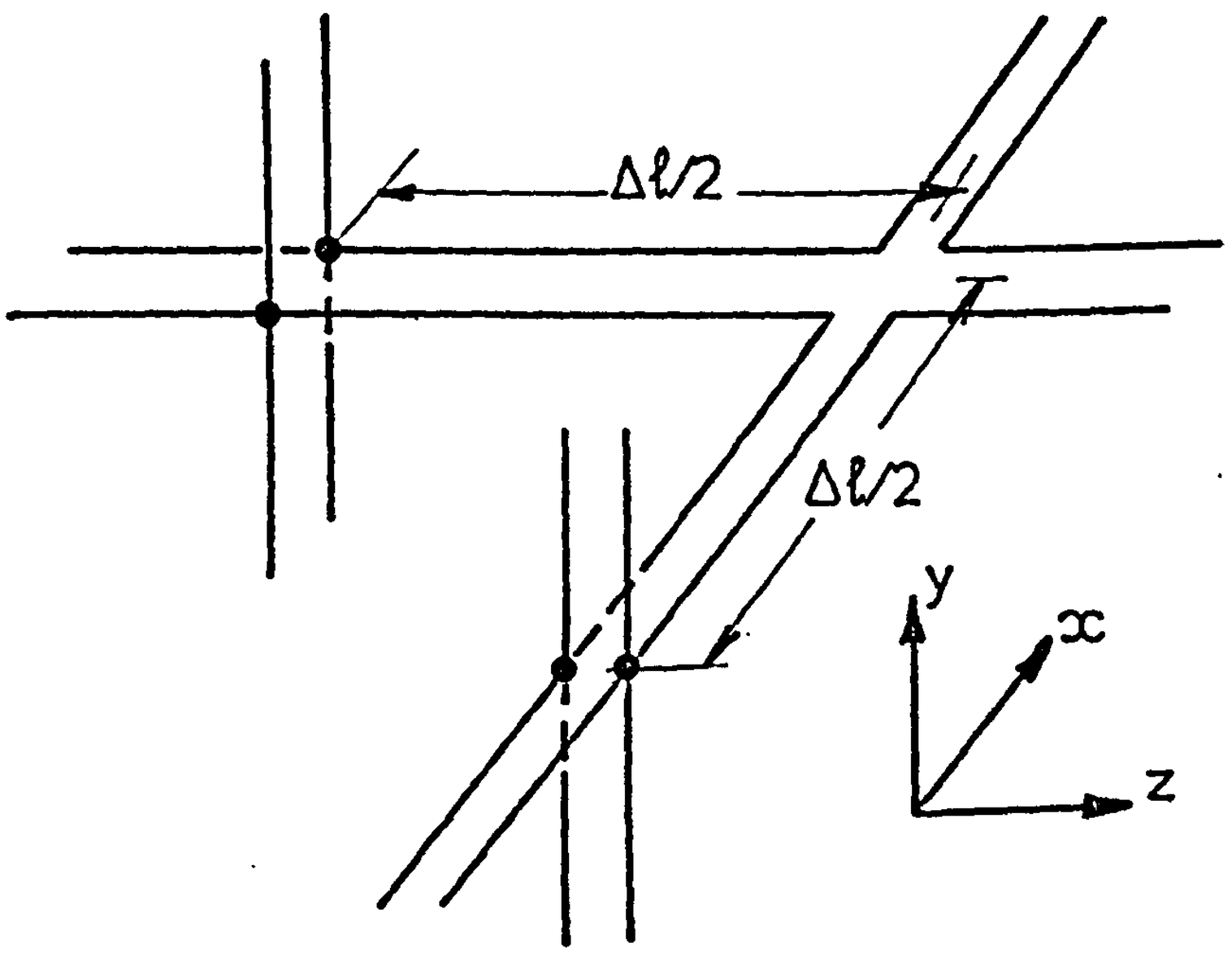

FIG. 5.4 Part of a 3-D node containing one shunt and two series connected nodes

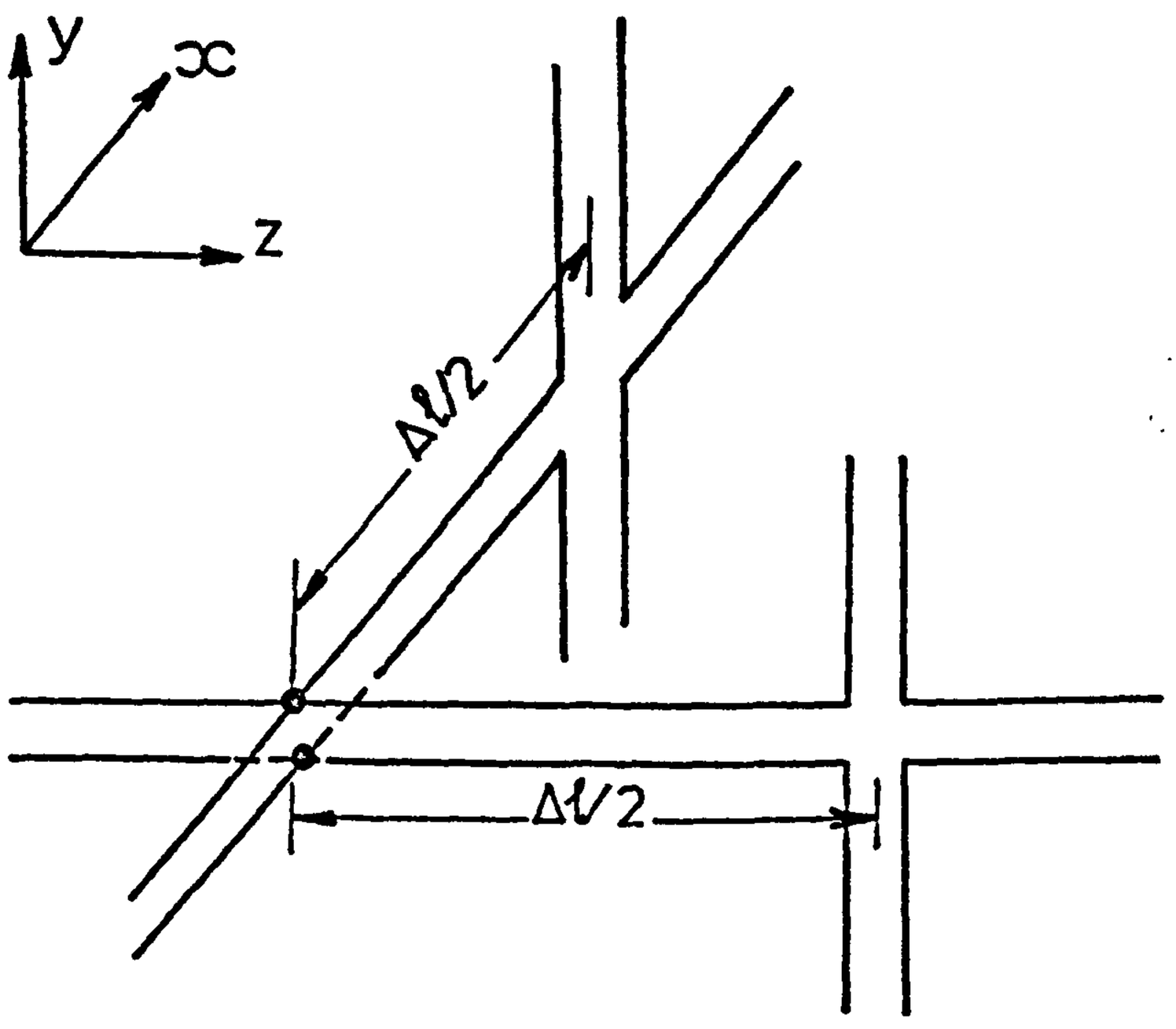

FIG. 5.5 Part of a 3-D node containing two shunt and one series connected nodes

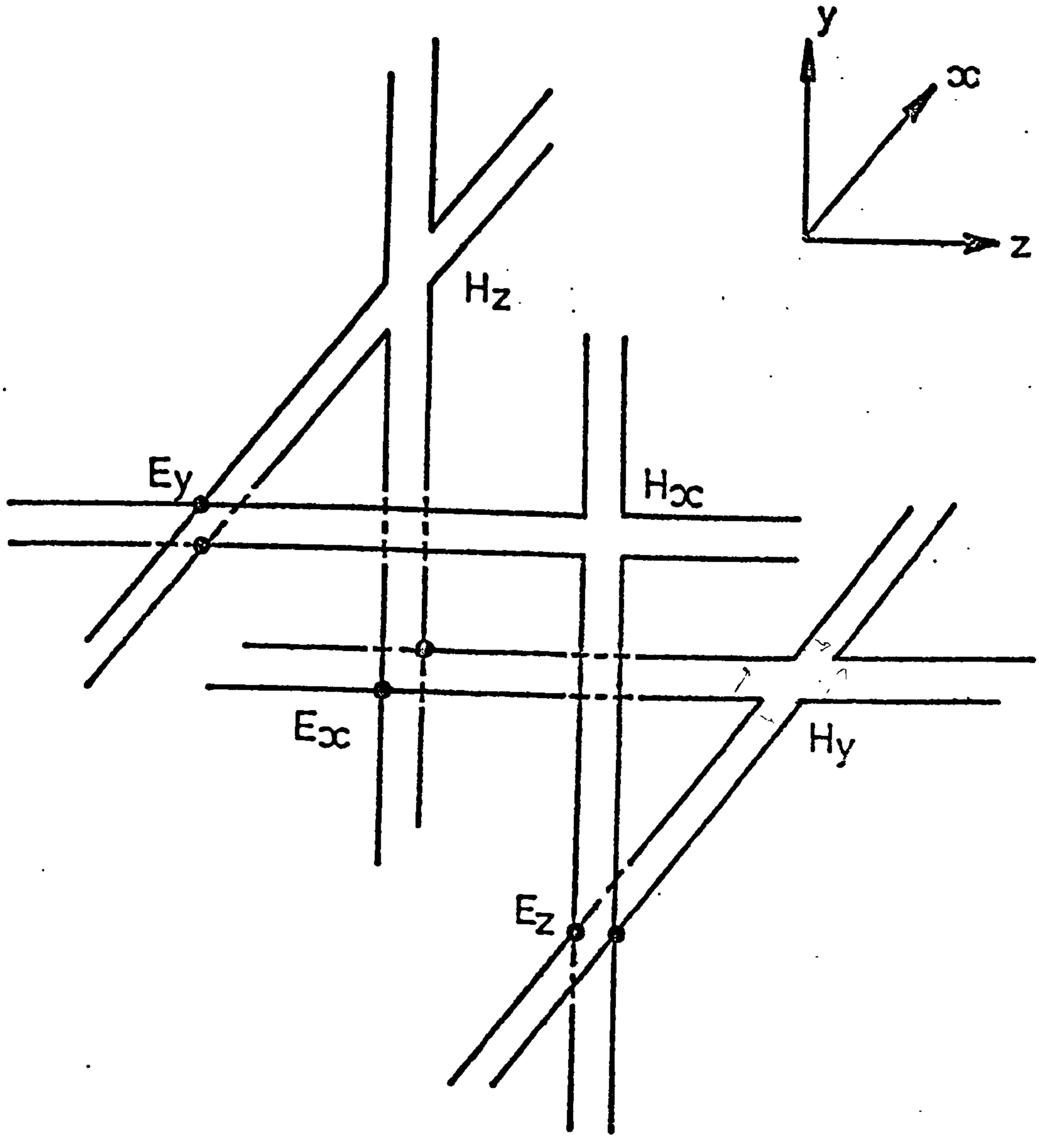

FIG. 5.6 A three-dimensional node

If the circuit of Fig. 5.4 is connected to the circuit of Fig. 5.5, a complete description of Maxwell's equations is given. The configuration is shown in Fig. 5.6 and this may be used to produce a three-dimensional network model as shown in Fig. 5.7. (Note that in Fig. 5.7 single lines are used to represent a pair of wires.) The model produced in this way has alternate series and parallel planes in any of the co-ordinate directions as originally envisaged at the beginning of this section.

5.4 PROPERTIES OF THE THREE-DIMENSIONAL MATRIX

Like the two-dimensional matrix, the three-dimensional matrix of Fig. 5.7 is also a slow-wave structure, and its slow wave properties may be understood by considering the propagation of plane waves. For example, consider the propagation of a one-dimensional plane wave along one of the co-ordinate axes, say z-axis. This can be represented by propagation along a one-dimensional line with short-circuited series stubs and open-circuited shunt stubs as shown in Fig. 5.8. This line may be examined by following a similar procedure used for the two-dimensional matrices.

If $\theta = \frac{\omega \Delta \ell}{c} = 2\pi \frac{\Delta \ell}{\lambda}$, and

$$\mathbf{T} = \begin{bmatrix} \cos\theta/4 & j\sin\theta/4 \\ j\sin\theta/4 & \cos\theta/4 \end{bmatrix} \qquad (5.14)$$

then the voltage and current propagation, taking permittivity- and permeability-stubs (not shown in Fig. 5.8) into account, is described by,

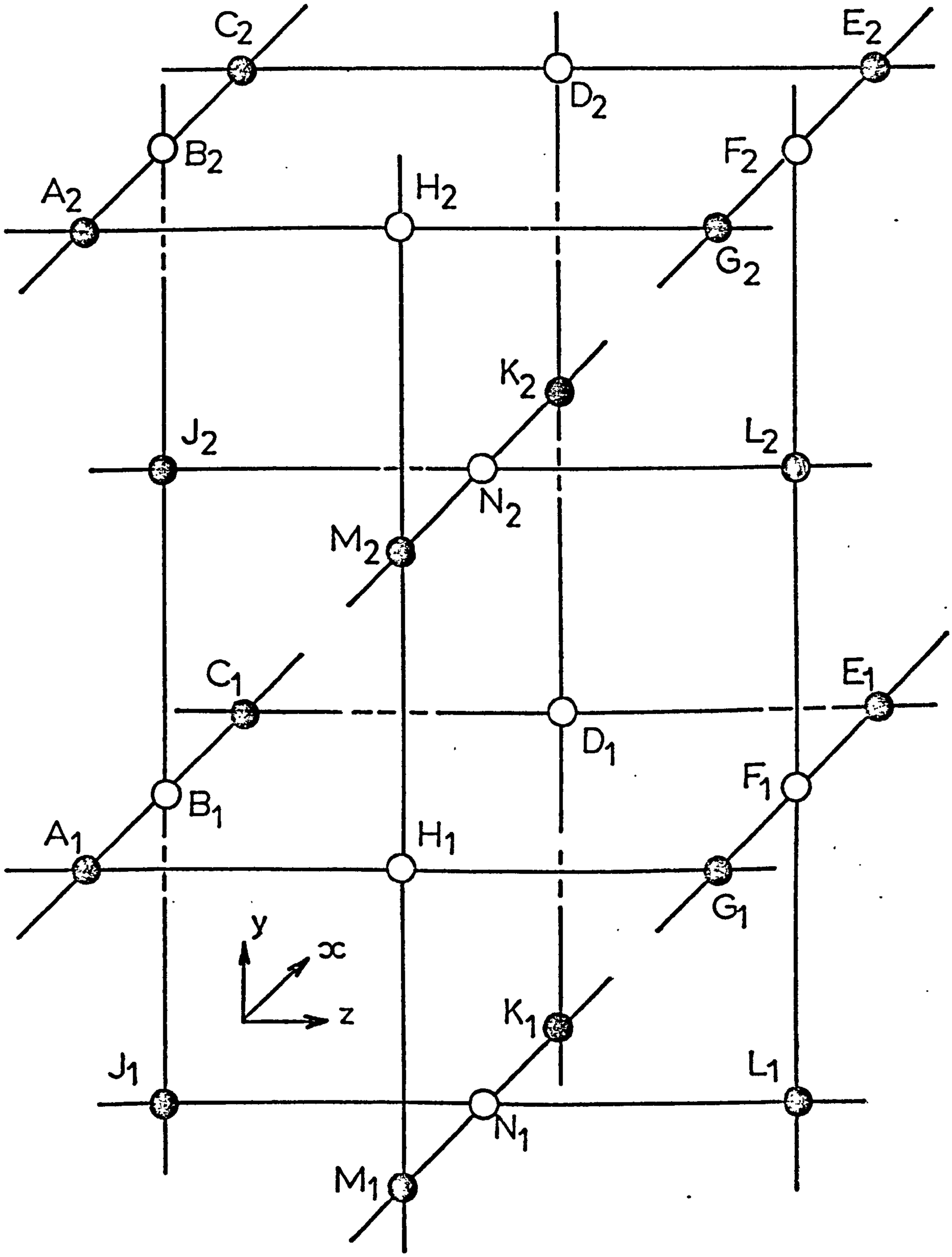

FIG. 5.7 Three-dimensional network model

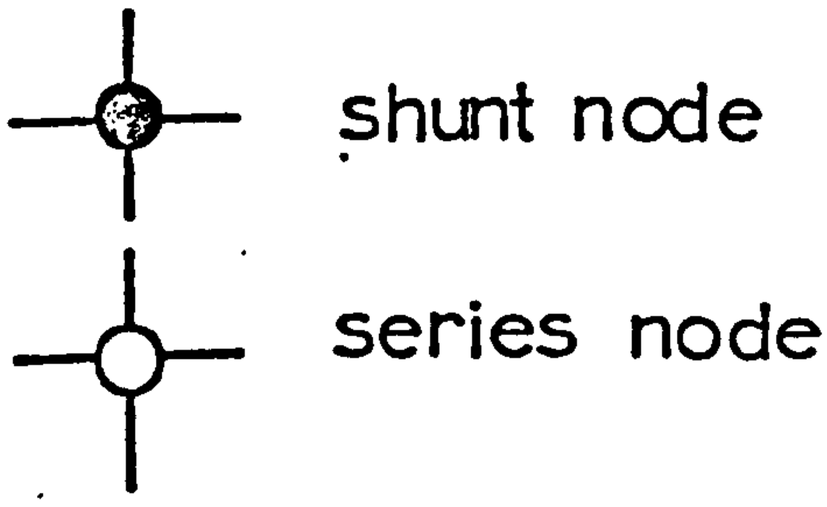

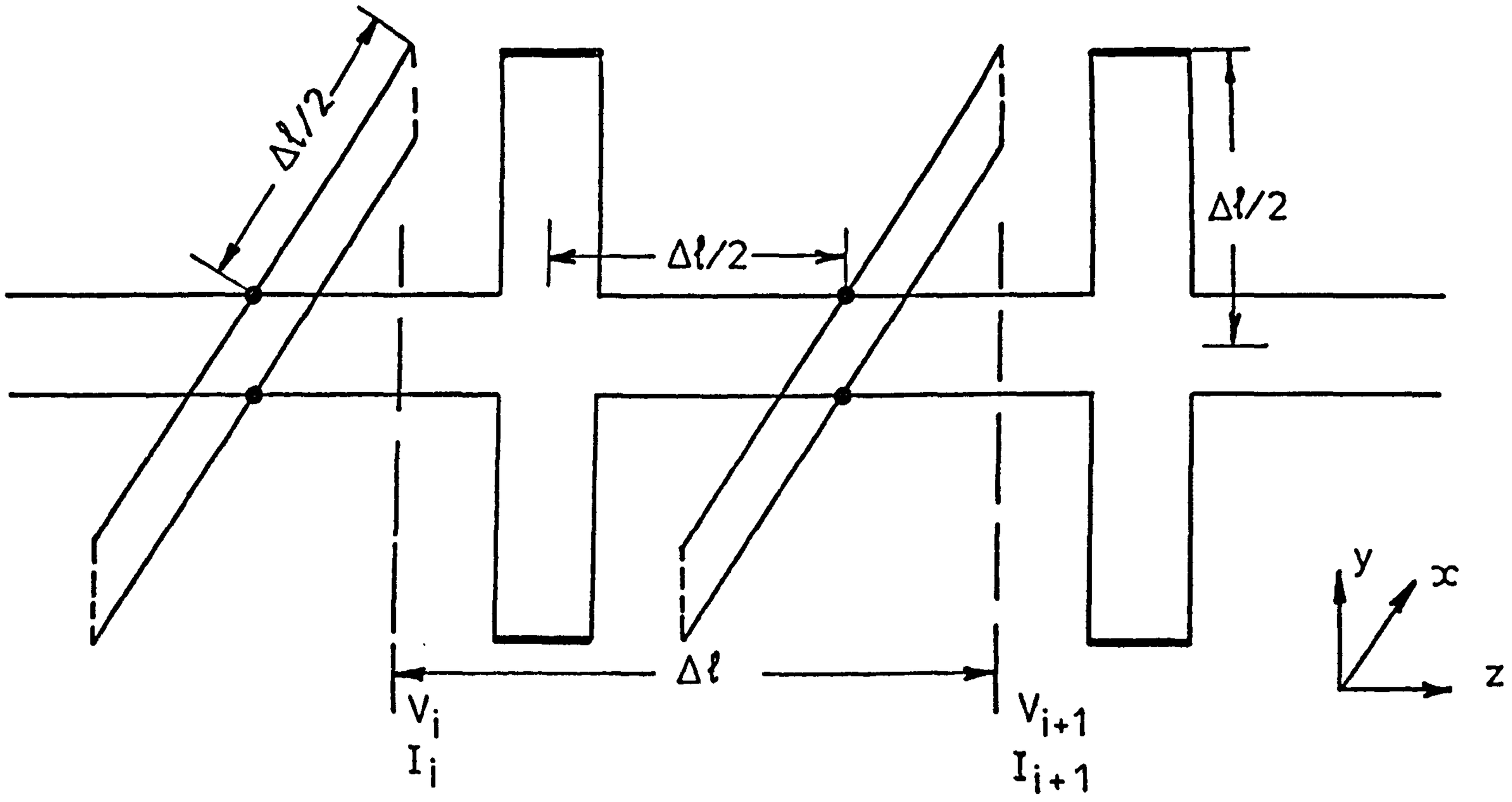

FIG. 5.8 Equivalent network for the waves propagating in the z direction only

short circuit

open circuit

$$\begin{pmatrix} V_i \\ I_i \end{pmatrix} = T \cdot \begin{pmatrix} 1 & j(2+Z_o)\tan\theta/2 \\ 0 & 1 \end{pmatrix} \cdot T \cdot$$

$$T \cdot \begin{pmatrix} 1 & 0 \\ j(2+Y_o)\tan\theta/2 & 1 \end{pmatrix} \cdot T \cdot \begin{pmatrix} V_{i+1} \\ I_{i+1} \end{pmatrix} \qquad (5.15)$$

If the waves on the periodic structure have a propagation constant $\gamma_n = \alpha_n + j\beta_n$ then,

$$\begin{pmatrix} V_i \\ I_i \end{pmatrix} = \begin{pmatrix} e^{\gamma_n \Delta\ell} & 0 \\ 0 & e^{\gamma_n \Delta\ell} \end{pmatrix} \cdot \begin{pmatrix} V_{i+1} \\ I_{i+1} \end{pmatrix} \qquad (5.16)$$

Solution of equations 5.15 and 5.16 gives

$$\text{Cosh}\ \gamma_n \Delta\ell = 1 - 8(1+Y_o/4)(1+Z_o/4)\sin^2\theta/2 \qquad (5.17)$$

which for the low frequency pass-band reduces to

$$\sin(\beta_n \frac{\Delta\ell}{2}) = 2\sqrt{(1+Y_o/4)(1+Z_o/4)}\ \sin(\frac{\omega\Delta\ell}{2c}) \qquad (5.18)$$

Equation 5.18 indicates that for low frequencies the "mass action" wave on the matrix travels at $1/2\sqrt{(1+Y_o/4)(1+Z_o/4)}$ times the velocity of the individual pulses. This result is consistent with the low frequency lumped approximation that the shunt stubs increase the capacitance (C) per unit length of the line by $(2+Y_o/2)$ times and the series stubs increase the inductance (L) per unit length by $(2+Z_o/2)$ times. Thus, if the free space velocity, c, is given by

$$c = \frac{1}{\sqrt{LC}} \qquad (5.19)$$

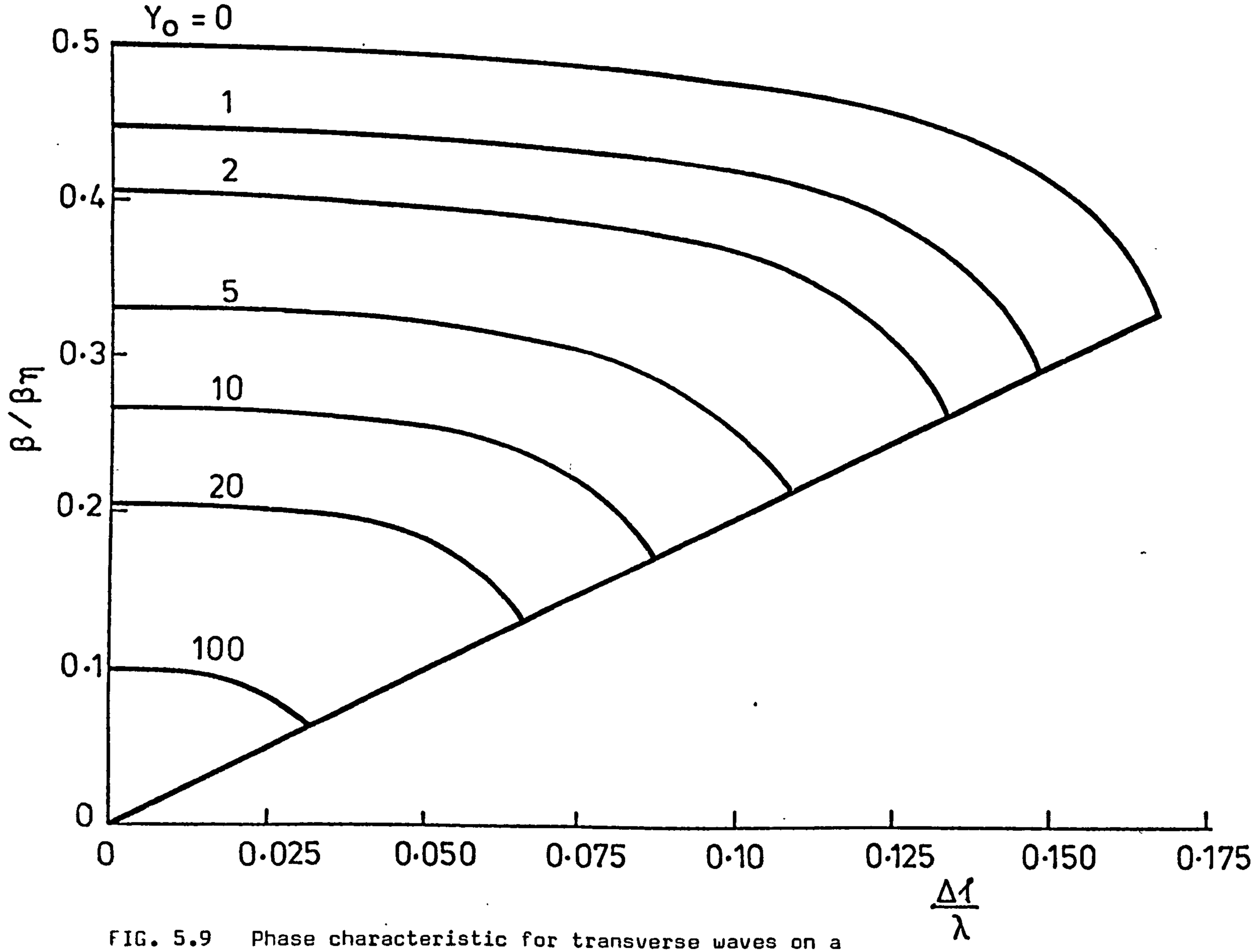

FIG. 5.9 Phase characteristic for transverse waves on a three-dimensional matrix

then the low frequency velocity of waves on the matrix v_n is given by,

$$v_n = \frac{1}{\sqrt{(2+Z_o/2)L.(2+Y_o/2)C}} = \frac{c}{2\sqrt{(1+Y_o/4)(1+Z_o/4)}} \qquad (5.20)$$

In the same way, it can be shown that the low frequency velocity of the wave propagationalong any other direction other than the co-ordinate directions is still $c/2\sqrt{(1+Y_o/4)(1+Z_o/4)}$.

Graphical representation of equation 5.18 for the case $Z_o=0$ is shown in Fig. 5.9. This figure clearly shows that the waves on the matrix along the co-ordinate axes cut off at some frequency, $\frac{\Delta\ell}{\lambda}$. The cut-off frequency is determined by the values of Y_o and Z_o and from equation 5.18. This is given by

$$\left(\frac{\Delta\ell}{\lambda}\right)_{\text{cut off}} = \frac{1}{\pi}\sin^{-1}\left[\frac{1}{2\sqrt{(1+Y_o/4)(1+Z_o/4)}}\right] \qquad (5.21)$$

5.5 DIELECTRIC LOSSES IN THREE-DIMENSIONS

The dielectric losses in the three-dimensional method are treated in a similar way to that explained for the two-dimensional method (section 2.3). To account for any dielectric losses present in a medium, the three-dimensional node of Fig. 5.6, further to permittivity- and permeability-stubs (not shown) is equipped with stubs of infinite length and characteristic admittance G_o (relative to the unity for that of the main lines) at shunt nodes (Fig. 5.10). At low frequencies, the effect of the loss-stub is to increase the conductance per unit length of the main lines by $\frac{G_o}{Z_o\Delta\ell}$, where Z_o is the characteristic impedance of the free space. Bearing in mind that any pulse reflected on

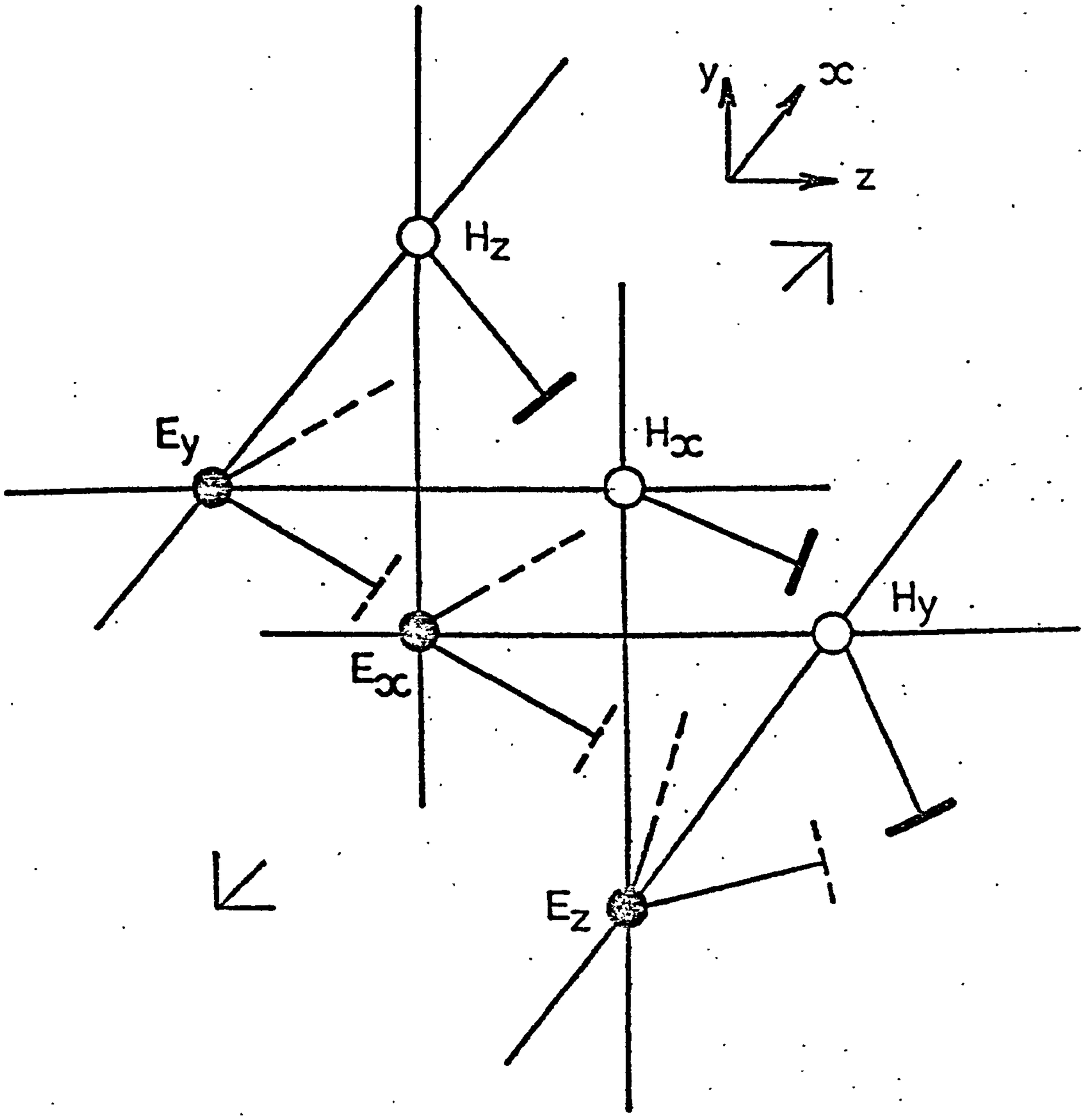

FIG. 5.10 Schematic diagram of a three-dimensional node including the permittivity, permeability- and loss-stubs (two-dimensional node separation and stub length = $\Delta\ell/2$)

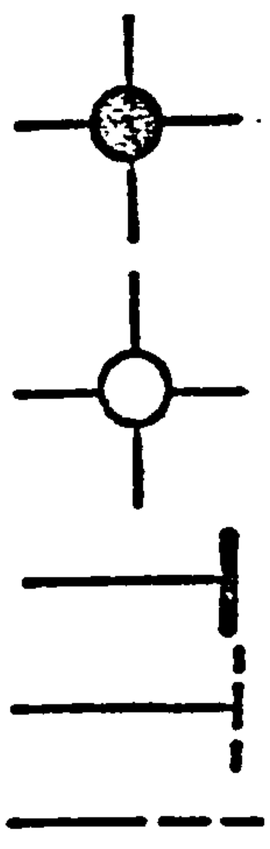

shunt node

series node

short circuited stub (permeability - stub)

open circuited stub (permittivity - stub)

infinitley long stub (loss-stub)

the loss-stub will not return to the node, the three-dimensional model network will then represent a lossy space of conductivity

$$\sigma = \frac{G_o}{Z_o \Delta \ell} \tag{5.22}$$

Thus, the losses on the matrix may be made variable simply by altering the value of the constant G_o. The voltage scattering matrix for a shunt node, including the loss-stub, is as given in equations 2.2 and 2.4.

5.6 BOUNDARIES

Having established a model for describing the space in three dimensions, it is now necessary to define a way of representing the boundaries of a problem. For this purpose, the conducting boundary planes of a problem are represented by short-circuit planes on the matrix. The open-circuit walls of symmetry are represented by open-circuit planes on the matrix. The symmetry wall in the matrix must be positioned so it will not disturb the periodicity of the matrix model. For example, an open-circuit boundary cutting through a line half-way between a series and a shunt node in Fig. 5.6 is not acceptable since the periodicity of the matrix will be disturbed. This is because one would expect a mirror image of series (or shunt) node on either side of the symmetry wall. Therefore, we are restricted to having walls of symmetry which actually cut through the nodes. Of course, this would satisfy the above condition; however, we are at liberty to position a conducting (short-circuit) boundary in any desired plane, whether half-way on the lines or indeed through the nodes.

With due regard to the above positioning alternatives for a boundary, one must try to search for the best choice to obtain a simple and easy numerical procedure. With this aim in mind, let us further examine the possibilities of boundary planes through the nodes. Referring to Fig. 5.6, we see that if a short-circuit boundary passes through shunt nodes in planes at right angles to it, then all the lines joining at these nodes will automatically be short-circuited. The opposite will be true for an open-circuit boundary. But if the particular nodes at a boundary lie in the plane of the boundary, the matter will be complicated due to change in impedance of the lines (and hence scattering matrix of the nodes) lying on the boundary. Therefore, all the above possibilities were considered in much detail and after much programming and observing the results, the best choice emerged as follows.

Referring to Fig. 5.7, a conducting plane in the x-y plane is represented by short-circuiting the shunt nodes A, C and J or E, G and L, and in the x-z plane by short-circuiting the nodes J, K, L and M and finally in the y-z plane by short-circuiting the nodes A, G and M. The open-circuit boundaries are set through series nodes that lie in planes at right angles to the boundaries. In this way, as already explained, the symmetry of the matrix on either side of the open-circuit boundary is preserved.

Having defined our boundaries as such, we can now represent exactly a rectangular cavity in three dimensions. The cavity could also be of a more complicated configuration with right angle corners. Cavities with curved boundaries and non-right angular corners can be approximated by using finer meshes.

Now let us examine the dielectric boundaries due to inhomogeneities inside a cavity. In the TLM model, auxiliary stubs (permittivity, permeability and losses) on a main line, control the properties of the represented medium in the line direction. The influence of the stub extends $\Delta\ell/2$ on the line either side of the stub. For example, in Fig. 5.7, the permittivity-stubs (not shown) on the shunt nodes K_1, L_1, M_1 and J_1 describe the permittivity of the medium in the positive y-direction, as far as a plane through the shunt nodes A_1, C_1, E_1 and G_1. Therefore, the boundary of a dielectric discontinuity, say in the y-direction, always falls on a plane through the shunt nodes A_n, C_n, E_n and G_n. All permittivity stubs below this plane will have a value of, say, Y_o and a value of Y_o' above the plane. Now a question arises - do we assume dielectric stub values of Y_o or Y_o' for the shunt nodes lying on the boundary plane? Or, indeed, should we assume an average value $(Y_o + Y_o')/2$, which seems to be most ideal? Careful examination of the alternatives showed that the latter, although best suited, would be undesirable from the computing point of view. This is because the computer program will have to deal with more than one value of permittivity within a 3-D node which would increase the storage requirements considerably. However, it was found that the error in taking a value of Y_o or Y_o' for the stubs on the boundary is comparatively small and perfectly acceptable in all cases considered. An example of this is shown in the next chapter (Fig. 6.1).

Conducting strips inside a cavity are treated and positioned in the same way as the conducting boundaries. However, it is required to define straight edges for the strip with no corrugation since the strips do not necessarily extend across any dimensions of the cavity. For this requirement to be possible, the strip in a plane must have its edges coincide with a row of shunt nodes in that plane. This would satisfy the above condition since all these shunt nodes will be short-circuited and no voltage impulse will be able to penetrate the strip edges.

From these discussions we realise that a conducting boundary such as a strip, and a dielectric discontinuity boundary, may not lie on the same plane in the model. This means that, say, for a strip laid on a dielectric we would have some dielectric overflow over the sides of the strip. The dielectric overflow has been found to be acceptable through numerous examples of microstrip cavities performed. The effect is especially negligible if the dielectric thickness is defined with no less than two or three 3-D nodes. In fact, as shown in Fig. 6.8, the results for a microstrip cavity with the dielectric thickness defined with only one 3-D node has proved highly successful.

5.7 NUMERICAL PROCEDURE

Any of the six electromagnetic field components may be excited by introducing impulses at various points in the network. These impulses travel along the ideal TEM lines and are scattered at the individual two-dimensional nodes according to equations 2.2 and 5.4. In this way, the time domain propagation of all six

field components is obtained simultaneously. Dielectric losses are accounted for by the procedure described in section 5.5. The boundaries may be made lossy by using imperfect reflection coefficients as described in chapter 3 or by introducing losses at the nodes on the boundary.

A solution for any (or all) of the field components is available anywhere within the geometry of the problem. The output consists of a stream of impulse amplitudes corresponding to the output impulse function for the particular field component under consideration. For analysis purposes, it is usual to take the Fourier transform of this function to yield the response to an excitation varying sinusoidally with time.

5.8 THREE-DIMENSIONAL COMPUTER PROGRAM

A general three-dimensional program has been written on the preceding analysis. The final form of this program,as listed in Fig. 5.11, is highly efficient and versatile. Considerable effort was put into minimising the storage requirements of the method. One real memory store is used to store the value of the pulse on a main line that joins a shunt node to a series node. For this to be possible, pulses throughout the model must converge on the similar nodes (shunt or series) at any instant of time. This, in turn calls for a purely E-field (or H-field) initial excitation, i.e. the pulses on the model at the start of the first iteration process need to be incident on shunt nodes (or series nodes).

```
      MASTER TLM

      DIMENSION V(26,8,8,27)IS(S1,6),IE(S1,7)
      DIMENSION EU(S1),SX(S1),SY(S1)SZ(S1),VA(S1),LS(S1),IEC(S,3)
      COMMON/COM3/EH(800)
      DATA IEC,NX,NY,NZ,KS,KE/1,2,3,4,13,5,6,7,8,14,9,10,11,12,15,S*0/

C     READ IN BLOCKS OF MEDIA AND BOUNDARIES
 23   KS=KS+1
      READ(S,200)(IS(KS,M),M=1,6),EU(KS),SX(KS),SY(KS),SZ(KS),LS(KS)

      IF(NZ.LT.IS(KS,6)) NZ=IS(KS,6)
      IF(NY.LT.IS(KS,4)) NY=IS(KS,4)
      IF(NX.LT.IS(KS,2)) NX=IS(KS,2)

      IF(IS(KS,1))24,24,23
 24   KS=KS-1

C     READ IN EXCITATION VALUES
 33   KE=KE+1
      READ(5,100)(IE(KE,M),M=1,7),VA(KE)
      IF(IE(KE,1)) 44,44,33
 44   KE=KE-1

C     READ IN REQUESTED OUTPUT POINT, COMPONENT FIELD AND NO. OF
      ITERATIONS
      READ(S,100)IO,JO,KO,L,NI

 100  FORMAT(7IS,F10.6)
 200  FORMAT(6IS,4f10.6,I1)

C     CLEAR THE MATRIX
      NZZ=NZ+1
      NYY=NY+1
      NXX=NX+1
      DO 1 K=1,NZZ
      DO 1 J=1,NYY
      DO 1 I=1,NXX
      DO 1 M=1,26
 1    V(M,I,J,K)=0.0

C     SET INITIAL VALUES
      DO 7 NS=1,KS
      LX=4*LS(NS)
      DO 7 K=IS(NS,5),IS(NS,6)
      DO 7 J=IS(NS,3),IS(NS,4)
      DO 7 I=IS(NS,1),IS(NS,2)
      V(16+LX,I,J,K)=4.*(EU(NS)-1.)
      V(17+LX,I,J,K)=2./(4.+V(16+LX,I,J,K)+SX(NS))
      IF(SX(NS).EQ.999.) V(17+LX,I,J,K)=0.0

      V(18+LX,I,J,K)=2./(4.+V(16+LX,I,J,K)+SY(NS))
      IF(SY(NS).EQ.999.) V(18+LX,I,J,K)=0.0

      V(19+LX,I,J,K)=2./(4.+V(16+LX,I,J,K)+SZ(NS))
      IF(SZ(NS).EQ.999.) V(19+LX,I,J,K)=0.0

      DO 2 NE=1,KE
      DO 2 K=IE(NE,5),IE(NE,6)
      DO 2 J=IE(NE,3),IE(NE,4)
      DO 2 I=IE(NE,1),IE(NE,2)
      DO 2 N=1,5
 2    V(IEC(N,IE(NE,7)),I,J,K)=VA(NE)

C     START THE ITERATION PROCESS
      DO 6 IC=1,NI
      DO 5 K=1,NZ
      DO 5 J=1,NY
      DO 5 I=1,NX
      CALL S(V(11,I,J,K),V(7,I,J,K),V(9,I,J+1,K),V(5,I,J,K+1),
     X       V(24,I,J,K),V(20,I,J,K),V(21,I,J,K))
      CALL S(V(10,I,J,K),V(4,I,J,K),V(12,I+1,J,K),V(2,I,J,K+1),
     X       V(25,I,J,K),V(20,I,J,K),V(22,I,J,K))
 5    CALL S(V(3,I,J,K),V(8,I,J,K),V(1,I,J+1,K),V(6,I+1,J,K),
           V(26,I,J,K),V(20,I,J,K),V(23,I,J,K))
      DO 4 K=1,NZZ
      DO 4 J=1,NYY
      DO 4 I=1,NXX
      CALL P(V(1,I,J,K),V(2,I,J,K),V(3,I,J,K),V(4,I,J,K),V(13,I,J,K),
     X       V(16,I,J,K),V(17,I,J,K))
      CALL P(V(5,I,J,K),V(6,I,J,K),V(7,I,J,K),V(8,I,J,K),V(14,I,J,K),
     X       V(16,I,J,K),V(18,I,J,K))
 4    CALL P(V(9,I,J,K),V(10,I,J,K),V(11,I,J,K),V(12,I,J,K),V(15,I,J,K)
     X       V(16,I,J,K),V(19,I,J,K))

C     EVALUATE AND STORE REQUESTED OUTPUT IMPULSE FUNCTION
      GO TO (66,77,88),L
 66   X=2.0*(V(1,IO,JO,KO)+V(2,IO,JO,KO)+V(3,IO,JO,KO)+V(4,IO,JO,KO)+
     X       V(16,IO,JO,KO)*V(13,IO,JO,KO))/(4.0+V(16,IO,JO,KO))
      GO TO 6
 77   X=2.0*(V(5,IO,JO,KO)+V(6,IO,JO,KO)+V(7,IO,JO,KO)+V(8,IO,JO,KO)+
     X       V(16,IO,JO,KO)*V(14,IO,JO,KO))/(4.0+V(16,IO,JO,KO))
      GO TO 6
 88   X=2.0*(V(9,IO,JO,KO)+V(10,IO,JO,KO)+V(11,IO,JO,KO)+V(12,IO,JO,KO)
     X       V(16,IO,JO,KO)*V(15,IO,JO,KO)/(4.0+V(16,IO,JO,KO))
 6    EH(IC)=X

C     CALL FOURIER TRANSFORM ROUTINE
      CALL OUTPUT(NI)

      STOP
      END
```

```
      SUBROUTINE P(V1,V2,V3,V4,V5,YO,Y)

C     SHUNT NODAL CALCULATIONS
      A=Y*(V1+V2+V3+V4+YO*V5)
      V1=A-V1
      V2=A-V2
      V3=A-V3
      V4=A-V4
      V5=A-V5

      RETURN
      END

      SUBROUTINE S(V1,V2,V3,V4,V5,ZO,Z)

C     SERIES NODAL CALCULATIONS
      A=Z*(-V1+V2+V3-V4-V5)
      V1=V1+A
      V2=V2-A
      V3=V3-A
      V4=V4+A
      V5=-V5-A*ZO

      RETURN
      END
```

```
      SUBROUTINE OUTPUT(NI)

C     FOURIER TRANSFORM ROUTINE
      COMMON/COM3/EH(800)

      READ(5,1000)D1,D2,DS
 1000 FORMAT(3F10.5)

      D=D1
 111  EHRE=0.0
      EHIM=0.0
      DO 1  IC=1,NI
      FC=6.283184*FLOAT(IC)*D
      EHRE=EHRE+EH(IC)*COS(FC)
 1    EHIM=EHIM-EH(IC)*SIN(FC)
      AMP=SQRT(EHRE*EHRE+EHIM*EHIM)
      WRITE(6,1000)D,AMP
      IF(D.GE.D2) RETURN
      D=D+DS
      GO TO 111

      RETURN
      END
```

FIG. 5.11 The general three-dimensional TLM computer program listing

A computer program on the proposed method basically requires 12 real memory stores per 3-D node (a 3-D node is comprised of 6 two-dimensional elementary nodes). However, a maximum of 23 memory stores is needed if a 3-D node was to be completely equipped with all three kinds of stubs to describe varying permittivity, permeability and also losses in a medium. An additional 3 memory stores will provide for use of planes of symmetry in any one of the three co-ordinate directions. One-fold, two-fold or three-fold symmetry of a problem will help to reduce the storage requirements by about 1/2, 1/4 or 1/8 respectively.

The general program of Fig. 5.11 has been used to obtain all the variety of the results presented in the next chapter. It uses a total of 26 real memory stores per 3-D node. (Note that this general program was used for all examples so that it could be constantly debugged and its efficiency improved in the course of extensive programming). This program has been written in about 110 lines of FORTRAN, including the subroutines. In the program a Fourier transform subroutine similar to the one described in chapter 4 is included. This subroutine provides for the time-to-frequency spectrum transformation of time impulse function obtained in the main program. A different short subroutine is used to calculate the time decay in a lossy wall or lossy dielectric cavity.

5.9 DISCUSSION

The three-dimensional version of the TLM method described in this chapter is an extension of the two-dimensional method and embodies the advantages and experiences gained in the two-dimensions. For example, in the two-dimensions, the conducting boundaries were set half-way between the nodes. This meant that in the computer program, boundary conditions had to be imposed on the neighbouring nodes before each iteration of the matrix, but in the three-dimensional method as explained in section 5.6, the boundaries lie on the nodes. This way, the boundary conditions will automatically be dealt with by simply short-circuiting the permittivity-stubs on the shunt nodes or open-circuiting the permeability-stubs on the series nodes lying on the boundary.

A simple and short program on the three-dimensional method was developed based on the same principles and techniques used in the two-dimensional program described in chapter 4. This program has been used to check the accuracy of the method for a wide range of propagation problems. In particular, some completely and also partially filled cavities with or without conducting strips have been studied. In all cases, results compared with other known methods in the literature have shown good agreement. Results for resonant frequencies and power decay time of some completely and partially filled lossy dielectric cavities are given in chapter 6. Also in chapter 6, the dispersion characteristics of a wide class of microstrip line cavities are presented. These include cavities with the strip conductor laid on a dielectric or

magnetic substrate, the abrupt change in width of a microstrip line and also some coupled lines results. In all cases where comparisons can be made, there has been excellent agreement.

REFERENCES

5.1 AKHTARZAD, S. and JOHNS, P.B. "Solution of 6-component electromagnetic fields in three space dimensions and time by the TLM method", Electron. Lett., 10, pp 535-537, December, 1974.

5.2 JOHNS, P.B. "The solution of inhomogeneous waveguide problems using a transmission-line matrix", I.E.E.E. Trans., MTT-22, pp 210-215, March, 1974.

5.3 AKHTARZAD, S. and JOHNS, P.B. "Generalized elements for the TLM method of numerical analysis", Submitted to Proc. I.E.E., (March, 1975).

5.4 AKHTARZAD, S. and JOHNS, P.B. "The solution of Maxwell's equations in three space dimensions and time by the TLM method of numerical analysis", Submitted to Proc. I.E.E., (March, 1975).

CHAPTER 6

NUMERICAL COMPUTATIONS FOR A WIDE VARIETY OF THREE-DIMENSIONAL RESONATORS USING THE GENERAL TLM COMPUTER PROGRAM

6.1 INTRODUCTION

In this chapter, the general and unique three-dimensional TLM program of Fig. 5.11 is used to analyse a wide variety of three-dimensional microwave cavity structures. The results presented here include the resonant frequency of some empty, completely and also partially filled cavities. The power decay time of some lossy dielectric cavities are also given. In particular, the cavities containing microstrip lines have been studied and the resonant frequency of cavities of various length are used to plot frequency (GHZ) versus dispersive phase constant (β) curves. The microstrip solutions include cavities with strip laid on a magnetic substrate, change in strip width discontinuity and also coupled microstrip lines' cavities. In all cases, whenever possible, the TLM results have been compared with those of analytical or other methods.

With a slight modification to the general program, it is possible to obtain the field distribution for the six components of the electromagnetic field in any desired plane through a cavity. To demonstrate this, the electric and magnetic field distribution of a typical microstrip cavity for different cross-sectional planes are also shown in this chapter.

6.2 COMPLETELY FILLED CAVITIES

6.2.1 Empty Rectangular Cavity

The method is first applied to the simplest form of a three-dimensional problem, i.e. an empty rectangular cavity. Table 6.1

TABLE 6.1

Empty rectangular cavity (dimensions a×b×c)

b/a = 2/3, c/a = 1/2

Mode, True Resonant Frequency	a/Δℓ	Resonant Frequency $k_c a$			
		Albani & Bernardi	Error %	This Method	Error %
TM_{110}, TE_{110}	6			5.5877	1.34
$k_c a$ = 5.6636	12	5.5439	2.11	5.6405	0.41
TE_{101}	6			6.8471	2.53
$k_c a$ = 7.0249	12	6.7560	3.83	6.9743	0.72
TM_{210}, TE_{011}	6			7.6916	2.07
$k_c a$ = 7.8540	12	7.5558	3.80	7.7942	0.76

shows the resonant frequencies of the first few modes in such a cavity. TLM results shown in this table are compared with the analytical results. They are also compared with results given in reference 6.1 by Albani and Bernardi. Albani and Bernardi obtain the solution of six-component electromagnetic fields by direct discretisation of Maxwell's equations in the integral form. The other purpose of Table 6.1 is also to draw a direct comparison between the two numerical methods. In the TLM method, it has been shown that a high degree of accuracy is obtained with only a very few number of nodes, unlike the method adopted by Albani and Bernardi.

6.2.2 Homogeneous Cube Cavity

The method has also been used to calculate the dominant mode resonant frequency of a cube cavity for various combinations of permittivity, ε_r, and permeability, μ_r, values. Results for the homogeneous cube cavity in Table 6.2 show that the TLM method is accurate for permeability-stubs and also for a combination of permeability- and permittivity-stubs.

6.3 PARTIALLY FILLED CAVITIES

Fig. 6.1 shows the structure of a cavity partially filled with dielectric. The dominant mode is LSM (H_y=0), the dispersion equation of which has been derived by Marcuvitz[6.2]. This structure was chosen to test the two cases where values of Y_o=0·0 for ε_r = 1·0 and then Y_o' = 11·28 for ε_r = 3·82 are used on the nodes

TABLE 6.2

Cube cavity (dimension a, $a/\Delta\ell = 7$)

State of Cavity	Resonant Frequency $k_c a$ of Dominant Mode (true $k_c a = 2.7768$)	Error %
$\mu_r = 1.0$ $\varepsilon_r = 2.56$	2.7568	0.66
$\mu_r = 2.56$ $\varepsilon_r = 1.0$	2.7586	0.66
$\mu_r = \sqrt{2.56}$ $\varepsilon_r = \sqrt{2.56}$	2.7595	0.62

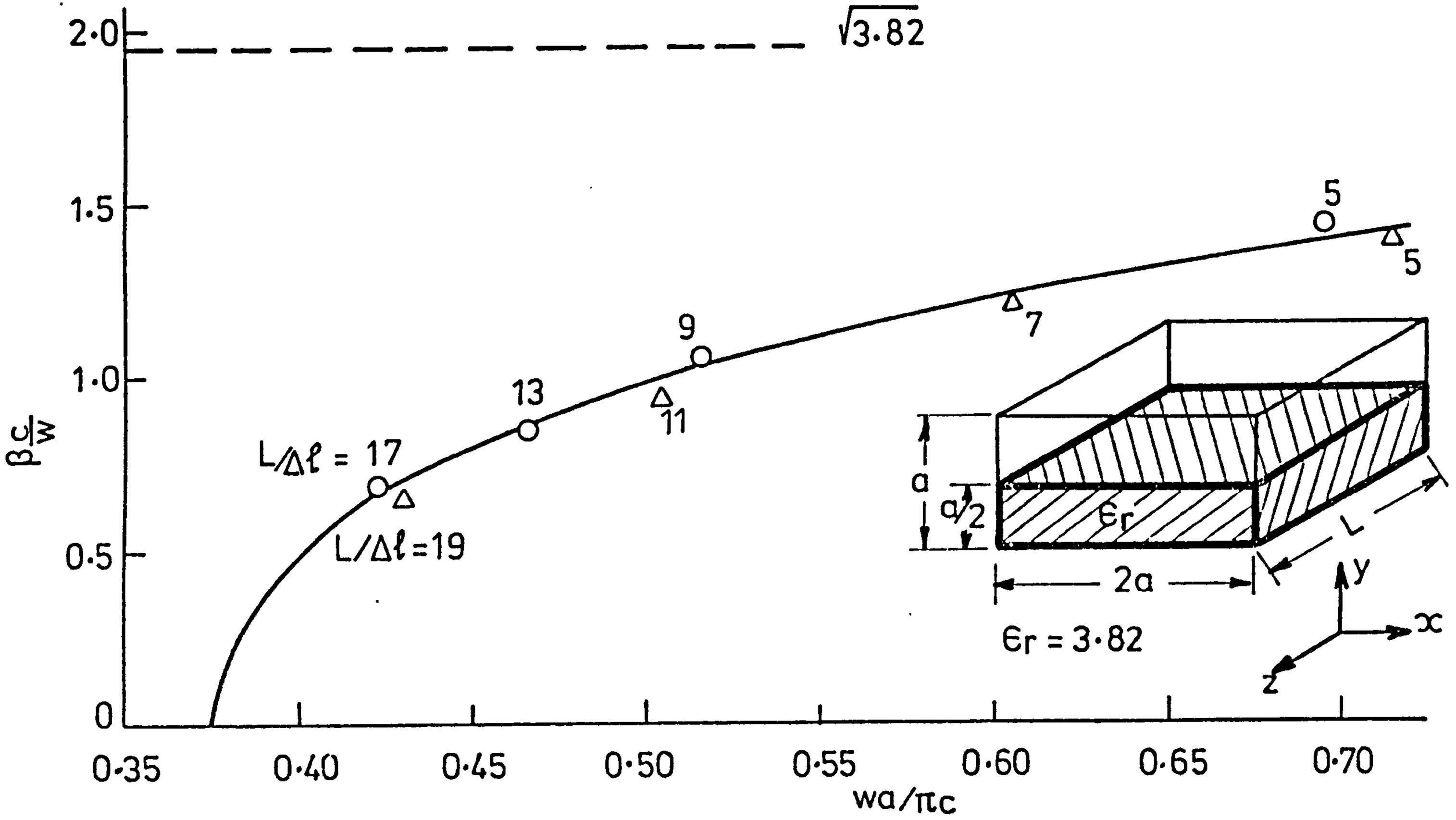

FIG. 6.1 Variations of β with 2a/λ for dominant LSM mode ($a/\Delta\ell = 5$)

△ TLM - dielectric stubs up to Exc, Ez, Hy plane

○ TLM - dielectric stubs up to Ey, Hxc, Hz plane

——— Analytical results

actually at the dielectric boundary (see section 5.6). Results for $\sqrt{\varepsilon_{eff}}$ versus frequency, $2a/\lambda$, are shown in Fig. 6.1. From Fig. 6.1, it can be seen that for values of Y_o equal to zero, results are an upperbound curve, and for values of Y_o' equal to 11·28 results are a lower bound curve compared with the theoretical results. Upperbound and lowerbound behaviour of the numerical curves are due to the slight change in ratio of air-to-dielectric thickness in favour of one or the other.

6.3.1 Dominant LSM Mode Cavity

The accuracy of the method for partially filled cavities is illustrated by calculating the resonant frequencies of the rectangular cavity of Fig. 6.2 for varying values of length, b. The cavity is excited with a single line of the field E_y in order to enhance the $H_{mo\ell}$ type of modes, of which the H_{101} type of mode is the dominant. Of course, the dielectric perturbs the mode from the true $H_{mo\ell}$ rectangular mode to yield fields varying in the three co-ordinate directions, and in this case, the result is the LSM mode for which analytical answers are available[6·2]. The asymptotic behaviour of the $\bar{\beta}$-frequency curve for this mode makes it realistic to compare numerical and analytical results for $2a/\lambda$ in some cases, and $\bar{\beta}$ in others. These results are shown in Table 6.3.

6.3.2 Cavity with Dielectric Discontinuity in One, Two and Three Directions

Some examples of inhomogeneous rectangular cavities given by Albani and Bernardi[6·3] were tried for the purpose of comparison

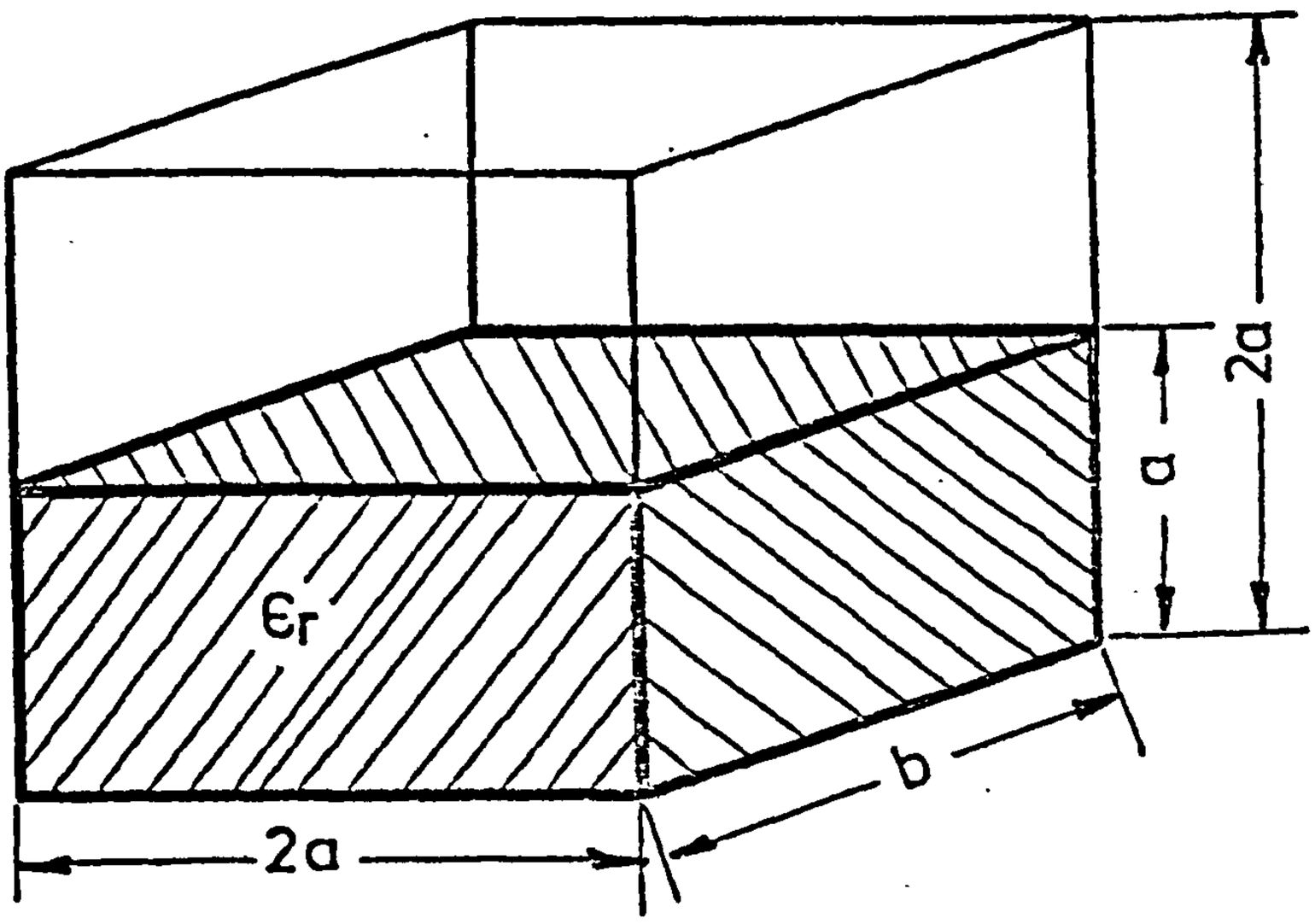

FIG. 6.2 Rectangular cavity loaded with a dielectric slab ($\epsilon_r = 2.45$, $\frac{2a}{\Delta\ell} = 7, \frac{b}{\Delta\ell} = 3,4,5,6,7,8,9,10$)

TABLE 6.3

Cavity of Fig. 6.2. Dominant LSM mode.

$\frac{b}{\Delta \ell}$	$\bar{\beta} = \frac{\beta c}{\omega}$			$\frac{2a}{\lambda} = \frac{\omega a}{\pi c}$		
	TLM	theoretical	error %	TLM	theoretical	error %
3	1.3959	1.3483	3.40	0.8358		
4	1.2626	1.2470	1.24	0.6930		
5	1.1494	1.1493	0.01	0.6090		
6	1.0495			0.5558	0.5506	0.93
7	0.9626			0.5208	0.5132	1.45
8	0.8853			0.4942	0.4868	1.49
9	0.8194			0.4746	0.4683	1.32
10	0.7599			0.4606	0.4541	1.41

of the results. Figs. 6.3, 6.4 and 6.5 show the structure of three examples with Fig. 6.3 having dielectric discontinuity in one direction only, Fig. 6.4 in two directions and Fig. 6.5 in all three directions. Table 6.4 shows the results for dominant resonant frequency of these structures by the TLM method in comparison with the results obtained by Albani and Bernardi.[6.3] Theoretical result for Fig. 6.3 is available and is given in Table 6.4. From this table, it is noticed that for the same mesh coarseness ($a/\Delta\ell = 20$) the TLM result for Fig. 6.3 is much more accurate than the result given by reference 6.3. In reference 6.3, Albani and Bernardi predict an 8% error for the results of Fig. 6.4 and Fig. 6.5. Estimated error of the TLM results for these figures is less than 1%.

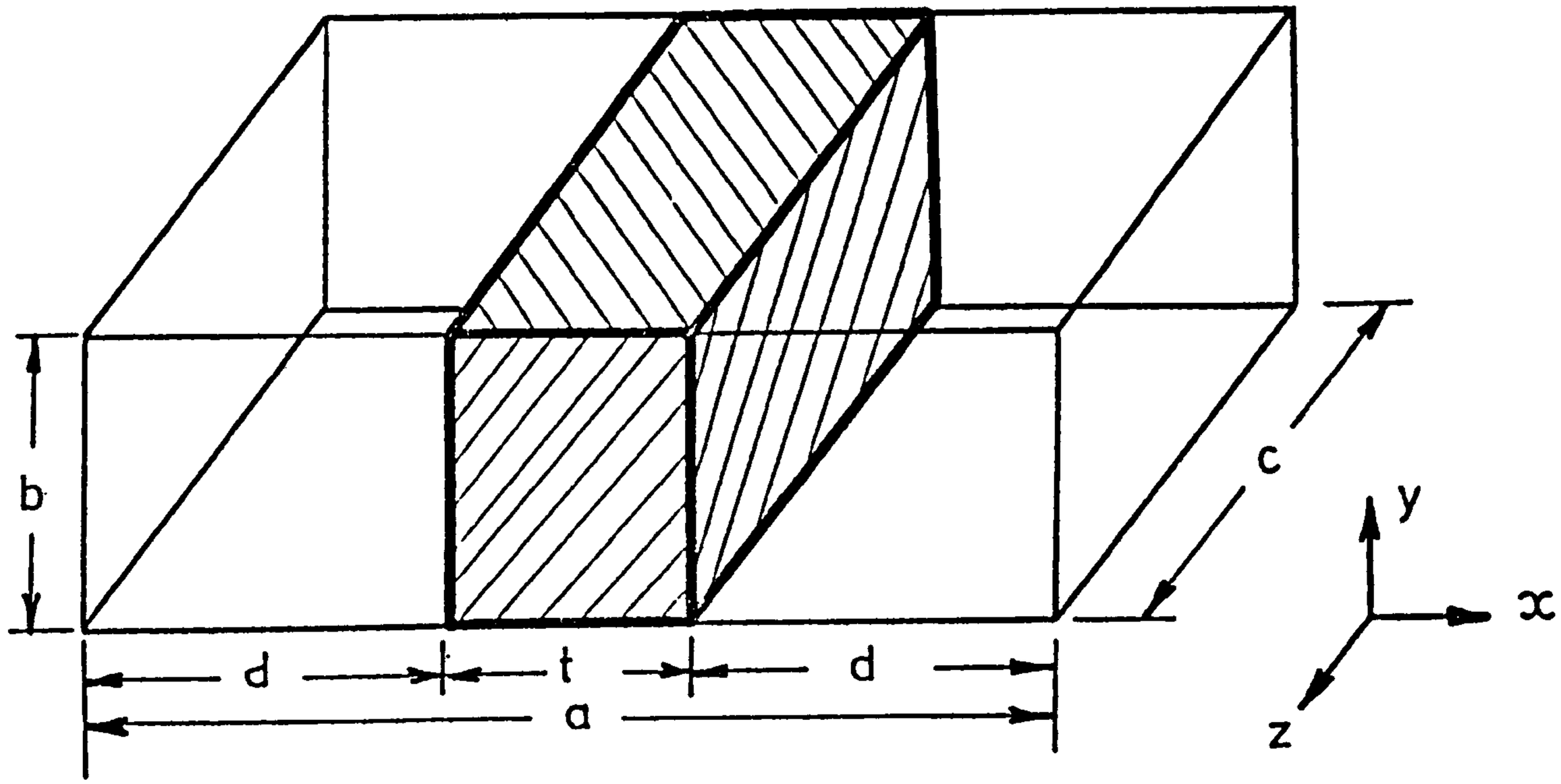

FIG. 6.3 Rectangular cavity loaded with a dielectric slab ($\varepsilon_r = 16$), t/a = 1/4, b/a = 3/10, c/a = 4/10

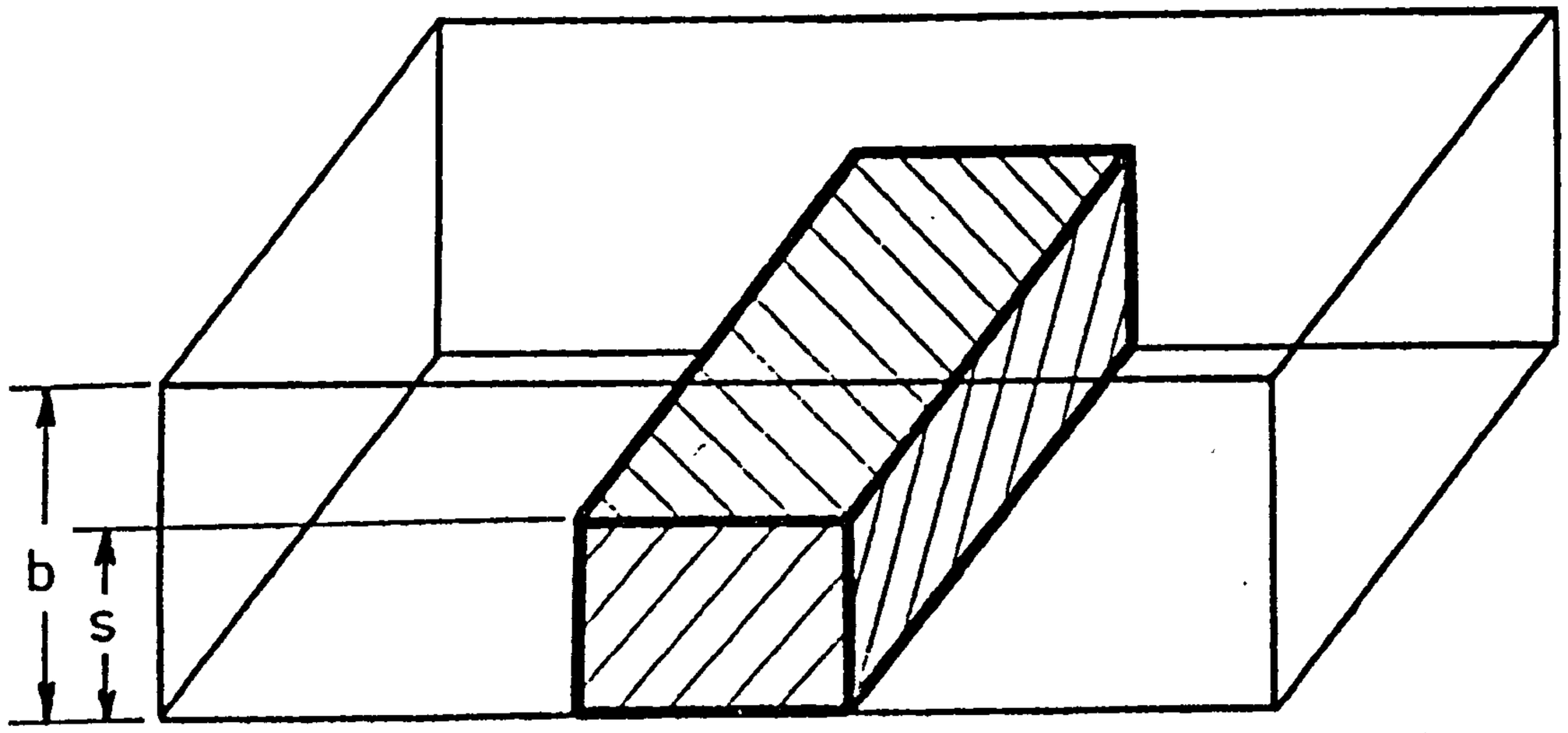

FIG. 6.4 Same as Fig. 6.3, s/b = 7/12

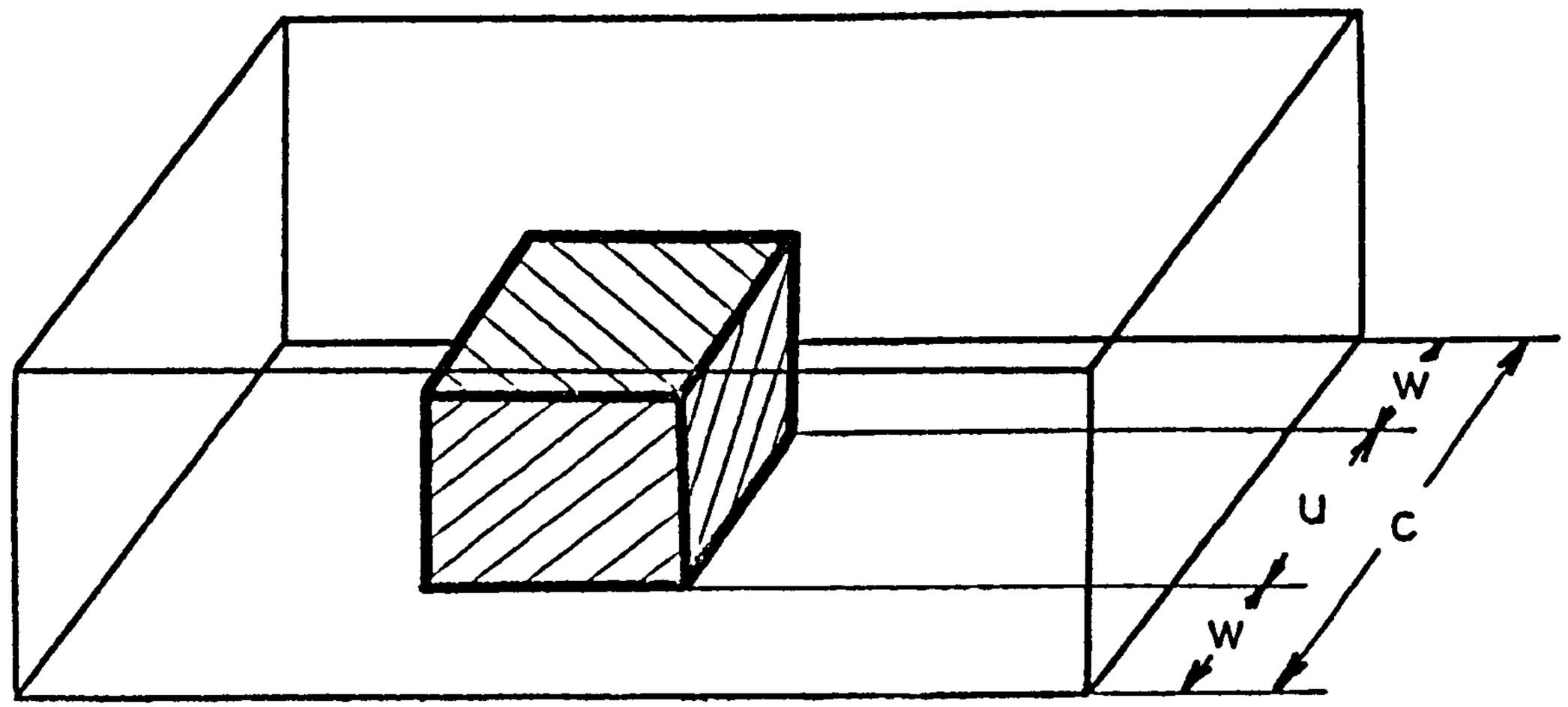

FIG. 6.5 Same as Fig. 6.4, u/c = 3/8

TABLE 6.4

Cavities in Figs. 6.3, 6.4, 6.5. Dominant Mode

Cavity $a/\Delta\ell = 20$	Resonant Frequency $k_c a$				
	Theoretical	Albani & Bernardi	Error %	This Method	Error %
Fig. 6.3 (TE_{101} Mode)	2.5829	2.4292	5.95	2.5761	0.26
Fig. 6.4		3.447	8.0*	3.5387	<1.0*
Fig. 6.5		4.907	8.0*	5.5920	<1.0*

* estimated

6.4 EXAMPLE OF AN OPEN BOUNDARY STRUCTURE

To demonstrate the flexibility of the method, the open boundary structure of Fig. 6.6 is considered next. Fig. 6.6 shows an infinitely wide conducting plane with a thin dielectric coating. It can be shown that one of the particular properties of this structure is the exponentially dying field in the space away from the dielectric-air interface[6.4,6.5]. In this case, the TLM method has to cater for an imaginary boundary at infinity in space as well as an infinite width of the structure in the x-direction. The latter is simply overcome by placing two open-circuit boundary planes in the x-direction. However, as for the imaginary boundary at infinity we can think of a lossy boundary nearer to the dielectric-air interface. This is possible because of the field decay in the space. How far we can bring in this lossy boundary depends mainly on the frequency. To analyse Fig. 6.6, in the TLM method a non-reflective boundary was used at only a few number of nodes away from the dielectric surface. The dispersion diagram for the dominant TM mode of the structure has been shown in the same figure.

6.5 LOSSY DIELECTRIC CAVITIES

Consider the lossy dielectric cavities shown in Fig. 6.7. Keeping the air loss-free requires G_o (normalised characteristic admittance of loss-stub) to have a value of zero on all the shunt nodes inside the air region. The value of G_o inside the dielectric medium on the shunt nodes is given by equation 5.22 as $G_o = \sigma \Delta\ell Z_o$.

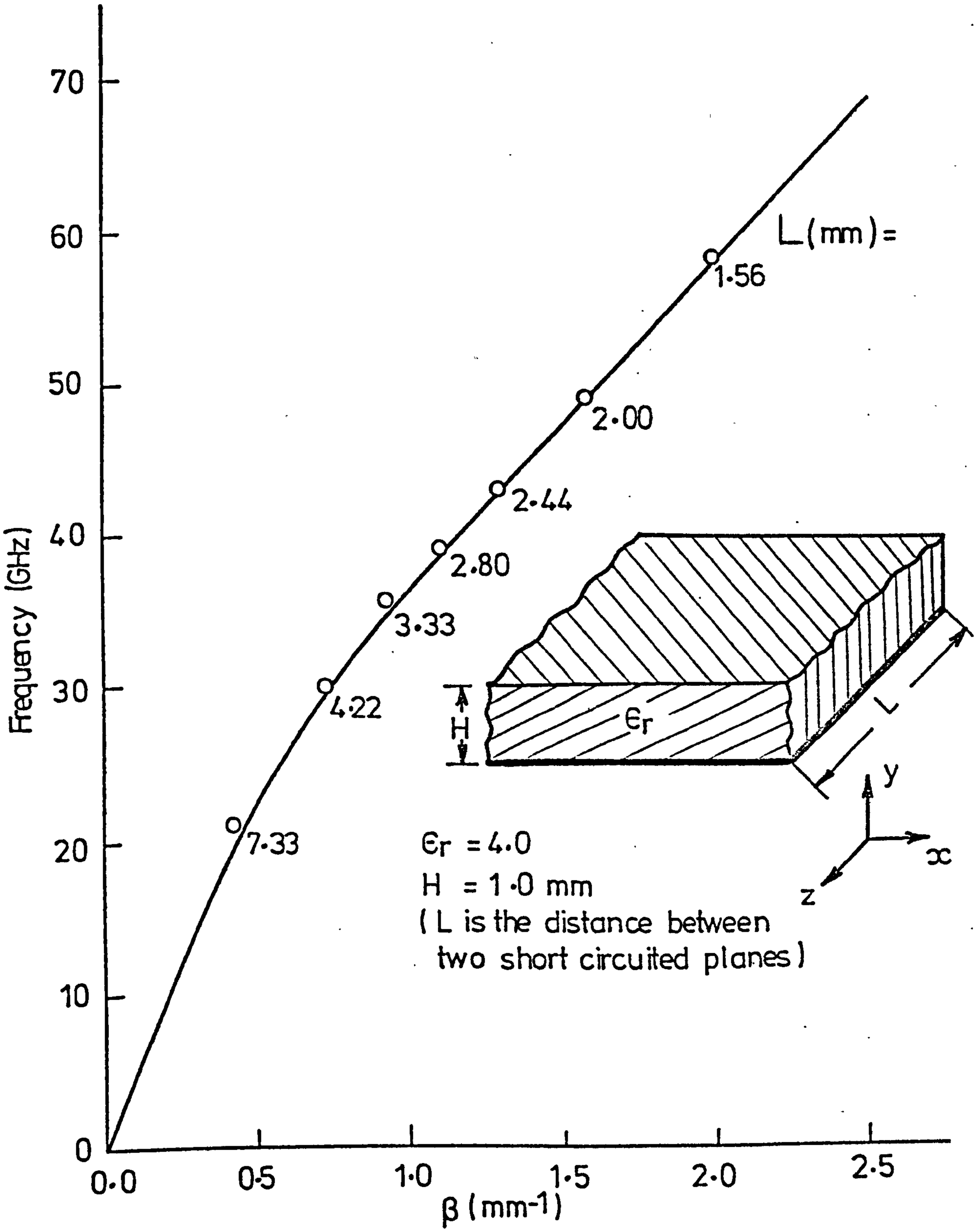

FIG. 6.6 The dispersion diagram for the dominant TM mode of a dielectric coated conducting plane ($H/\Delta\ell = 4$)

o This method (TLM)

——— Analytical results

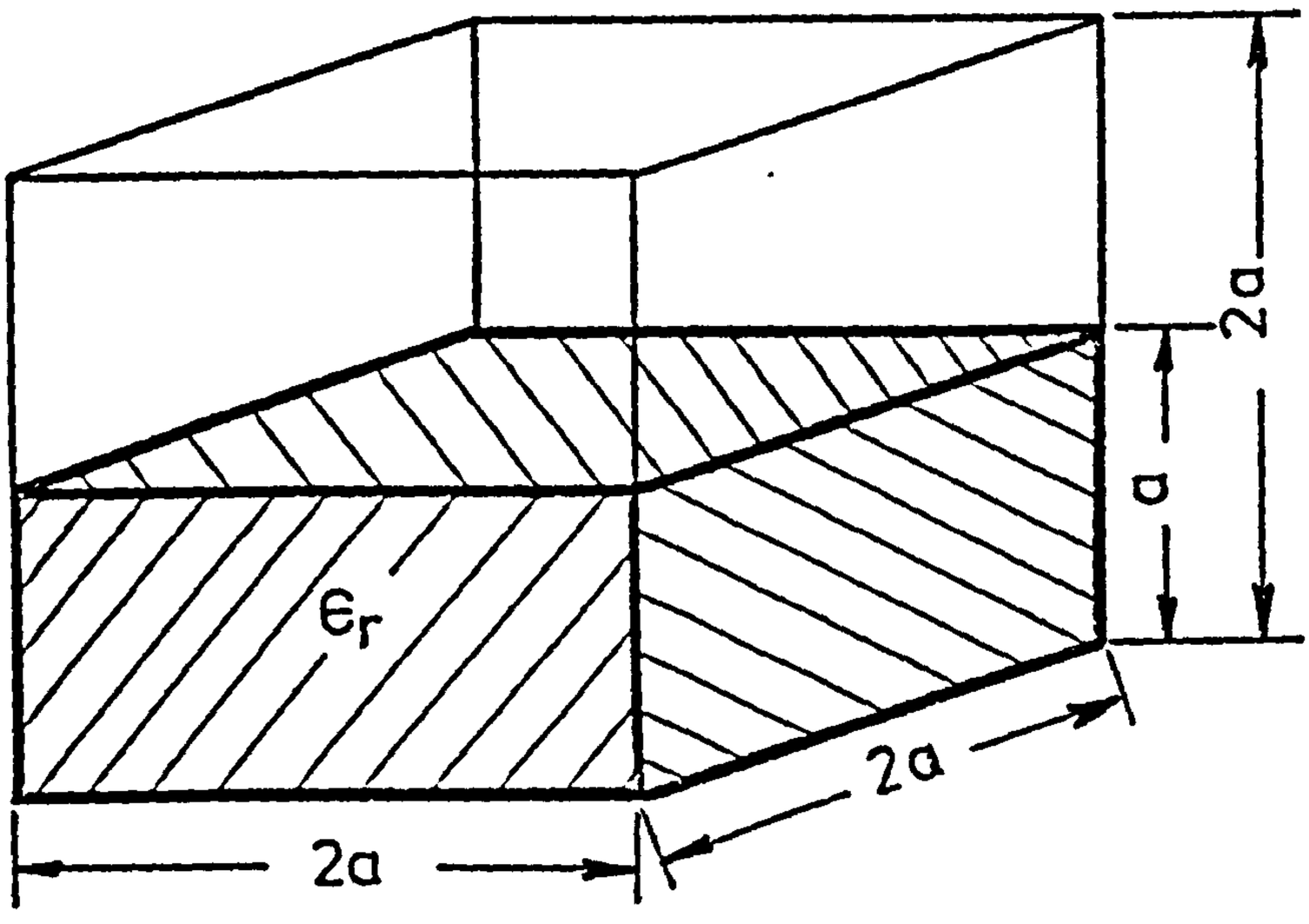

(a)

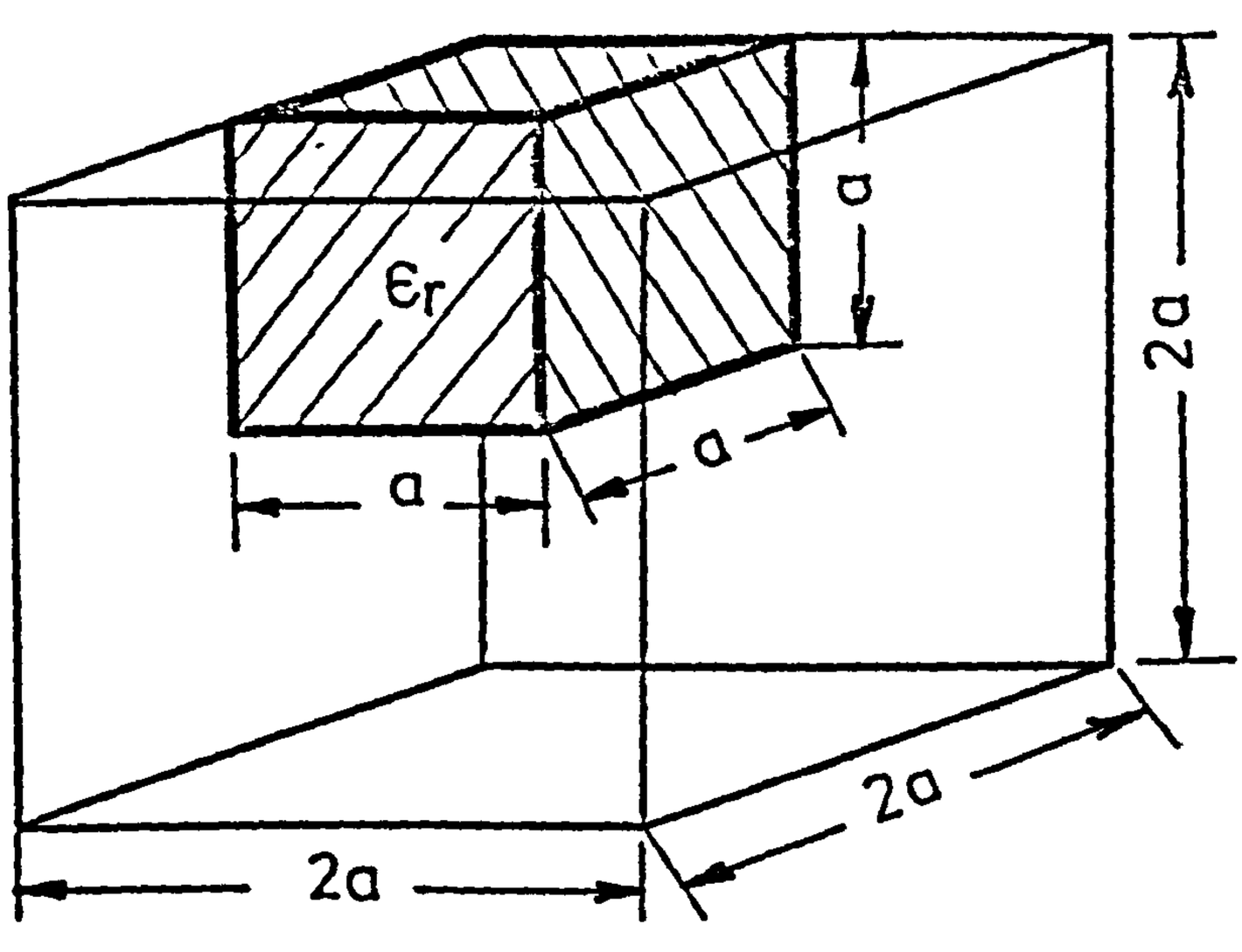

(b)

FIG. 6.7 Rectangular cavity loaded with a lossy dielectric slab ($\epsilon_r = 2.45$, $\frac{2a}{\Delta\ell} = 7$, $\Delta\ell = 0.3$ cm)

TABLE 6.5

Cavity of Fig. 6.7

State of the cavity	$(\frac{\Delta \ell}{\lambda})$ for resonance of dominant mode (σ = 0.0)			Time taken for the power in the cavity to fall to 1/e of its original value (σ = 0.0885 S/m)		
	TLM	theoretical	error %	TLM ns	theoretical ns	error %
empty	0.0503	0.0505	0.39	∞	∞	
structure of Fig. 6.7(b)	0.0440			1.560		
structure of Fig. 6.7(a)	0.0371	0.0369	0.53	0.724		
completely filled with dielectric	0.0321	0.0322	0.31	0.493	0.490	0.61

The time taken for the total power in each of the cavities of Fig. 6.7 to decay to 1/e of its original value is shown in Table 6.7. A conductivity of $\sigma = 0{\cdot}0885$ S/m and node separation $\Delta\ell = 0{\cdot}3$ cm is assumed. In all cases, the initial field excitation consisted of equal amplitudes of E_y at each of the nodes, and hence the decay time is not to be associated with any one particular mode. If the decay time for a particular mode is required, then the field configuration for that mode must be found by normal loss-free TLM procedures and then the losses introduced after the field is established. Table 6.7 also shows the dominant frequency cut-offs of Fig. 6.7 cavities for a conductivity of $\sigma = 0{\cdot}0$ S/m (non-lossy dielectric).

6.6 MICROSTRIP CAVITIES

The general TLM program has also been used to find the resonant frequencies of three-dimensional cavities containing microstrip. The first microstrip cavity checked on the computer corresponded to the structure of Fig. 6.8. In the TLM method, the resonant frequency of various lengths, L, of the cavity is used to plot the frequency, GHz, versus phase constant, β, curve shown in Fig. 6.8. The result is compared with Mittra and Itoh[6.6] and Hornsby and Gopinath[6.7] in the same figure. The quasi-TEM solution for open microstrip line based on Wheeler's curves[6.8] is also shown for comparison. The frequency versus phase constant curve for the quasi-TEM analysis shows no dispersion. This is due to the fact that the propagation effect is neglected in such an analysis.

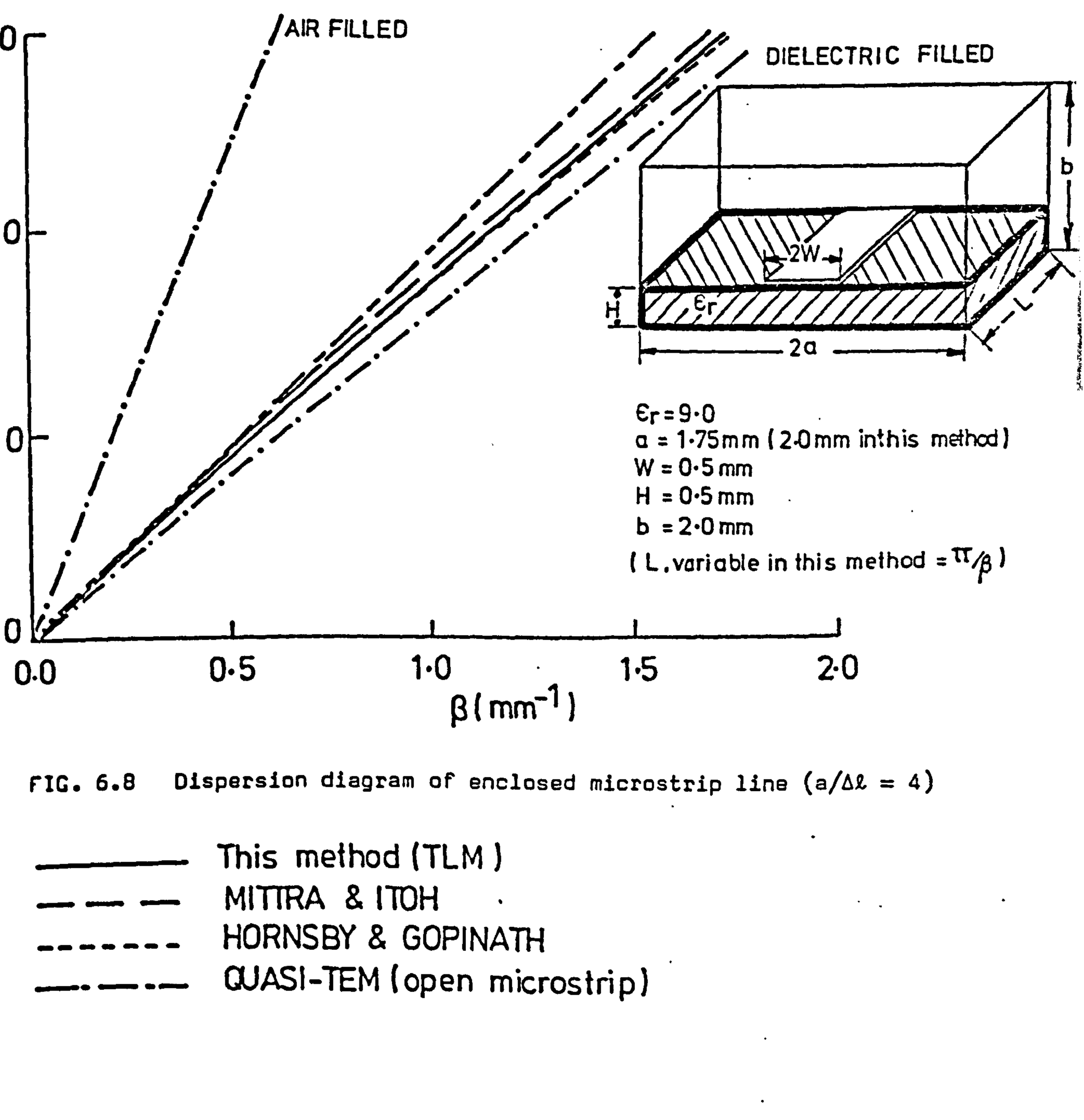

FIG. 6.8 Dispersion diagram of enclosed microstrip line ($a/\Delta\ell = 4$)

——— This method (TLM)

— — — MITTRA & ITOH

------- HORNSBY & GOPINATH

—·—·— QUASI-TEM (open microstrip)

The curves of Fig. 6.8 demonstrate the high accuracy of the results obtained by this method, even though a very few number of nodes (see the figure) have been used to describe the geometry. As already pointed out in section 5.6, the dielectric overflow over the edges of the strip (due to the boundary difficulties in the model) seem to have a very little effect on the outcome.

Longitudinal field components effect a phase velocity decrease with increasing frequency. Therefore, the phase constant, β, and hence the effective permittivity, ε_{eff}, increase with increasing frequency. $\beta/\beta_o = \sqrt{\varepsilon_{eff}}$ describes the frequency dependent behaviour of the effective permittivity. Fig. 6.9 shows the frequency dependence of ε_{eff} for a microstrip cavity shown in the same figure. In this figure, the effective permittivity versus frequency curve obtained by the TLM method for the various lengths of cavity, L, are compared with that given by Itoh and Mittra[6.9]. A full description of the method used in reference 6.9 has been given in reference 6.10. Note that the method used in reference 6.10 by the author, Itoh, differs from that given in reference 6.6 by Mittra and Itoh.

In references 6.9 and 6.10 some numerical and experimental results have been compared by the authors. From the study of these results, it has become apparent that the experimental curve say in Fig. 6.9 would lie slightly below the curve given by Itoh and Mittra. This will probably mean a higher accuracy for the results of this method, since the experimental curve might fall nearer to the TLM curve.

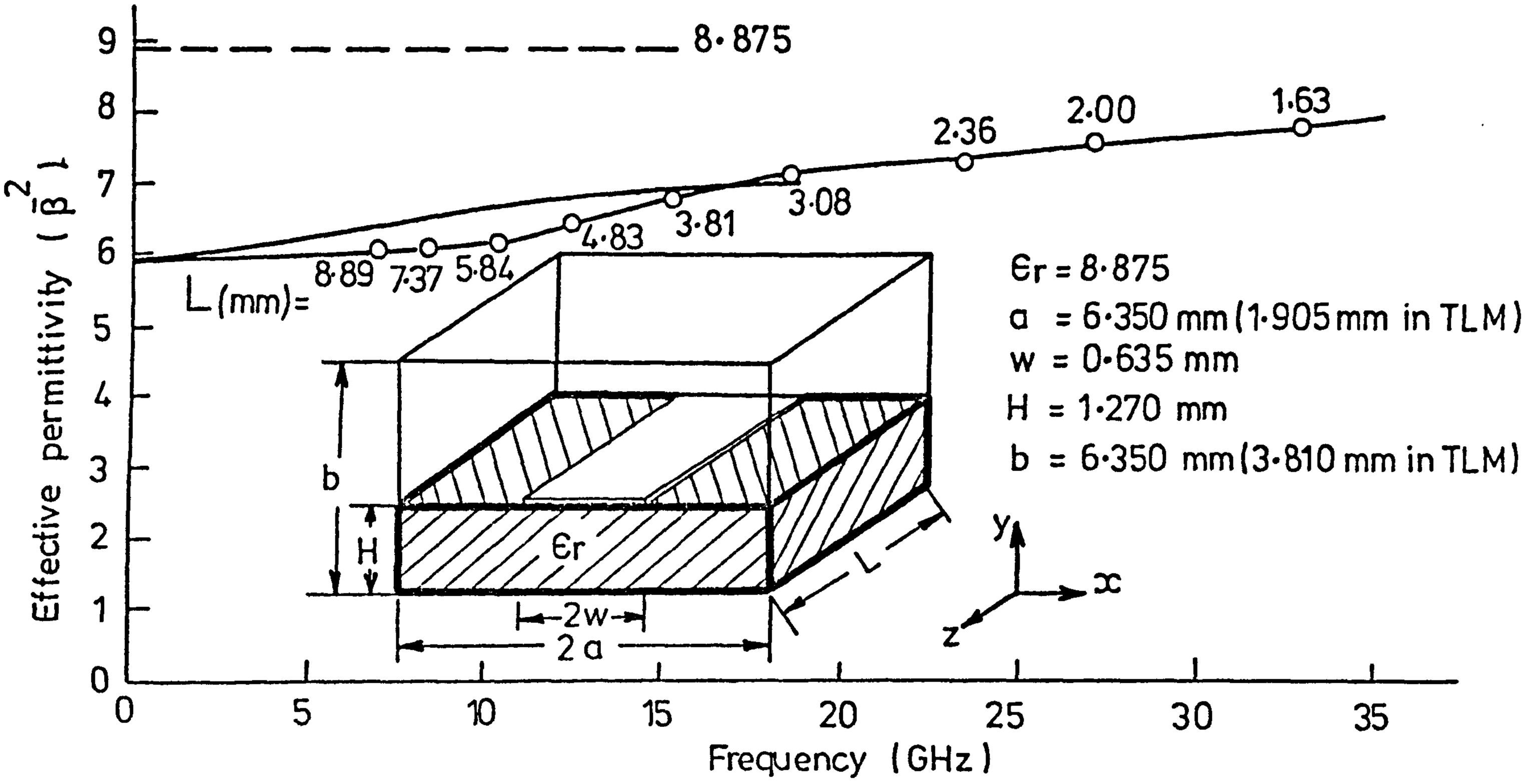

FIG. 6.9 Effective dielectric constant versus frequency ($2a/\Delta\ell$ = 15,21)

—o—o— This method (TLM)

——— ITOH & MITTRA

6.7 INVESTIGATION OF THE LOW-LOSS MICROSTRIP MODE

It is well known that the dominant mode of propagation in the inhomogeneous structures is basically the quasi-TEM mode with a d.c. cut-off frequency. However, in reference 6.11 using the finite element method of numerical analysis[6.12] the author, P. Daly, has predicted the existence of a second type of mode also with a d.c. cut-off frequency. The particular mode has been referred to as "surface wave" due to the heavy concentration of all field components near the air-dielectric interface. The longitudinal fields for this mode decay rapidly away from the interface as in the surface waveguides[6.4,6.5]. Daly argues that due to the smallness of the electric field at the conductor, for a given surface resistivity the losses in the surface wave would be very much smaller than for the quasi-TEM waves. The same general argument would also hold if the dielectric were lossy.

Dispersion in the surface mode has been shown to be negligible compared to that for the TEM mode. This has been correctly argued to be due to an almost symmetrical value of longitudinal fields[6.11] about the interface over a wide range of frequency. These symmetrical values in turn will account for a substantially constant ratio of the stored average energy in the dielectric to that in the air region at ε_r, over the same frequency range. Consequently, the phase velocity will remain practically unaltered at its d.c. value $c/\sqrt{\frac{(\varepsilon_r+1)}{2}}$.

The importance of the surface or low-loss mode, if it exists, is readily apparent from the above discussions. Therefore, with this in mind, the possible existence of the low-loss mode was

investigated using the present method. For this purpose, the exact structure of the example used by Daly[6.11] was simulated in the computer. This was done in order to directly compare Daly's results with the TLM results, since at no time during the extensive process of computation for other microstrip structures did we come across such a mode. The geometry of the structure is shown in Fig. 6.10. For the purpose of representation, in Fig. 6.10 results are compared for frequency versus phase constant rather than frequency versus effective permittivity[6.11]. Considerable care was taken to try to excite the surface mode as suggested by Daly[6.11]. We also deliberately excited the cavities with Daly's field values as given in reference 6.11, but as can be seen in Fig. 6.10 there has been no resonant frequency corresponding to this mode, even though higher order waveguide modes are readily detected. (Note that in section 6.4, the same microstrip structure, but without the strip, was used to obtain the highly accurate surface waveguide mode results.)

Fig. 6.11 and Fig. 6.12 show a typical E_y-field amplitude versus normalised frequency, $\Delta\ell/\lambda$, for the cavity of Fig. 6.10 with L = 3·75 mm. (The effect of truncating the iteration process is to cause the field values, expressed as a function of frequency, to be convolved with a sinf/f type curve as shown in these figures. This causes smoothing out of high narrow peaks of the output function.) Fig. 6.11 clearly shows the resonant peaks corresponding to the quasi-TEM, the first and the second higher order waveguide modes. Any resonant frequency corresponding to the surface mode would have appeared between the quasi-TEM and the first waveguide

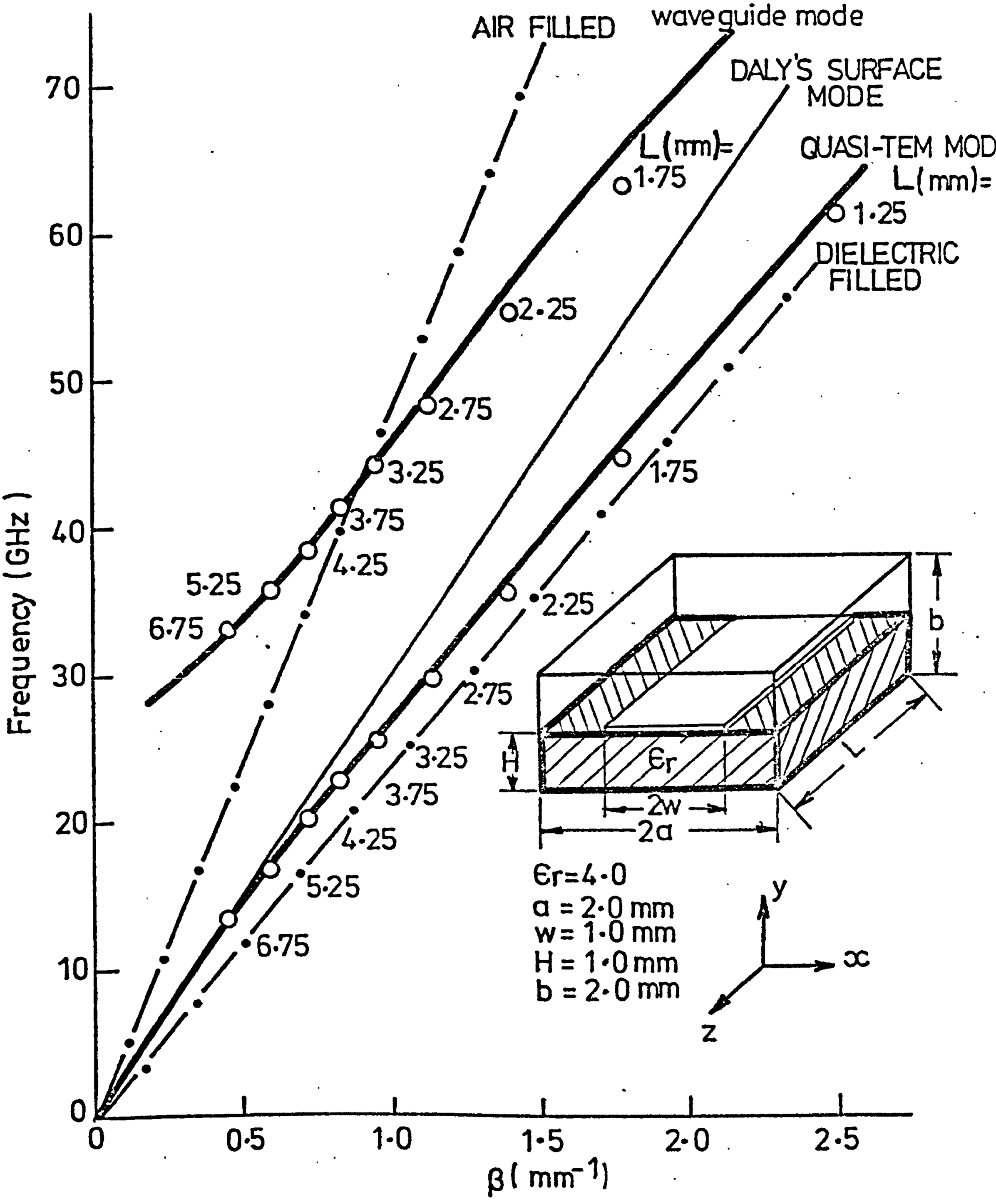

FIG. 6.10 Dispersion diagram of enclosed microstrip line ($a/\Delta\ell = 8$)

o This method (TLM)

—— Daly

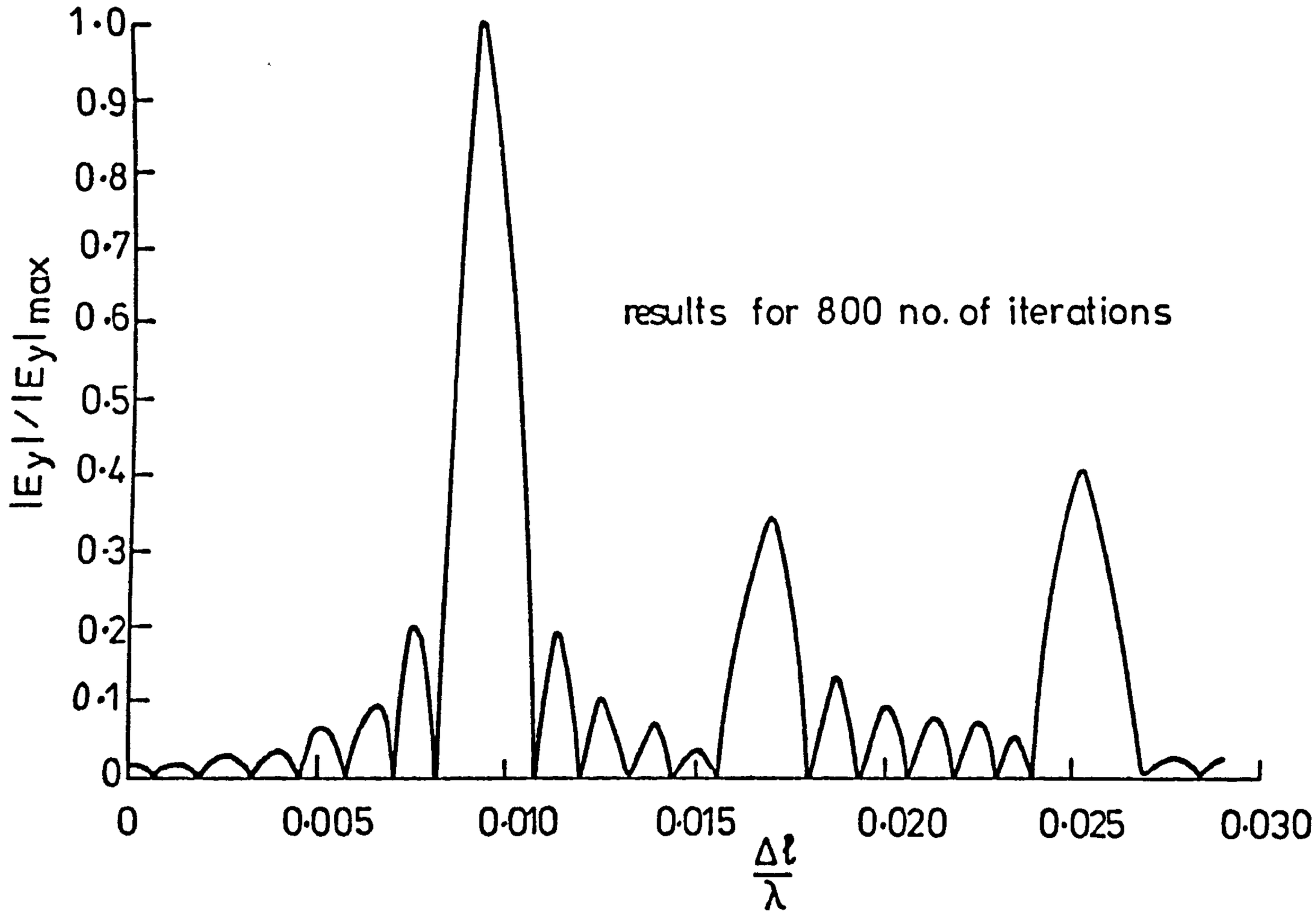

FIG. 6.11 A typical E-field spectrum for the resonator of Fig. 6.10 (L = 3.75 mm), clearly showing the resonant peaks corresponding to the quasi-TEM, the first and the second waveguide modes

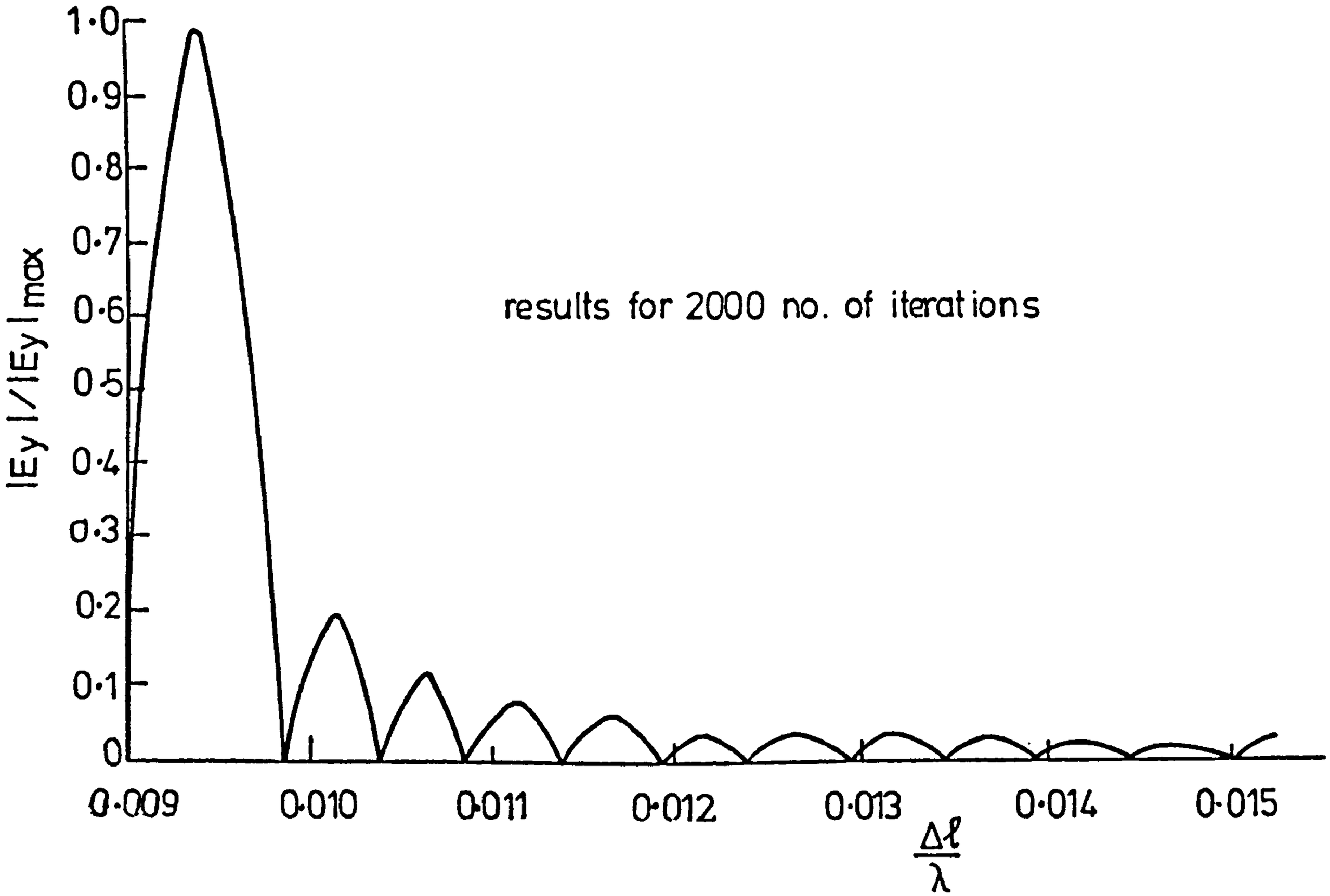

results for 2000 no. of iterations

FIG. 6.12 A closer inspection of Fig. 7.4 for the range between resonant peaks of the quasi-TEM and the first waveguide mode in search of the possible existance of Daly's surface mode resonance

mode resonant frequencies (see Fig. 6.10). Fig. 6.12 shows a close-up of this region, but still no sign of a resonance corresponding to the surface or low-loss mode. Therefore, we have concluded that such a mode is most possibly non-existent. The result obtained by Daly[6.11] for surface modes might have been due to a possible error in the finite element computer program routine.

6.8 MICROSTRIP LINE ON MAGNETIC SUBSTRATES

In this section, the use of stubs at series nodes (permeability-stubs) is demonstrated. It should be noted that the reflection coefficients at the boundaries used in two dimensions[6.13] are not required. This is because the permeability-stubs provide the correct properties for a permeable medium as do the stubs at shunt nodes (permittivity-stubs) for dielectrics. The results for the homogeneous cube cavity in Table 6.2 showed that the TLM method is accurate for permeability-stubs and also for a combination of permeability-permittivity stubs.

The method is used to calculate the dispersion relationship for a microstrip line on an isotropic magnetic substrate. The example is given for a relative permeability of $\mu_r = 0{\cdot}8$ which is within a practical range of permeabilities for substrates biased along the direction of propagation[6.14]. The results are shown in Fig. 6.13 and are compared with the result obtained by Pucel and Masse[6.14] assuming TEM propagation. As expected, the results agree for low frequencies and the discrepancy between the TEM assumption and the true dispersive result obtained by the TLM method only becomes important at high frequencies.

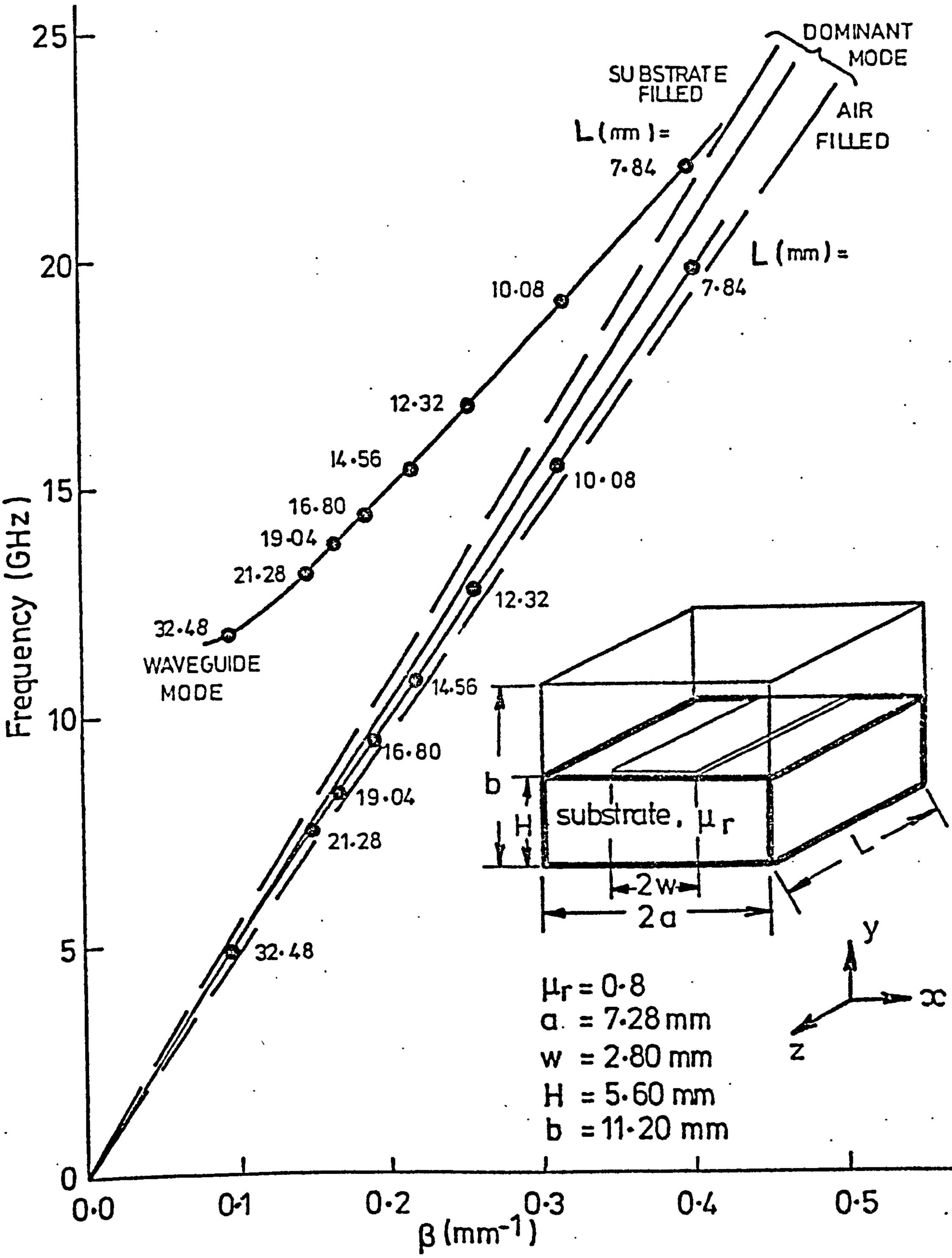

FIG. 6.13 Dispersion diagram of enclosed microstrip line on an isotropic magnetic substrate ($2a/\Delta\ell = 13$)

—o—o— This method (TLM)

——— QUASI-TEM (open microstrip)

TABLE 6.6

Variation of effective permeability
and effective permittivity with frequency

Frequency (GHz)	ε_{eff} (ε_r=1.25)	μ_{eff} (μ_r=0.8)	$\varepsilon_{eff}.\mu_{eff}$
6.57	1.1518	0.9301	1.0713
7.34	1.1522	0.9431	1.0866
9.56	1.1601	0.9488	1.1007
11.30	1.1672	0.9590	1.1193
13.71	1.1774	0.9680	1.1397
17.54	1.1891	0.9745	1.1588

Pucel and Masse have derived a duality relationship between magnetic and dielectric substrates, again assuming TEM propagation. This relationship allows calculation of the effective permeability μ_{eff} in terms of effective permittivity ϵ_{eff} by the formula[6.14],

$$\mu_{eff}(W/H,\mu) = \frac{1}{\epsilon_{eff}(W/H,\mu^{-1})}$$

Table 6.6 shows how the product $\mu_{eff}.\epsilon_{eff}$ varies with frequency for substrates with $\mu_r = 0{\cdot}8(\epsilon_r = 1)$ and $\epsilon_r = 1{\cdot}25(\mu_r = 1)$. From the result of Table 6.6 it can be seen that at low frequencies the TEM approximation applies since the product is near unity. At high frequencies μ_{eff} tends to unity and the product then assymtotes to ϵ_{eff}. The near linear variation of ϵ_{eff} with frequency suggests that the approximate method for calculating μ_{eff} used by Pucel and Masse[6.15] yields good results.

6.9 MICROSTRIP DISCONTINUITIES

The versatility of both the TLM method and the TLM program is further illustrated here by calculating the resonant frequencies of cavities containing microstrip with an abrupt change in width. Such discontinuities constitute a true three-dimensional problem. Only limited amounts of theoretical[6.10,6.16,6.17] or experimental[6.18] data on discontinuities in microstrip have been reported, although there is extensive data on (homogeneous) balanced strip transmission-line[6.19] and coaxial-line[6.20] discontinuities. For example, in reference 6.16 Farrar and Adams use a matrix method to reduce the defining integral equation to an approximate matrix equation in

order to obtain the solution of a wide range of microstrip discontinuity problems. However, the method is based on the quasi-static approximations which assume a TEM mode of propagation. The TLM method may be used to analyse microstrip discontinuities inside a cavity without making any propagation assumptions.

Fig. 6.14 shows the geometry of a dielectric loaded cavity with a microstrip line. The width of the centre line is non-uniform with an abrupt change. Some representative numerical results of this geometry are shown in Fig. 6.15. The TLM results are compared with a curve calculated by TEM analysis with a capacitive discontinuity given by Farrar and Adams[6.16]. From Fig. 6.15, it is apparent that the relative values of frequency for short lengths, 2L, of the cavity are considerably lower than those computed by the quasi-static approximations. This is partly a result of employing the TEM analysis rather than a dispersive analysis to calculate the results. The error between the discontinuity curves of Fig. 6.15 is also due to the fact that in reference 6.16 there is no equivalent lumped capacitance to account for the fringing field effects between the discontinuity edges and the front conducting plane of the cavity (Fig. 6.14). For short lengths of L in Fig. 6.14, the fringing capacitance will have a comparable effect with that of the discontinuity. Therefore, larger discrepancies between the TLM method and reference 6.16 occur at higher frequencies.

In Table 6.7, discontinuity results of Fig. 6.15 are numerically compared with those obtained by the TLM method for uniform lengths of lines. Two extreme cases of uniform line with $W = W_o = 0{\cdot}75$ mm

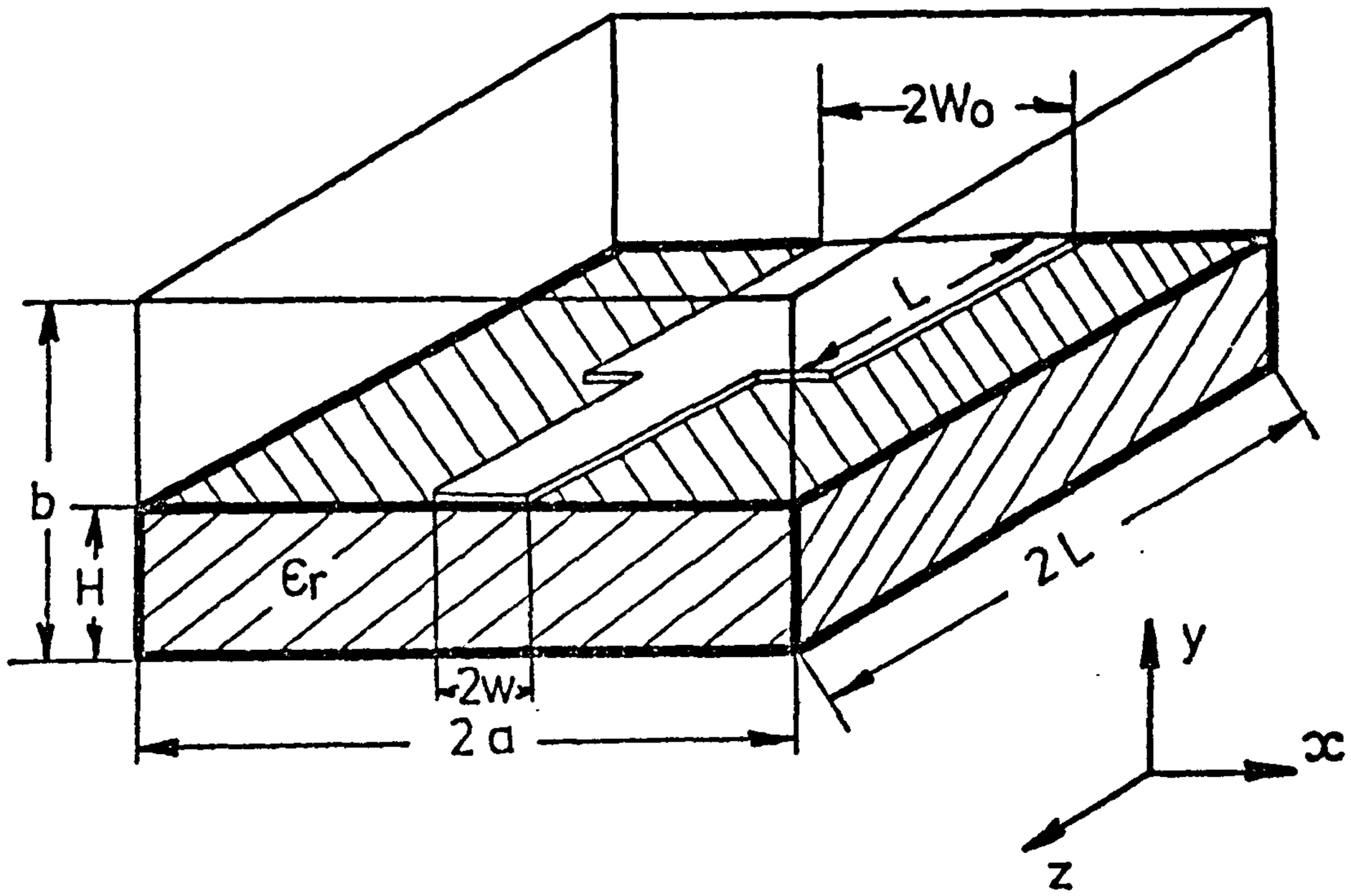

FIG. 6.14 Microstrip cavity with an abrupt change in line width

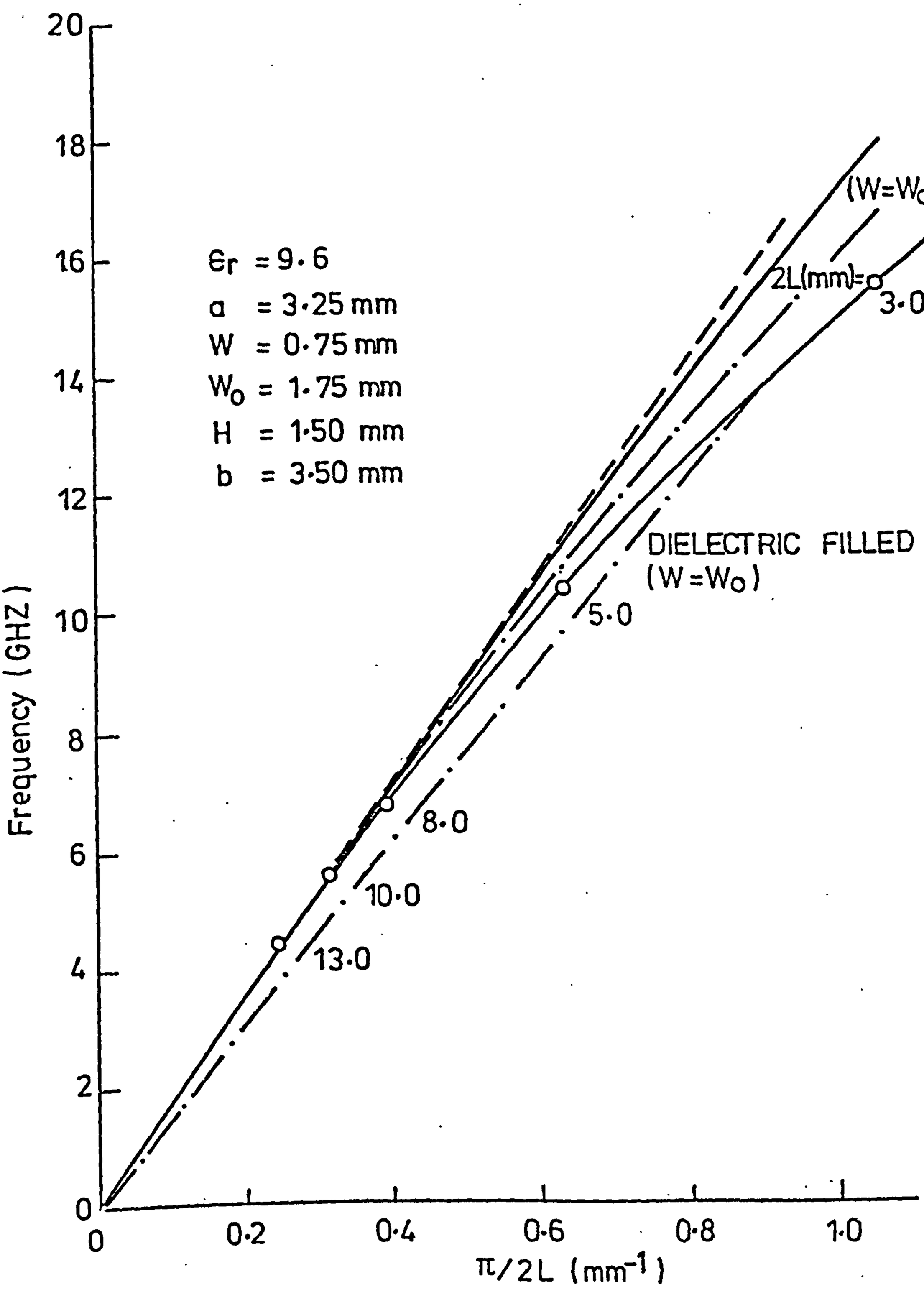

FIG. 6.15 Dispersion diagram for structure of Fig. 6.14 ($2a/\Delta\ell$ = 13)

—o—o— This method (TLM)

——— FARRAR & ADAMS (QUASI-TEM, open structure)

TABLE 6.7

Cavity of Fig. 6.14

Length of Cavity (2L) mm	Dominant Resonant Frequency			
	Farrar & Adams * 2W =1.5mm $2W_o$=3.5mm GHz	This Method 2W =1.5mm $2W_o$=3.5mm GHz	This Method 2W =1.5mm $2W_o$=1.5mm GHz	This Method 2W =3.5mm $2W_o$=3.5mm GHz
3.0	18.060	15.480	16.920	16.800
5.0	11.040	10.320	10.774	10.704
8.0	6.960	6.768	6.996	6.972
10.0	5.580	5.556	5.605	5.604
13.0	4.466	4.464	4.466	4.466

* quasi-TEM, open structure

and also $W = W_o = 1{\cdot}75$ mm for structure of Fig. 6.14 have been considered. From this table, it is apparent that the dispersion due to the change in line width given by Farrar and Adams is virtually negligible up to about 7 GHz ($2L > 8{\cdot}0$ mm). Nevertheless, it is greater than those of the uniform lines. However, it is noticed that at higher frequencies this dispersion is comparatively much smaller than the dispersive effect of the lines with no discontinuity. Therefore, we conclude that the dispersion due to the line itself is far more important than the dispersion due to the discontinuity. Hence, a solution based on the quasi-TEM analysis of the line would be misleading.

6.10 COUPLED MICROSTRIP LINE CAVITIES

Coupled microstrip lines are generally used in microwave integrated circuits for making control devices such as direction couplers and filters. Hence, for design purposes, accurate information on coupled lines in necessary.

As in the case of microstrip transmission lines, the lowest order mode for wave propagation along parallel microstrip lines in a homogeneous medium is a TEM mode. When inhomogeneities in the dielectric medium are present,the wave propagation is no longer TEM due to the different phase velocities in the different media, but is of quasi-TEM nature. For sufficiently low frequencies the quasi-TEM theory can be employed to obtain the characteristics of coupled lines of microstrip (references 6.21-6.23 for example). However, at higher frequencies, when the wavelength in microstrip line becomes comparable to the transverse dimensions of the line, the deviation from quasi-TEM behaviour becomes significant and

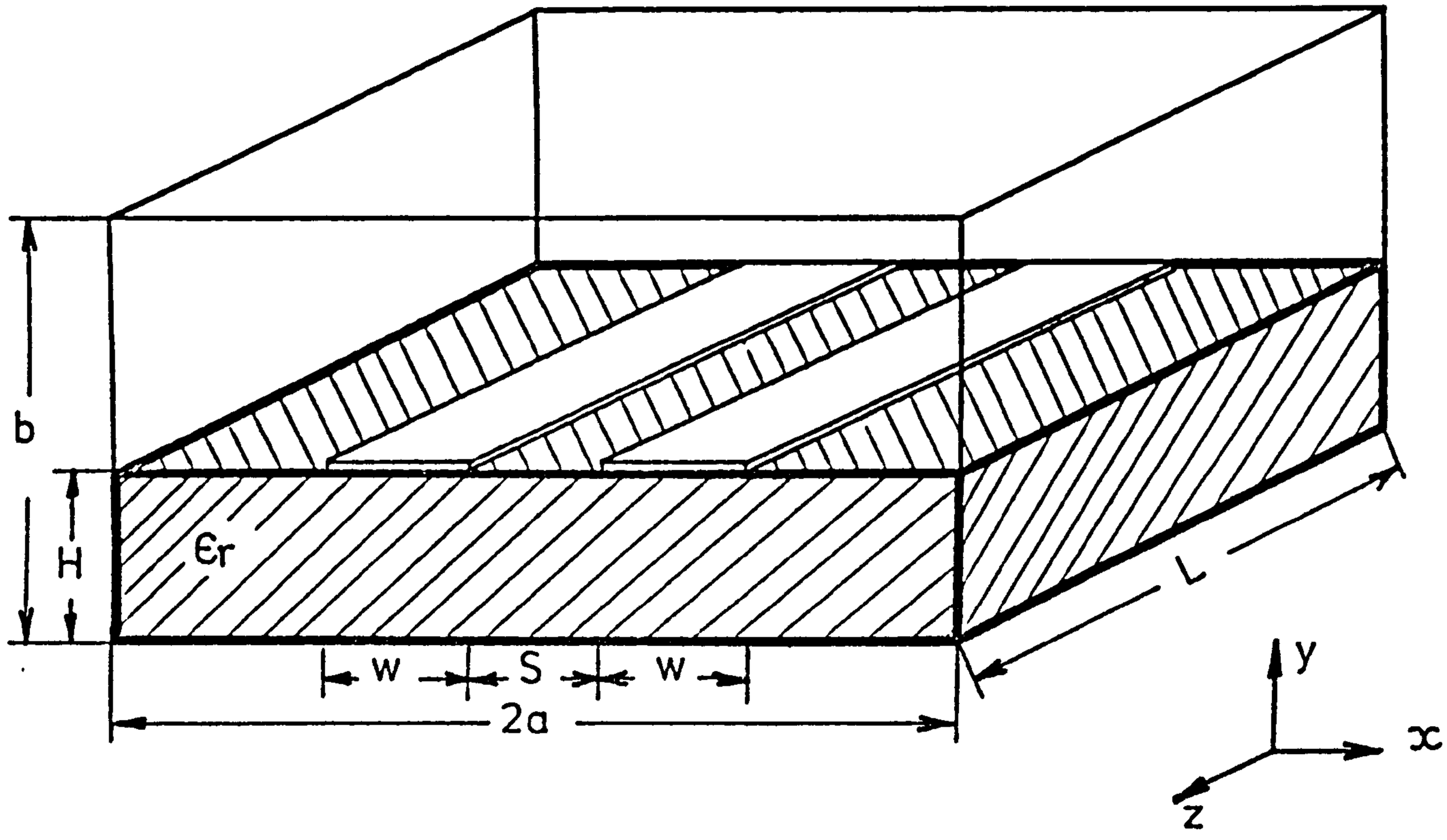

FIG. 6.16 Enclosed coupled pair of microstrip lines

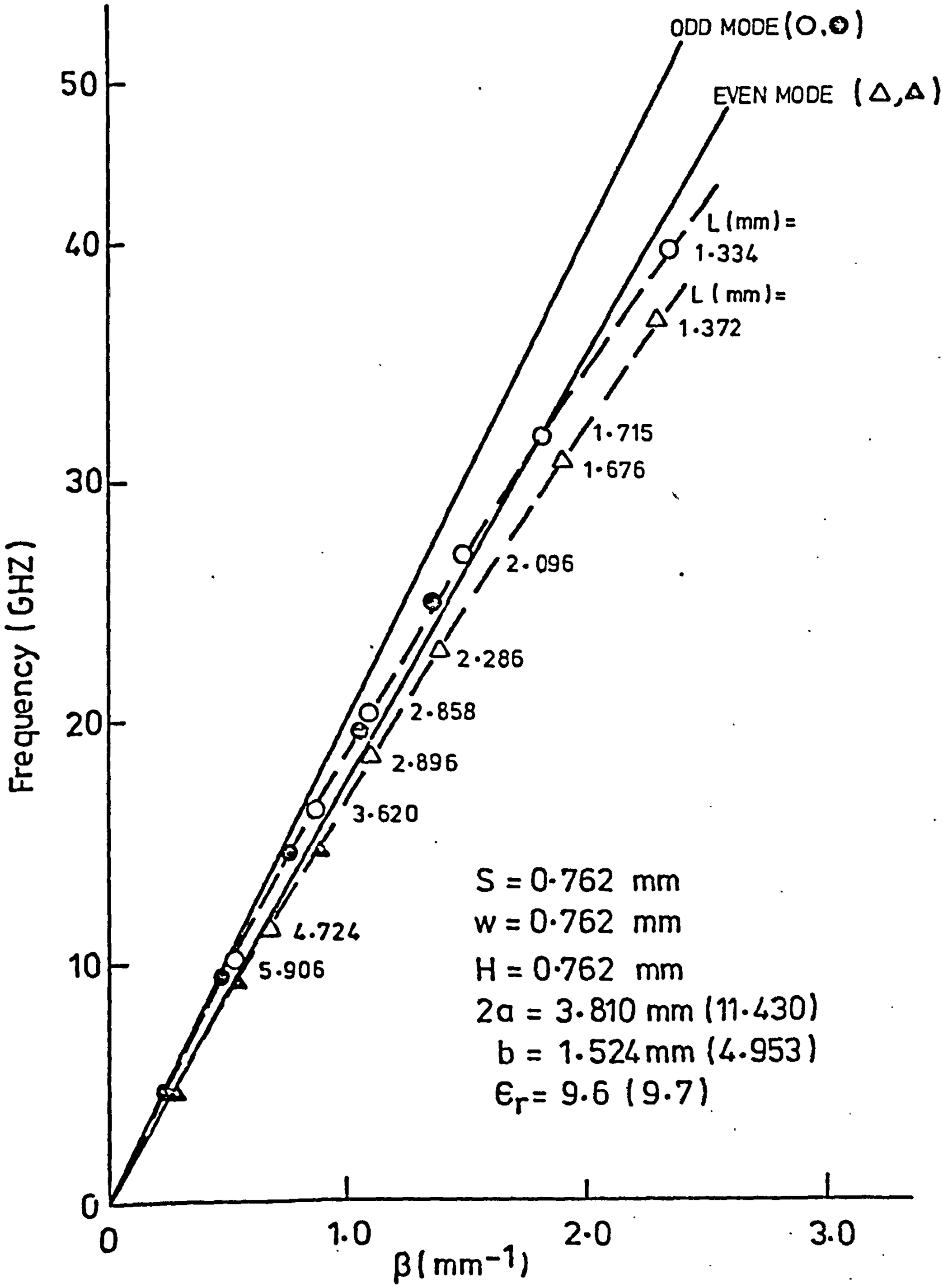

FIG. 6.17 Dispersion diagram for structure of Fig. 6.16
($2a/\Delta\ell$ = 20 for odd mode, 25 for even mode)

O , Δ This method
O , ▲ CORR & DAVIES
——— AKHTARZAD et al
(QUASI-TEM, open structure)

higher order modes of propagation become possible (see references 6.24-6.27 for example). The TLM method of numerical analysis as described in this thesis, falls in the latter category of references where it can be used to obtain the dispersive results of coupled lines enclosed in a cavity.

The physical construction of an enclosed coupled pair of microstrip lines is shown in Fig. 6.16. Some representative results for the structure of Fig. 6.16 are shown in Fig. 6.17. The TLM results are compared with Corr and Davies[6.24]. Corr and Davies have used the finite difference methods to obtain the dispersion curves. The quasi-TEM solution for open coupled microstrip lines based on the design theory given by Akhtarzad et al[6.23] is also shown in Fig. 6.17 for comparison. Results of Fig. 6.17 indicate a very good agreement between the TLM and Finite difference curves for all frequencies shown.

6.11 SIX-COMPONENT ELECTROMAGNETIC FIELD DISTRIBUTIONS

With a slight modification to the general TLM program, values of the six components of electromagnetic fields at any frequency are readily available at all the nodes inside a cavity. This is considered to be important not only for the value of seeing the field distribution, but also for the following reason. In section 6.5, the results for the power decay times of a number of partially filled lossy dielectric cavities were shown. However, in all cases the initial field excitation consisted of equal amplitudes of E_y at each of the nodes and hence the decay time was not to be associated with any one particular mode, but using the field distribution information, it is possible to find the decay time for a particular mode as explained in section 6.5.

Figs. 6.18-6.20 show the distribution of the six electric and magnetic field components across various planes of microstrip cavity in Fig. 6.10. The field values are for a frequency of 35·59 GHz corresponding to the dominant mode (quasi-TEM) frequency resonance of this cavity with L = 2·25 mm. Cross-sections in the z co-ordinate direction have been chosen at various distances $z = \ell$ from the front s/c plane of the cavity so that the particular field components in that plane will exhibit maximum values. The general characteristics of the fields are much as would be expected, i.e. the fields are mostly concentrated in the dielectric and the normal electric fields and tangential magnetic fields at or near the strip and the surrounding conductors reach a maximum.

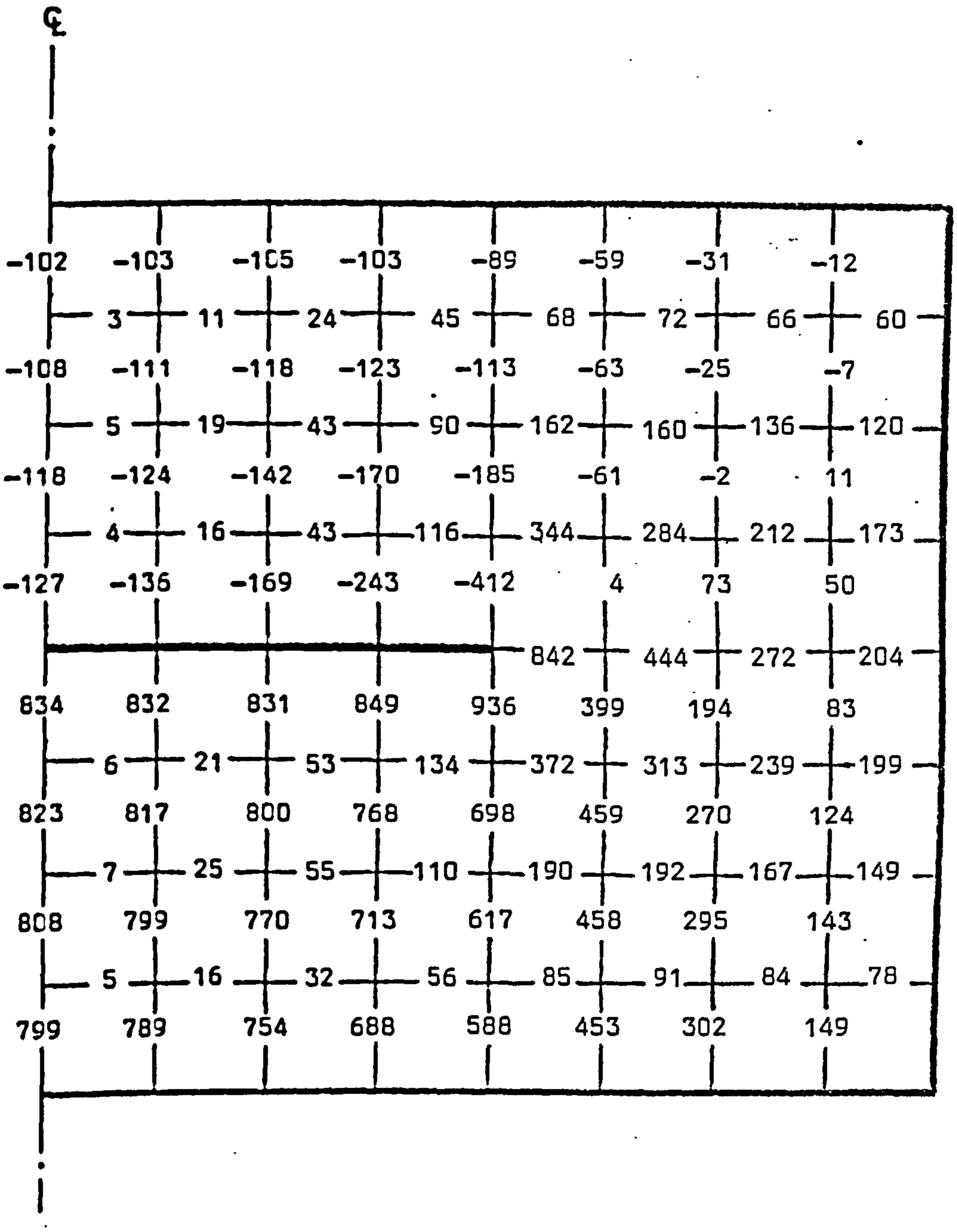

FIG. 6.18 Transverse electric field distribution in the x-y plane and $z = \ell$ for the dominant microstrip mode of Fig. 6.10 structure at 35·59 GHz ($L = 2{\cdot}25$ mm, $\ell = 1{\cdot}0$ mm); horizontal number E_x, vertical number E_y.

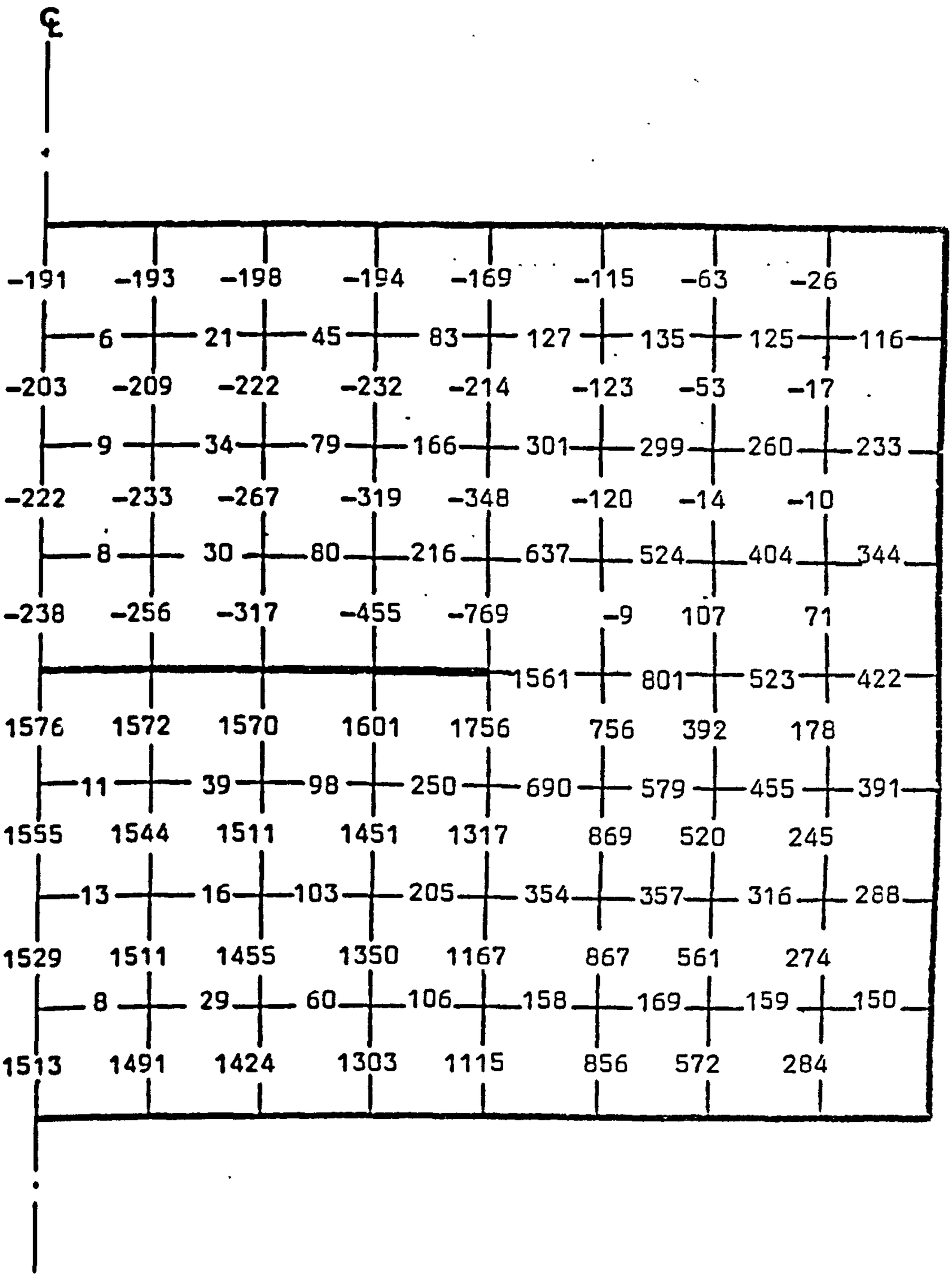

FIG. 6.19 Transverse magnetic field distribution in the x-y plane and $z = \ell$ for the dominant microstrip mode of Fig. 6.10 structure at 35·59 GHz ($L = 2{\cdot}25$ mm, $\ell = 0{\cdot}25$ mm); vertical number H_x, horizontal number H_y.

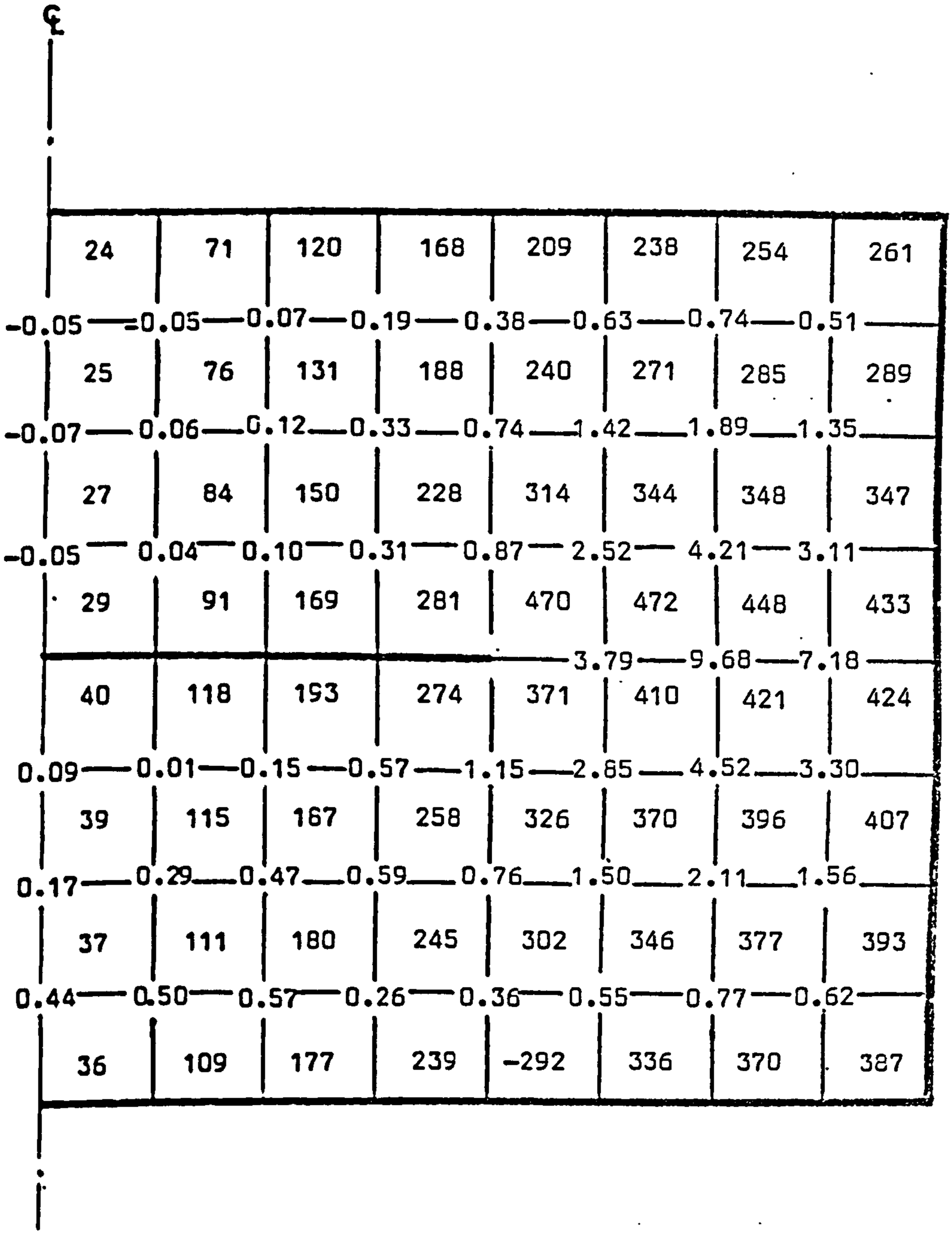

FIG. 6.20 Longitudinal electric and magnetic field distributions in the x-y planes with $z = \ell_1$ and $z = \ell_2$ respectively, for the dominant microstrip mode of Fig. 6.10 structure at 35·59 GHz ($L = 2{\cdot}25$ mm, $\ell_1 = 0{\cdot}25$ mm, $\ell_2 = 1{\cdot}0$ mm); decimal number - E_z, integer number H_z.

6.12 DISCUSSION

This chapter has demonstrated the application of the TLM method of numerical analysis to three-dimensional microwave cavities. The main advantages of the TLM method are its ease of application, its versatility and accuracy.

The ease of application arises because of the close connection between the numerical routine and the actual physics of wave propagation[6.28]. For example, provided the capacitance of the lines in the TLM method are increased somehow (by using stubs in this thesis) then, because all six components of the field are accounted for, the dielectric boundary will also be properly accounted for. Thus, there is no need to introduce special numerical routines to take account of the boundary. The same argument applies to lossy materials (from zero conductivity to infinite conductivity) and hence for metallic boundaries also.

The versatility arises for similar reasons. The properties of a medium are described at each node by the two stubs - the permittivity and permeability-stub at shunt and series nodes and the loss-stub at shunt nodes. The TLM program consists, therefore, of setting the properties of the medium at each node in the first instance, and then performing the iteration process to find the way in which the fields propagate. Thus, the complication of the geometry, in terms of ε, μ and σ is limited only to the mesh coarseness and does not affect the program listing.

The accuracy of the method is mainly dependent on the number of nodes used to describe the geometry of a problem and also the number of iterations performed. Therefore, the errors can be minimized by using enough number of nodes and iterations[6.29].

While it is not possible to present formulae for the general case, it is hoped that the following figures demonstrate that the running time and storage of the TLM method are at least comparable with other methods. The first case is for the geometry of Fig. 6.8 for L = 2·5 mm using 5 x 9 x 6 = 270 three-dimensional nodes (no symmetry properties used) and 200 iterations of the matrix. In this problem the running time was 2·16 minutes and the total storage was 20 k words. The second example is for Fig. 6.14 for 2L = 5·0 cm using 8 x 8 x 11 = 704 three-dimensional nodes (symmetry property used) and 400 iterations. Here the time was 11·26 minutes using 46 k words. These results are quoted for the ICL 1906A computer.

REFERENCES

6.1 ALBANI, M. and BERNARDI, P. "A numerical method based on the discretization of Maxwell equations in integral form", I.E.E.E. Trans., MTT-22, pp 446-449, April, 1974.

6.2 MARCUVITZ, N. "Waveguide handbook", McGraw-Hill, New York, 1951.

6.3 ALBANI, M. and BERNARDI, P. "A numerical method for 6-component electromagnetic fields", Inst. Electronics, Univ. Roma, Rome, Italy, internal rep. 51, February, 1973.

6.4 COLLIN, R.E. "Field theory of guided waves", McGraw-Hill, New York, 1960.

6.5 WILLIAMS, C.G. and CAMBRELL, G.K. "Numerical solution of surface waveguide modes using transverse field components", I.E.E.E. Trans., MTT-22, pp 329-330, March, 1974.

6.6 MITTRA, R. and ITOH, T. "A new technique for the analysis of the dispersion characteristics of microstrip lines", I.E.E.E. Trans., MTT -19, pp 47-56, January, 1971.

6.7 HORNSBY, J.S. and GOPINATH, A. "Numerical analysis of a dielectric-loaded waveguide with a microstrip line - finite difference methods", I.E.E.E. Trans., MTT-17, pp 684-690, September, 1969.

6.8 WHEELER, H.A. "Transmission-line properties of parallel strips separated by a dielectric sheet", I.E.E.E. Trans., MTT-13, pp 172-185, March, 1965.

6.9 ITOH, T. and MITTRA, R. "A technique for computer dispersion characteristics of shielded microstrip lines with the application to the junction problems", 4th European Microwave Conference, Montreux, Switzerland, pp 373-377, September 10th-13th, 1975.

6.10 ITOH, T. "Analysis of microstrip resonators", I.E.E.E. Trans., MTT-22, pp 946-952, November, 1974.

6.11 DALY, P. "Hybrid mode analysis of microstrip by finite-element methods", I.E.E.E. Trans., MTT-19, pp 19-25, January, 1971.

6.12 ZIENKIEWITZ, O.C. and CHEUNG, Y.K. "The finite-element method in structural and continuum mechanics", McGraw-Hill, New York, 1967.

6.13 JOHNS, P.B. "The solution of inhomogeneous waveguide problems using a transmission-line matrix", I.E.E.E. Trans., MTT-22, pp 209-215, March, 1974.

6.14 PUCEL, R.A. and MASSE, D.J. "Microstrip propagation on magnetic substrates - Part I: Design theory", I.E.E.E. Trans., MTT-20, pp 304-308, May, 1972.

6.15 PUCEL, R.A. and MASSE, D.J. "Microstrip propagation on magnetic substrates - Part II: Experiment", I.E.E.E. Trans., MTT-20, pp 309-313, May, 1972.

6.16 FARRAR, A. and ADAMS, A.T. "Matrix methods for microstrip three-dimensional problems", I.E.E.E. Trans., MTT-20, pp 497-504, August, 1972.

6.17 JANSEN, R. "Shielded rectangular microstrip disc resonators", Electron. Lett., 10, pp 299-300, July, 1974.

6.18 SILVESTER, P. "TEM wave properties of microwave transmission lines", Proc. I.E.E., 115,pp 43-48, January, 1968.

6.19 PATEL, P.D. "Calculation of capacitance coefficients for a system of irregular finite conductors on a dielectric sheet", I.E.E.E. Trans., MTT-19, pp 862-869, November, 1971.

6.20 DAVIS, P.J. and RABINOWITZ, P. "Numerical integration", Waltham, Mass., Blaisdell, 1967.

6.21 BRYANT, T.G. and WEISS, J.A. "Parameters of microstrip transmission lines and of coupled pairs of microstrip lines", I.E.E.E. Trans., MTT-16, pp 1021-1027, December, 1968.

6.22 JUDD, S.V., WHITELEY, I., CLOWES, R.J. and RICKARD, D.C. "An analytical method for calculating microstrip transmission line parameters", I.E.E.E. Trans., MTT-18, pp 78-87, February, 1970.

6.23 AKHTARZAD, S., ROWBOTHAM, T.R. and JOHNS, P.B. "The design of coupled microstrip lines", I.E.E.E. Trans., MTT-23, June, 1975.

6.24 CORR, D.G. and DAVIES, J.B. "Computer analysis of the fundamental and higher order modes in single and coupled microstrip", I.E.E.E. Trans., MTT-20, pp 669-678, October, 1972.

6.25 KRAGE, M.K. and HADDAD, G.I. "Frequency dependent characteristics of microstrip transmission lines", I.E.E.E. Trans., MTT-20, pp 678-688, October, 1972.

6.26 GETSINGER, W.J. "Dispersion of parallel coupled microstrip", I.E.E.E. Trans., MTT-21, pp 144-145, March, 1973.

6.27 JANSEN, R. "Computer analysis of edge-coupled planar structures", Elect. Lett., 10, pp 520-521, November, 1974.

6.28 JOHNS, P.B. "A new mathematical model to describe the physics of propagation", Radio and Electron. Eng., 44, pp 657-666, December, 1974.

6.29 JOHNS, P.B. "Application of the transmission-line matrix method to homogeneous waveguides of arbitrary cross-section", Proc. I.E.E., 119, pp 1086-1091, August, 1972.

6.30 AKHTARZAD, S. and JOHNS, P.B. "The solution of 6-component electromagnetic fields in three space dimensions and time by the TLM method", Electron. Lett., 10, pp 535-537, December, 1974.

6.31 AKHTARZAD, S. and JOHNS, P.B. "The solution of Maxwell's equations in three space dimensions and time by the TLM method of numerical analysis", Submitted to Proc. I.E.E. (March, 1975).

6.32 JOHNS, P.B. and AKHTARZAD, S. "Three-dimensional numerical analysis of microwave cavities using the TLM method", I.E.E.E., MTT-S International Microwave Symposium, Palo Alto, California, U.S.A., May 12-14, 1975.

6.33 AKHTARZAD, S. and JOHNS, P.B. "TLM analysis of the dispersion characteristics of microstrip lines on magnetic substrates using three-dimensional resonators", Electron. Lett., 11, pp 130-131, March, 1975.

6.34 AKHTARZAD, S. and JOHNS, P.B. "The dispersive analysis of microstrip line width change by the TLM method", To be submitted to Electron. Lett., (1975).

6.35 AKHTARZAD, S. and JOHNS, P.B. "Three-dimensional TLM computer analysis of microstrip resonators", I.E.E.E. Trans., MTT-23, December, 1975.

6.36 AKHTARZAD, S. and JOHNS, P.B. "A computer program for the analysis of a wide range of microwave resonators", 5th European Microwave Conference, Hamburg, Germany, September 1-4, 1975.

6.37 AKHTARZAD, S. and JOHNS, P.B. "A new model for the numerical solution of Maxwell's equations in three space dimensions and time", 5th Iranian Conference on Electrical Engineering, Pahlavi University, Shiraz, Iran, October 27-30, 1975.

CHAPTER 7

CONCLUSIONS AND ACKNOWLEDGEMENTS

7.1 CONCLUSIONS

The TLM method of numerical analysis in two dimensions, as described in chapters 1-3, has proved to be a useful general tool for the analysis of waveguide cross-sections and scattering problems. The introduction of the loss component described in these chapters makes the method very general indeed. The general TLM program used in two dimensions is similar to that described in chapter 4 and is applicable to a very wide range of problems simply by using different input data.

The extension of the TLM method to three space dimensions is obviously a desirable step and in chapter 5, by introducing the series node, the foundation for that extension is provided. Also in chapter 5, it is shown how the shunt nodes are used in conjunction with the series nodes to form a basic three-dimensional node to represent a true three-dimensional space. All six components of the electromagnetic field are properly accounted for by the three-dimensional model made up of many such basic 3-D nodes. The loss component in three dimensions may be introduced into the model in a similar manner as in the two dimensions.

Programming forms a significant part of any numerical method. With a proper technique, the programmer will save both computer time and storage. This saving could prove to be of great importance when limited time or storage, especially the latter, is available on the computer. It is perhaps equally important that a new user of the program should be able to adopt to it in a short while and also be able to feed into the computer the general data on a problem. With this in mind, a general purpose computer program based on the analysis of chapter 5 has been presented in the same chapter. The merits of

this program lies in its versatility and ease of application to general three-dimensional cavities. All the information relating to a three-dimensional cavity, such as conducting boundaries, strip patterns, permeability and permittivity at different points and also losses are simply fed into the computer as data. The three-dimensional program is an extension of the two-dimensional TLM program introduced in chapter 4 and has been written in only 110 lines of FORTRAN including three short subroutine programs.

In chapter 6, a wide range of microwave cavities have been analysed using the general three-dimensional TLM computer program. The results presented include the resonant frequencies of some empty, completely and partially filled cavities, the dispersion characteristic for an open-bounded surface waveguide and the power decay time of some lossy dielectric cavities. Also given, are some results for the dispersion characteristics of single microstrip line on dielectric and magnetic substrates, coupled microstrip lines on dielectric substrates and an example of a microstrip discontinuity, namely an abrupt change in line width. In all cases where comparisons could be made there has been excellent agreement. These results serve to demonstrate the ease of application and versatility of both the TLM method and the program. They also demonstrate the high accuracy of the method. By quoting some actual figures for run time and storage requirements of some examples in section 6.12, it is hopedthat these figures will demonstrate that the running time and storage of the TLM method are at least comparable with other methods.

The accuracy of the TLM method is due to the sophistication of the internodal field function which is used when the Fourier transform is taken. In effect, the act of taking the Fourier transform puts a section of a sinusoidal function between each node. For

example, in a homogeneous rectangular cavity the field functions are not solved approximately but exactly. It is for this reason that field description errors in the TLM method tend to be less than for many other methods.

The other sources of error in the TLM method are truncation and velocity errors (see section 1.4.1). Truncation error is predictable. It is associated with mathematical effect of taking the Fourier transform of a truncated function. The velocity error is also well defined and is dependent on the number of mesh nodes describing the geometry of a problem. These errors are minimal for enough number of nodes and iterations. A full description of the errors in the TLM method has been presented in reference 1.2.

The surface mode phenomenon of microstrip has been investigated also in this thesis (see chapter 6). Although considerable care was taken to try to excite the surface mode, there was no resonant frequency corresponding to this mode even though higher order waveguide modes are readily detected in this method. Therefore, it was concluded that such a mode most likely does not exist.

Finally, although the TLM method has been applied essentially to electromagnetic field problems, it may be adapted to form an analysis of other problems such as diffusion. The state-of-the-art of the method as explained in this thesis has shown to possess a remarkable degree of versatility and affords not only the user with a powerful numerical technique, but also the potential researcher to develop the method and ideas raised thoughout this project.

7.2 ACKNOWLEDGEMENTS

The author wishes to extend his thanks to Professor J.E. Parton for the use of University facilities and to Professor R.L. Beurle for taking an interest in this research. The author is also grateful to Mrs. K.M. Samwell for typing this thesis, to Miss E. Morris for proof reading and to his parents for continuous support.

Financial support for this study by the United Kingdom Ministry of Defence under contract AT/2024/037/CVD is also gratefully acknowledged. Last, but by no means least, the author wishes to express his sincere thanks to Dr. P.B. Johns for his constant encouragement and invaluable suggestions throughout this research project.

APPENDIX A

COMPUTER PROGRAM LISTING

```
      MASTER TLM - SINA

      DIMENSION V(4,12,11),IB(11,8),IE(11,7),R(11),VA(11)
      COMMON EH(200)

C     READ IN - LIMITS OF MATRIX
      READ(5,100)NX,NY
 100  FORMAT(4I5,I2,3I1,F10.6)

C     READ IN BOUNDARIES - X MIN, X MAX, Y MIN, Y MAX,
C     BOUNDARY CODE AND REFLECTION COEFFICIENT.
      KB=0
 11   KB=KB+1
      READ(5,100)(IB(KB,M),M=1,8),R(KB)
      IF(IB(KB,1))22,22,11
 22   KB=KB-1

C     READ IN EXCITATION POINTS OR LINES-X MIN, X MAX, Y MIN, Y MAX.
C     EXCITATION CODE AND INITIAL EXCITATION VALUE
      KE=0
 33   KE=KE+1
      READ(5,200)(IE(KE,M),M=1,7),VA(KE)
 200  FORMAT(4I5,I3,2I1,F10.6)
      IF(IE(KE,1))44,44,33
 44   KE=KE-1

C     OUTPUT POINT (IO,JO), OUTPUT CHOICE (L) AND
C     NUMBER OF ITERATIONS (NI).
      READ(5,100)IO,JO,L,NI

C     CLEAR THE MATRIX.
      DO 1  J=1,NY
      DO 1  I=1,NX
      DO 1  M=1,4
 1    V(M,I,J)=0.0

C     SET MATRIX TO PRESCRIBED INITIAL VALUES.
      DO 2 NE=1,KE
      DO 2 J=IE(NE,3),IE(NE,4)
      DO 2 I=IE(NE,1),IE(NE,2)
      DO 2 M=IE(NE,5),IE(NE,7),IE(NE,6)
 2    V(M,I,J)=VA(NE)

C     SET LIMITS OF MATRIX FOR ITERATION PURPOSE.
      NX=NX-1
      NY=NY-1

C     START THE ITERATION PROCESS
      DO 5  IC=1,NI
```

```
C       PERFORM BOUNDARY REFLECTIONS ACCORDING TO BOUNDARY CODE AND
C       REFLECTION COEFFICIENT.
        DO 3  NB=1,KB
        DO 3  J=IB(NB,3),IB(NB,4)
        DO 3  I=IB(NB,1),IB(NB,2)
        VXY=V(IB(NB,6),I,J)
        V(IB(NB,6),I,J)=R(NB)*V(IB(NB,5),I+IB(NB,8),J+IB(NB,7))
 3      V(IB(NB,5),I+IB(NB,8),J+IB(NB,7))=R(NB)*VXY

C       PERFORM NODAL CALCULATIONS.
        DO 4  J=1,NY
        DO 4  I=1,NX
        A=0.5*(V(1,I,J+1)+V(1,I,J)+V(2,I,J)+V(2,I+1,J))
        V(1,I,J)=A-V(1,I,J)
        V(2,I,J)=A-V(2,I,J)
        VY=A-V(1,I,J+1)
        VX=A-V(2,I+1,J)
        V(2,I+1,J)=V(4,I,J)
        V(1,I,J+1)=V(3,I,J)
        V(3,I,J)=VY
 4      V(4,I,J)=VX

C       EVALUATE AND STORE THE REQUIRED INFORMATION (ACCORDING TO
C       IO,JO AND L) FOR OUTPUT IMPULSE FUNCTION.
        GO TO(77,66,55),L
 55     EH(IC)=0.5*(V(1,IO,JO)+V(2,IO,JO)+V(3,IO,JO)+V(4,IO,JO))
        GO TO 5
 66     EH(IC)=V(3,IO,JO)-V(1,IO,JO)
        GO TO 5
 77     EH(IC)=V(4,IO,JO)-V(2,IO,JO)

C       REPEAT THE ITERATION PROCESS FOR NI NO. OF ITERATIONS.
 5      CONTINUE

C       CALL FOURIER TRANSFORM ROUTINE (OUTPUT).
        CALL OUTPUT(NI)


        STOP
        END
```

```
      SUBROUTINE OUTPUT(NI)

      COMMON EH(200)

C     READ IN- LOSS FACTOR (T).
      READ(5,100)T
  100 FORMAT(3F10.6)

C     READ IN FREQUENCY- (AS A RATIO OF MATRIX MESH SIZE TO FREE-
C     SPACE WAVELENGTH) FOR INITIAL VALUE OF D1 UP TO D2, INSTEPS
C     OF DS.
      READ(5,100)D1,D2,DS

      WRITE(6,1000)
 1000 FORMAT(///,19H      D         EHMOD,//)

C     EVALUATE COMPONENT LINE'S PROPAGATION CONSTANTS USING T.
      R=0.5*SQRT(1.0+T*T)
      RA=0.0
      IF(T.NE.0.0) RA=6.283184*SQRT(-0.5+R)
      RB=6.283184*SQRT(+0.5+R)

C     PERFORM THE FOURIER TRANSFORMATION.
      D=D1
   11 EHRE=0.0
      EHIM=0.0
      UK=EXP(-D*RA)
      U=UK

      DO 1  IC=1,NI
      CS=IC*RB*D
      EHRE=EHRE+EH(IC)*COS(CS)*UK
      EHIM=EHIM-EH(IC)*SIN(CS)*UK
    1 UK=UK*U

C     CALCULATE THE OUTPUT MAGNITUDE (EHMOD).
      EHMOD=SQRT(EHRE*EHRE+EHIM*EHIM)

C     WRITE OUT THE TABLE OF EHMOD VERSUS D.
      WRITE(6,100)D,EHMOD

C     FREQUENCY RANGE EXHAUSTED?
      D=D+DS
      IF(D.LE.D2) GO TO 11

      RETURN
      END
      FINISH
```

```
PGM     TLM - SINA
DATA

     12   11
      2    3     6     6 1310   1.000000
      3    3     6     6 2401   1.000000
      4    5     5     5 1310   1.000000
      5    5     4     5 2401   1.000000
      6    6     3     3 1310   1.000000
      6    6     2     3 2401   1.000000
      7   11     1     1 1310   1.000000
     11   11     2    10 2401   1.000000
      2   11    10    10 1310   1.000000
      1    1     7    10 2401  -1.000000
      0    0     0     0 0000   0.000000
     10   10     2    10  114   1.000000
      0    0     0     0  000   0.000000
      2    8     1   200
  0.000000
  0.000000   0.025500   0.000500
```

D	EHMOD
0.000000	19.024551
0.000500	18.138422
0.001000	15.551606
0.001500	11.474605
0.002000	6.249257
0.002500	0.798801
0.003000	6.040162
0.003500	11.929740
0.004000	17.007356
0.004500	20.772529
0.005000	22.811141
0.005500	22.816568
0.006000	20.611113
0.006500	16.160127
0.007000	9.580175
0.007500	1.322959
0.008000	8.956182
0.008500	19.959823
0.009000	31.457548
0.009500	42.850323
0.010000	53.546449
0.010500	62.990975
0.011000	70.698626
0.011500	76.282550
0.012000	79.476504
0.012500	80.149032
0.013000	78.308840
0.013500	74.101189
0.014000	67.795772
0.014500	59.767082
0.015000	50.468774
0.015500	40.403917
0.016000	30.093294
0.016500	20.044317
0.017000	10.725369
0.017500	2.611763
0.018000	4.421728
0.018500	9.571468
0.019000	13.052634
0.019500	14.855618
0.020000	15.094843
0.020500	13.973539
0.021000	11.762973
0.021500	8.781036
0.022000	5.374936
0.022500	1.974957
0.023000	1.853519
0.023500	4.600752
0.024000	6.813235
0.024500	8.257057
0.025000	8.861718

NUMBER OF TRANSFERS	100
TOTAL MILL TIME USED	20 SECS
MAXIMUM CORE USED	6 THOUSAND
COMPUTING UNITS USED	2.5